NASA CONTRACTOR REPORT

NASA CR-1267

NASA CR-1267

AN EXPERIMENTAL AND THEORETICAL ANALYSIS OF THE CONVECTED BALANCED ARC

by Leland Malcolm Nicolai

Prepared by
UNIVERSITY OF MICHIGAN
Ann Arbor, Mich.
for

NATIONAL AERONAUTICS AND SPACE ADMINISTRATION • WASHINGTON, D. C. • FEBRUARY 1969

NASA CR-1267

AN EXPERIMENTAL AND THEORETICAL ANALYSIS OF THE CONVECTED BALANCED ARC

By Leland Malcolm Nicolai

Prepared under Grant No. NGR 23-005-128 by
UNIVERSITY OF MICHIGAN
Ann Arbor, Mich.

for

NATIONAL AERONAUTICS AND SPACE ADMINISTRATION

For sale by the Clearinghouse for Federal Scientific and Technical Information
Springfield, Virginia 22151 – CFSTI price $3.00

ACKNOWLEDGMENTS

The author wishes to express his appreciation to the members of the Doctoral Committee. He is especially grateful to Professor Kuethe for the advice and guidance given throughout the research. Professor Kuethe has an outstanding "feel" for the physical phenomena involved and this was a tremendous help on many occasions. The many discussions with Professor Kuethe were most helpful and will long be remembered warmly. Professor Phillips was very generous in sharing his time, experience and reports during the investigation. These three items were invaluable as they considerably reduced the time spent searching for information. A special thanks to Professor Bowen for his interest and enthusiasm in the research problem. The ideas expressed in Section 5. 6 are largely his.

The assistance of Dr. Robert L. Harvey is gratefully acknowledged. The help in the laboratory of Francis Donovan and Ronald Kapnick, and the photographic assistance of Robert Brando was greatly appreciated. These men would always do more than what was asked of them. Many thanks also to Mrs. Eunice Sherbrook and Mrs. Jacqueline Biggers for their expeditious and conscientious typing of this dissertation.

The author is grateful to the National Aeronautics and Space Administration for their support of this research under NASA Grant No. NGR 23-005-128 and to the United States Air Force for making this continuing education possible.

Finally, the author wishes to extend a very special expression of gratitude to his wife, Carolyn, for her untiring encouragement and understanding.

TABLE OF CONTENTS

LIST OF ILLUSTRATIONS

LIST OF TABLES

NOMENCLATURE

B	Magnetic field strength
C_2	$\pi \bar{\sigma}/4$
C_3	Experimental constant, $Nu_{FC} = C_3 (Re_f)^2$
C_4	$\rho_f^2 \pi \phi_b C_3/\mu_f^2$
C_5	$\rho_f^2 4 \phi_b C_3/\bar{\sigma} \mu_f^2$
C_D	Drag coefficient (usually referenced to transverse dimension)
C_p	Specific heat for constant pressure process
D	Effective dimension for arc
d_1	Reference dimension
d_S	Arc streamwise dimension (based upon luminous region)
d_T	Arc transverse dimension (based upon luminous region)
d_{eff}	Effective diameter, diameter of circular cylinder having the same surface area as elliptic cylinder, $\approx (d_T + d_S)/2$
E	Electric field strength
E_o	Electric field strength for a free-burning arc
E_x	Exposure, (intensity) (time)
e	Charge on an electron, 1.6×10^{-19} coulombs
Gr	Grashoff number (see Appendix A)
H	Nondimensional total enthalpy per unit mass

h	Static enthalpy, $\int C_p dT$
h_{NC}	Natural convection heat transfer coefficient
I	Arc current
I_1	Reference current, $\sigma_1 E d_1^2$
J_1	Reference current density, $\sigma_1 E$
j	Arc current density
K_1	Eckert number, u_1^2/h_1
K_{JH}	Joule heating parameter, $EI_1/\phi_1 Pr_1\sqrt{L_c}$
k	Thermal conductivity
L_c	Lorentz number, $\rho_1 BID/\mu_1^2$
M_∞	Free stream Mach number
m_e	Mass of an electron, 9.1×10^{-31} Kg
m, n	Exponents
N	Radiance in watt/cm^2- steradian
Nu	Nusselt number
n_e	Electron number density
P	Pressure
P_L	Power gradient parameter, EI_1/ϕ_1
P_t	Total pressure
P_∞	Free stream pressure
Pr_1	Prandtl number evaluated at reference temperature, $\mu_1 h_1/\phi_1$
Q_{MT}	Energy transfer by mass transfer

Q_R	Energy transfer by radiation per unit volume
q_∞	Free stream dynamic pressure, $\rho_\infty u_\infty^2/2$
R	Gas constant
Re	Reynolds number
Re_1	Interior Reynolds number evaluated with reference quantities, $\sqrt{L_c}$
Re_∞	Free stream Reynolds number
r	Radial distance from origin
r_b	Radius of arc assuming a circular boundary
T	Temperature
T_1	Reference or characteristic temperature
T_e	Electron temperature
T_f	Film temperature, $(T_b + T_\infty)/2$
T_g	Gas temperature
T_σ	Effective temperature, i. e., temperature corresponding to mean electrical conductivity $\bar{\sigma} = I/(\pi d_S d_T/4)E$
T_∞	Free stream temperature
t	Time
t_{ex}	Exposure time or shutter speed
U_R	Total energy transfer by radiation/length
u_∞	Free stream velocity
u_{∞_n}	Free stream velocity normal to the arc leading edge

u_1	Characteristic velocity for arc core, $\sqrt{\sigma_1 EB\, d_1/\rho_1}$
u, v, w	Velocity components in x, y, z directions respectively
V	Total velocity, (u, v, w)
V_{arc}	Total arc voltage
x, y, z	Coordinates for a right hand system
Z_s	Charge number of particle (i. e., $Z_s = -1$ for electrons)
Z	Compressibility factor
α, β	Constant coefficients in power gradient relation
Γ	Exponent on P_∞ to account for change in σ as P_∞ varies (see Appendix D)
γ	Tangent of the slope of the film characteristic response curve
ε	Radiation emission coefficient
ϵ	Source strength, mass/sec
Θ	$(T_o - T)/(T_o - T_s)$
θ	Angle measured from the x axis
μ	Coefficient of viscosity
ρ	Density
ρ_e	Net free charge density
σ	Electrical conductivity
$\bar{\sigma}$	Mean electrical conductivity

τ_e	Electron - neutral collision time
τ_{ij}	Stress tensor
τ_{sys}	Transmission factor for viewing system
Φ	Viscous dissipation term
ϕ	Heat flux potential, $\int k dT$
ψ	Non-dimensional stream function
Ω	Solid angle for radiance measurements
ω_e	Electron cyclotron frequency, Be/m_e

Subscripts

1	Reference quantities
b	Conditions at the arc boundary
f	Quantity evaluated at film temperature T_f
i	Index on radial variable
j	Index on azimuthal variable
o	Conditions at the origin
s	Conditions at the surface or boundary
w	Conditions at the wall
FC	Conditions for forced convection
NC	Conditions for natural convection

Mathematical Notation

$\approx$	Approximately equal to
$\sim$	Proportional to
$\vec{\ }$	Vector symbol
$\lvert\ \rvert$	Absolute value
O(1)	Value of order one magnitude
∇	$\frac{\partial}{\partial x} + \frac{\partial}{\partial y} + \frac{\partial}{\partial z}$, Gradient operator
∇^2	$\frac{\partial^2}{\partial x^2} + \frac{\partial^2}{\partial y^2} + \frac{\partial^2}{\partial z^2}$, Laplacian operator

I. INTRODUCTION AND BACKGROUND

1.1 INTRODUCTION

The purpose of this investigation was to examine the behavior of a direct current electric arc in a cross-flow and transverse magnetic field. The external fields were such that the Lorentz force balanced the fluid dynamic drag force on the column. This arrangement is defined here as a convected balanced arc. This problem was one of basic research into the interaction and energy exchange processes between an electric arc, a velocity field, and a magnetic field.

One application of this investigation would be in the area of arc heater design and performance. Here the enthalpy of a cold fluid is increased by (1) the conversion of electric to thermal energy inside the arc and then (2) energy transfer across the arc boundary into the fluid. The electric arc has an unlimited power input capability, being limited only by the capability of the surroundings to remove this power input and by the capability of the arc's external power supply. If the surroundings were suddenly able to remove more energy from the arc (for example, by increasing the cross-flow velocity), the arc, for a constant current, would increase its electric field strength to accommodate this.

The most popular arc heater design (at present) is the electric arc burning in a tube with a co-axial gas flow. This configuration exhibits good arc stability and has been put on a sound theoretical footing by Stine and Watson (Ref. 14). In this design, however, a large fraction of the column energy input (EI) is transferred to the tube walls and is not available to heat the cold fluid.

Another configuration for arc heater design is the cross-flow configuration where the arc column moves, normal to its axis, through the gas or the arc is stationary and immersed in a moving fluid (i. e. the convected balanced arc). This configuration does not have the tube walls of the co-axial design, thus all of the energy put into the column must be transferred to the cold fluid flowing around the arc. The cross-flow configuration appears to be a more efficient arc heater design than the co-axial configuration, however, many questions must be answered before a valid performance estimate can be made of a cross-flow arc heater. For example, "How comparable is an arc in a cross-flow and a transverse magnetic field to a heated solid cylinder in a cross-flow?" The stability of the arc in a cross-flow is not as easily achieved as it is for the co-axial design. This is because the interaction processes between the arc, the velocity field and the magnetic field are still in question. Also, the theoretical treatment of the cross-flow design is much more difficult since all

the boundary conditions are not known a priori and the arc is not rotationally symmetric.

The experimental and theoretical investigation reported in this dissertation is arranged as follows. Section II reports the experimental information obtained on convected balanced arcs at high currents (200 to 500 amperes) in supersonic airstreams of Mach 2.5, 3.0 and 3.5. Section III presents a development of the theory for convected balanced arc columns. The governing equations and boundary conditions are formulated (assuming a continuum fluid) and the important similarity parameters are defined. In Section IV the experimental results from this investigation and from Ref. 19 are discussed and compared with the theory. The theory of Section III is advanced a little further as a result of the comparison with experimental data. Results from the numerical solution of the governing equations are presented in Section V and are compared with experimental information.

Appendix A discusses the analogy between the natural convection of heat in a horizontal tube and the convection of heat inside a convected balanced arc. Appendix B presents experimental correlation curves for the forced and natural convection heat transfer from heated solid cylinders. Probably the most striking observation of a

convected balanced arc in a supersonic airstream is the characteristic slant of the arc. Reasons for the slant are presented in Appendix C along with a discussion of the general arc configuration. The free-burning arc was of interest in this investigation since it represented the limiting case of the convected balanced arc when the cross-flow vanished. For this reason an experimental study of free-burning arcs at currents of 190 to 400 amperes and pressures of 1 atmosphere down to 0.0191 atmospheres was conducted and the results are shown in Appendix D.

1.2 GENERAL FEATURES OF AN ARC

An arc is a subdivision of the general electrical phenomena termed self sustaining gaseous discharges. Static discharge characteristics are shown in Fig. 25. The discharge is sustained by (1) the existence of a conducting fluid (usually a gas) between an anode and cathode electrode, and (2) the emission of electrons by the cathode under the bombardment of positive ions and light quanta from the gas.

Region A of Fig. 25 is characterized by a large voltage drop of several hundred volts, and a low current (usually less than 1 ampere) and is called the glow discharge region (Ref. 46, Chapter 15 and 16). The arc discharge is shown as region B of Fig. 25 and differs from the glow discharge in that it has a low voltage drop and is capable of

sustaining large currents (Ref. 4 and 45). The region between the electrodes of an arc is a fairly uniform plasma (that is to say free from electrode effects) and is a useful tool in plasma research.

The arc can be divided into three regions: the cathode drop region, positive column and the anode drop region. These three regions are shown in Fig. 28. The two drop regions are extremely short (on the order of an ion mean free path) and are characterized by sharp drops in potential near both electrodes. The potential drops (often called potential falls or drop voltages) are attributed to space charge accumulation close to the electrodes and the physical processes occuring in and near these areas are not too well understood (Ref. 1, 2, 3, 5, 6, and 13 give excellent discussions of the drop phenomena). It is the task of the drop region to bring about the electrical contact of the plasma column at a high gas temperature with the electrodes at a lower temperature. The region between the anode and cathode drop is called the positive column and as mentioned above is a fairly uniform region. The name "positive column" was given to this region of the arc by the early investigators who thought the plasma column was an extension of the anode or positive drop region.

In order for an arc to be self sustaining there must be a manufacture of electrons some where in the arc. This is obvious since electrons near the cathode move along the arc under the axial electric field

towards the anode while the ions, being much more massive than the electrons, are relatively stationary in the column and provide charge neutrality. Electrons are produced by the ionization of the neutral gas in the column but the primary source of electrons is the cathode itself. Ions are accelerated through the cathode fall and bombard the cathode, imparting energy and increasing the temperature of the cathode. Electrons are then emitted from the cathode by several mechanisms. The primary mechanisms are thermionic emission, field emission (electrons are drawn out of the metal by very high electrostatic fields) and a combination of thermionic and field emission called T-F emission (Ref. 3).

The cathode is further characterized by a strong constriction of the arc column at the cathode. The ion bombardment is more efficient when it concentrates its "conditioning" on a small spot rather than an area the size of the column cross-section. This constriction gives rise to a magnetic pressure gradient in the cathode fall region which accelerates the plasma in the axial direction into the uniform column. This action draws air in from the surroundings (Maecker, Ref. 1, refers to this as a pumping action) and provides a cathode jet along the column towards the anode (see also Ref. 3 and 13).

The anode, compared to the cathode, has a relatively passive role in the discharge process. The arc anodes do not to any significant extent

emit positive ions, however, at large currents a strong anode jet can exist (King, Ref. 57).

1.3 THERMAL AND NON-THERMAL ARCS

For a plasma in local thermodynamic equilibrium the number of collisions between electrons and heavy plasma particles is so large that the electrons transfer their total excess energy, which they derived from the electric field, to the heavy particles. In the weakly ionized arc column this energy transfer is primarily by elastic collisions (Ref. 28 and 46). Thus there must be many collisions since the amount of energy transferred in a single elastic collision is small (on the order of m_e/m_i).

For arcs operating at gas or vapor pressures of 1 atm or greater the conditions for thermodynamic equilibrium are particularly well met because of the large number of collisions between electrons, atoms and ions. Such arcs are called "thermal arcs" or simply "high pressure arcs".

Arcs operating at low gas pressures (something less than 1 mm Hg) are usually not in local thermodynamic equilibrium. At these low pressures there are not enough collisions to establish equilibrium between the electrons and the heavier plasma particles, and the electron temperature T_e is much larger than the gas temperature T_g. Such arcs are called "non-thermal arcs" or "low pressure arcs".

Figure 29 shows a typical temperature dependence on gas temperatures at various pressures. There is not, however, a defined pressure above which the arc qualifies as a thermal arc and below which it is a non-thermal arc. In general, high pressure arcs will refer to arcs at pressures of the order of 1 atm. An external transverse magnetic field can effectively increase the pressure in which an arc is operating. The magnetic field effectively decreases the mean free path of electron-neutral collisions since the trajectories of the electrons between collisions are not straight lines but gyrations around the field lines. Thus, the collision frequency is increased as though there were an increase in pressure. Blevin (Ref. 46, p. 125) defines the effective pressure P_∞' as

$$P_\infty' = P_\infty \sqrt{1 + \omega_e^2 \tau_e^2}$$

where $\omega_e = Be/m_e$, electron cyclotron frequency

τ_e = electron-neutral collision time (Ref. 24 and 25)

$\omega_e \tau_e$ = Hall parameter

Hence, for arcs operating in external transverse magnetic fields, the effective pressure should be used in determining whether an arc is thermal or non-thermal.

Tonks and Langmuir (Ref. 12) state that the fundamental relations for describing the column of the low pressure arc are:

(1) Plasma balance (i. e. species continuity equation)

(2) Ion generation and recombination equations

(3) Mobility equations for ions and electrons

(4) Ohm's law for electron current

(5) Energy balance equation

Champion (Ref. 11) and Thompson (Ref. 8) show that these five fundamental relations, plus Maxwell's equations form a necessary and sufficient set for a full description of the non-thermal arc. Hoh (Ref. 7) considers the effect of a magnetic field upon the low pressure arc. The non-thermal arc is an interesting and important facet of plasma physics but it is not considered further in this investigation.

The positive column of the high pressure or thermal arc is analyzed considering the plasma as a single specie gas or continuum fluid at some local pressure and temperature (Ref. 1 and 10). The theory for a thermal arc column in a transverse flow and magnetic field is discussed in detail in Section 3. 2.

1.4 CLASSIFICATION OF THERMAL ARCS

Steady arcs can be one of several different types depending upon the boundary conditions imposed by the surroundings. From this point of view, steady arcs are usually classified as electrode stabilized, wall stabilized or convection stabilized. Here the word "stabilize" means to impose boundary conditions which will guarantee the arc to be in a steady state.

For example an electrode stabilized arc has the steady state energy input in the column (i.e. joule heating) balanced primarily by energy transport to the electrodes. The column is very short and really not uniform since there is significant energy transfer in the axial direction (Ref. 44, 45, and 46). The electrode stabilized arc is difficult to analyze because a significant portion of its length is in the drop regions. The anode and cathode drop regions are not in thermodynamic equilibrium regardless of the gas pressure since the electron acceleration takes place so suddenly in the high electric field region that there are not enough collisions to establish equilibrium (Ref. 5 and 6).

A wall stabilized arc is an arc burning in a tube of fixed temperature. The arc length is long enough such that there is an interval of uniform column, free from electrode effects, where the joule heating is balanced by two-dimensional heat conduction and radiation to the wall. This arc can be analyzed very nicely because the boundary conditions are known and there is no convection involved in the problem. This problem has been studied extensively (see, for example, Ref. 9) and is fairly well understood.

A convection stabilized arc is an arc that is burning in a stationary fluid (free convection or free-burning arc) or a moving fluid (forced convection arc). The convection heat transfer at the arc

boundary is the primary energy transfer mechanism that balances the input energy. Radiation is usually negligible, however, it can become as much as 1/3 of the input energy for high pressure, high current arcs (see Ref. 55 and 56).

The arc in a moving fluid is swept downstream with the flow unless the arc column is held stationary by some means. Usually the arc is held stationary by impressing a transverse magnetic field of sufficient strength such that the resulting Lorentz force just balances the fluid dynamic "drag" force on the column.

1.5 REVIEW OF THE CONVECTED BALANCED ARC LITERATURE

Roman and Myers (Ref. 20) made a survey of all the investigations through early 1966 of electric arc interactions with magnetic and aerodynamic fields. Their review is an excellent account of the work done on travelling arcs (i.e. arcs moving along the electrodes due to the Lorentz force) as well as stationary arcs. Because of their survey of the literature, this review will be limited to the references which influenced this investigation.

Bond (Ref. 17) investigated the balanced convected arc in a Mach 2.0 and 2.5 airstream with the experimental set-up shown in Fig. 1 and 2 and described in Section 2.1. He examined a current range of 200 to 900 amperes, free-stream pressures P_∞ of 20 to 50 mm Hg and different electrode materials. The external magnetic field decreased

in the upstream direction such that the arc could move along the electrodes until a balance between the Lorentz force and fluid dynamic drag force was achieved. The arc was observed photographically and appeared to be quite steady.

Bond made the following observations:

(1) At $M_\infty = 2.5$ and $P_\infty = 29$ mm Hg the electric field was constant at 35.5 volts/in. over the current range of 300 to 700 amperes.

(2) The value of the magnetic field required for balancing the arc was dependent only upon the value of P_∞.

(3) The arc column slanted between the cone cylinder electrodes with the anode always upstream of the cathode. The angle of the slant was approximately that of the local Mach angle and did not vary with current, P_∞ or electrode material.

(4) With the cathode above the anode, the cathode spot was on the side of the cathode and not on the underside as one would expect.

(5) The arc configuration was quite steady when it could assume its characteristic slant, however it became very unsteady and resembled a ball of fire when conditions were such that it couldn't slant.

(6) From photographs, the arc diameter appeared to increase with current.

Roman (Ref. 19) investigated an arc in a subsonic cross-flow and transverse magnetic field at one atmosphere. Argon was blown past the tungsten cathode to prevent rapid oxidation. This resulted in an air seeded argon arc burning in air and introduced uncertainties about the physical and transport properties of the arc. Roman investigated a current range of 200 to 400 amperes, with free stream velocities up to 60 ft/sec and magnetic fields up to 50 gauss. His experimental results are shown in Fig. 12 and 13 and were used extensively in this investigation.

Roman's general observations were:

(1) Photographs of the arc showed an increase of the streamwise (d_S and transverse (d_T) dimensions with current. The arc appeared to have an elliptical cross-section with d_T/d_S about 1.5. The d_S decreased and d_T increased for a constant current and increasing flow velocity. The dimensions varied linearly with current and flow velocity.

(2) Using the force balance equation

$$BI = C_D \frac{1}{2} \rho_\infty u_\infty^2 d_T$$

Roman determined C_D values, based upon d_T, of 0.7 to 1.1. The free stream Reynold's number range was 4×10^2 to 4×10^3 and these C_D values were similar to the values for solid cylinders with the same cross flow Reynold's numbers.

(3) Miniaturized pitot, enthalpy and heat flux probes were used to determine the velocity and energy distribution in the region downstream of the arc. The velocity measurements showed a stagnant region directly behind the arc with a clearly defined wake formation. Flow visualization with a micron-size particle injection scheme was used in conjunction with high-speed photography to study the flow pattern near the arc boundary and in the wake region. These studies showed the separation point for the arc to be about the same as for a solid cylinder in incompressible flow. From this he concluded that the arc was impervious to the external flow.

(4) From photographs of the arc, the temperature at the edge of the luminous region was estimated to be $6000^{o}K \pm 1000^{o}K$.

(5) The Nusselt number for the column was determined and found to be within an order of magnitude of Hilpert's curve (Fig. B-1).

The characteristic curves (Fig. 13a) were fairly flat over the current range for $u_{\infty} < 40$ fps. For higher velocities the slope of the characteristic curve became slightly negative. The arc dimensions increased with current. Roman remarks in Ref. 20 that his experimental data (at the large current) might have been affected by wall interference due to the close proximity of the magnets.

Fischer and Uhlenbusch (Ref. 39) considered the theoretical problem of a wall stabilized nitrogen arc at one atmosphere with a transverse magnetic field. They were interested in determining the cross-sectional streamline pattern and temperature distribution due to the internal circulation generated by the Lorentz force. The internal flow was assumed to be steady, two-dimensional and incompressible. The self magnetic field and the inertia terms in the momentum equation were neglected. The boundary conditions at the wall, were the no-slip condition and a temperature of $0^{o}K$.

The solution of the vorticity and energy equations were carried out numerically with the heat flux potential and stream function expressed as Fourier series. The numerical solution was limited by computer storage and Fischer and Uhlenbusch were able to obtain valid solutions only for magnetic fields up to about 150 gauss.

The solution for the streamlines indicated a double-vortex pattern displaced in the direction of the Lorentz force. The temperature distributions were shifted with the peak temperature forward of the arc centerline. For a constant current, the calculated electric field increased as the magnetic field increased from 0 to 150 gauss.

Harvey (Ref. 31) made an experimental and theoretical investigation of convected balanced arcs. His experimental work was an extension of Bond's effort with more data taken at Mach 2.5 and new

data at Mach 3. 5. He introduced magnesium particles into the column at the anode and was able to observe their motion along the column using high-speed photography. The estimated speed of the tracer particles in the column was about 35 fps.

Harvey reported the following observations:

(1) On the basis of the high-speed motion pictures of the magnesium tracers, the arc column is essentially impervious to the free-stream.

(2) The luminous region of the arc appeared to be elliptical in shape with the transverse dimension d_T larger than the streamwise dimension d_S

(3) The force and heat transfer coefficients, based upon d_T and the normal component of the free-stream velocity, were within a factor of 3 of the analogous coefficients for solid cylinders with the same optical shape and free-stream conditions.

(4) The arc configuration had the same characteristic slant observed by Bond. The slant angle was approximately the local Mach angle at M_∞ of 2. 5 and 3. 5 and this angle did not change with current or P_∞.

Harvey extended the numerical work of Fischer and Uhlenbusch (Ref. 39) to higher values for the magnetic field. He retained the inertia terms in the momentum equation and considered a wall

temperature of 4400^{o}K. His solutions showed that as the magnetic field was increased to higher values the peak temperature shifted to the front of the arc and the temperature contours were distorted around the periphery of the cross-section.

The natural convection of heat in a horizontal tube is very similar to the flow behavior in a balanced convected arc in that the convection currents are generated in both cases by body forces dependent upon temperature. In this regard the efforts of Weinbaum (Ref. 32) and Ostrach and Menold (Ref. 33) were very helpful in the early stages of this investigation. The analogy between these two problems is made in Section 3. 5 and Weinbaum's work is presented in Appendix A.

II. EXPERIMENTAL RESULTS

2.1 EXPERIMENTAL SET-UP AND EQUIPMENT

The experimental apparatus consisted of two rail electrodes mounted in the University of Michigan 4 in. x 7 in. supersonic wind tunnel (blow-down) with water cooled field coils providing a transverse magnetic field. This set-up is shown in Fig. 2. This apparatus was designed and fabricated by Bond (Ref. 17) during his work at the University of Michigan.

The electrodes are cone cylinders, about six inches long and one half inch in diameter with a 7 $1/2^{o}$ half angle cone (Fig. 1). Carbon and OFHC* copper were used as the electrode materials. The anode was usually on the bottom.

The transverse magnetic field was supplied by two coaxial coils located on opposite sides of the tunnel (Fig. 2c). Each coil is water cooled and contains eleven pancake segments about 12 in. in diameter. The coils provide a maximum flux density at the tunnel centerline of 6400 gauss with 2000 amps flowing through the coils. The magnetic field decreases upstream in the vicinity of the electrodes as shown in Fig. 6. The coils could be moved upstream and downstream to balance the arc. The power supply for the coils and the arc was a 600 volt, 1600 amp d.c. generator.

---

*Oxygen free, high conductivity copper.

The arc, shown schematically in Fig. 6, was initiated by exploding a firing wire. The operation sequence was to start the tunnel and then close the firing switch which first energized the coils and, about 4 sec later, energized the arc circuit. A typical run was 1.5 sec in duration. Longer runs resulted in considerable damage to the electrodes since they were uncooled. If conditions were right for a steady arc to be established (i.e. stagnation pressure, Mach number, arc current, coil location and coil current) it was established very quickly (i.e. less than 10^{-2} sec). The arc was able to move along the electrodes until the balanced arc conditions were satisfied.

The measurements of currents and voltages were made using a light-beam oscillograph, Visicorder Model 1508. Hathaway galvonometers were used in the instrument.

Visual observations of the arc were made using a 16 mm Fastax (Model W 163269) and a 35 mm Nikon camera. A mirror arrangement (Fig. 2c) external to the supersonic tunnel permitted near head-on and side-on observations simultaneously. The film used in the Fastax was Dupont 931A (f/16) and Kodachrome II KR430 (f/5.6) at speeds of 4000 to 7000 frames/sec. The film used in the Nikon camera was ADOX KB14 (f/16 at 1/1000) and Kodak Panatomic X (f/11 at 1/1000).

2.2 RANGE OF EXPERIMENTAL TEST CONDITIONS

With the experimental set-up described in the last section, a balanced convected arc in a supersonic stream could be investigated at Mach numbers of 2.0 to about 3.5. This investigation considered Mach numbers of 2.5, 3.0, and 3.5. An attempt was made to have the same free stream pressure, P_∞ for all 3 Mach numbers, but this was not possible. With one atmosphere total pressure, the P_∞ for $M_\infty = 3.5$ was 9.6 mm of Hg. The lowest total pressure for $M_\infty = 2.5$ at which a steady arc could be established was $P_t = 13.0$ in. of Hg which gave a $P_\infty = 19.3$ mm of Hg. For total pressures less than 13.0 in. of Hg at $M_\infty = 2.5$ the tunnel was thermally choked due to the energy addition from the arc. The P_t for $M_\infty = 3.0$ was set at 21.0 in. of Hg which gave a $P_\infty = 14.5$ mm of Hg, an intermediate value between the free stream pressures at $M_\infty = 2.5$ and 3.5. The range of the other test conditions are given in Table I and Fig. 22.

2.3 VISUAL OBSERVATIONS

Photographs of steady and unsteady convected arcs in a supersonic stream are shown in Fig. 3, 4, and 5. One observes, first of all, that the steady arc has clearly defined boundaries slanted with the anode spot upstream of the cathode spot. Also, that the cathode spot for the steady arc is on the side of the cathode and not on the underside as one would expect. These observations were first made by Bond in Ref. 17.

The arc shown in Fig. 5 is termed an unsteady arc. The photograph shows the boundaries of the arc as fairly well defined, but not as clear and distinct as for the steady arc shown in Fig. 3 or 4. The arc of Fig. 5 is balanced but it is not steady as evidenced by the large fluctuations in voltage (i.e. greater than $\pm$ 7 volts) and (to a lesser degree) current as shown on the Visicorder trace. Also, the cathode root is not a well defined spot, but rather seems to encompass the entire perimeter of the cathode. This unsteady arc configuration was forced by locating the field coils such that the arc could not attain a steady arc configuration. If the field coils had been moved upstream about one inch the test condition would have been identical to those of Run 657 and the arc configuration would have looked like Fig. 10a.

All data used in this investigation were obtained from arcs qualifying as steady arcs. To qualify as a steady arc, its photograph had to show very distinct and well defined boundaries and a cathode spot on the side of the cathode. Also, and most important, its voltage and current traces had to be very steady as in Fig. 3 and 4.

The steady arcs showed a different slant angle for the lower and upper leading edges (anode on the bottom). These observed angles are shown on Fig. 7. The angles increase with increasing arc current* and appear to be related with the free-stream Mach angle, since

*This is contrary to the observations of Bond (Ref. 17) and Harvey (Ref. 31). This piece of experimental information is very important and results in the qualitative agreement between the data of this investigation and Roman (Ref. 19).

they change with Mach number. The reason for the arc slant appears to be fluid dynamic rather than an electromagnetodynamic, such as Hall effect. The reasons for this argument will be discussed in Appendix C. Also, the point where the leading edge slant changes (half way along the column) is the intersection region between the upper and lower electrode conical shocks.

It was observed that once the proper location for the field coils was found to establish a steady arc at a particular Mach number, the coils could be left at this location while the current was varied from 200 to 500 amps. The arc is free to move along the electrodes seeking the proper conditions for balancing. With the field coils fixed, however, the anode spot was also fixed, over the above current range. This indicated that the value of the magnetic field B at the reference station was fairly constant for fixed free stream conditions but variable current*. Actually, the value of B decreased slightly with increasing current due to the increasing slant of the reference station. The values of B/q_{∞_n} versus arc current I for this investigation are shown on Fig. 12 along with some of Roman's data (Ref. 19).

---

*The observation that B was independent of current but dependent on P_∞ and T_∞ was first made by Bond (Ref. 17).

About 2/3 of the distance along the column from the anode on the near head-on view one observes an "interaction region." This appears to be an interaction between the fluid flowing along the column from the anode and the plasma jet from the cathode. The fluid appears to stream out the side of the arc at about the location of minimum pressure or the separation point (see Figure 10) *. This behavior is identical to that observed by Morse et al. (Ref. 69) who observed this interaction between the cathode plasma jet and column flow from the anode. As the current is increased to 500 amps this plasma jet becomes stronger, causing the interaction region to get larger and move down the column.

Since the arc dimensions and value of the magnetic field vary along the arc column, a reference station was selected for these measurements. It was required that this reference station be in an interval of uniform column. A station 1/3 the distance from the anode to the cathode was selected as the reference station and all dimensions and values of magnetic field were measured there (Figure 6). It was observed in the free-burning arc experiments discussed in Appendix D that for P_∞ = 14. 5 mm Hg, the free - burning arc was convection stabilized for arc lengths greater than 2. 0 in. This means

*Roman (Ref. 19) observed a separation point and formation of a wake for convected balanced arcs.

that for arc lengths greater than 2 in. there exists an interval of column where the arc can be assumed uniform in the axial direction. This assumption becomes more valid the longer the arc. Thus, for distances greater than one inch from the electrodes the energy balance can be considered two-dimensional and none of the column energy is transported to the electrodes. Since the arc lengths for the convected balanced arc were greater than 3.0 in., the reference station appears to be far enough from the anode such that the input power gradient EI is balanced by two-dimensional radiation, forced convection and mass transfer at the boundary.

It appears from the photographs and from the drawing of Fig. 6 that the reference station is far enough away from the interaction regions of (1) the upper and lower conical shocks and (2) the confluence of the anode and cathode flow so that their influences should be negligible. Thus it is hypothesized that at this reference station the arc simulates, to a satisfactory approximation, a uniform column inclined to the free stream.

An interesting observation can be made from the arc photographs shown in Fig. 10. The brightest region at the reference station is near the leading edge. This observation is further strengthened by the microdensitometer scans of Fig. 10a (Run 657) shown in Fig. 26. These results indicate that the peak temperature occurs near the leading

edge and not at the arc centerline. This shift in the peak temperature in the direction of the Lorentz force is observed in numerical calculations and will be discussed more in Section V.

2. 4 ARC DIMENSIONS OF THE LUMINOUS REGION

The arc dimensions of the luminous region at the reference station were obtained from photographs using the Nikon camera with Kodak Panatomic X film at f/11 and 1/1000. The developing was in D-76 (diluted 1 to 4) for 5 min. This gave a film characteristic response curve (density versus log exposure *) with a very low gamma, $\gamma = 0.225$. These photographic conditions were used to insure that over the intensity range of interest the film response was linear so that the arc detail was preserved.

The photographs, such as Fig. 3, 4, and 10 show that the leading edge of the luminous region is very distinct and well defined, whereas the sides and back are less clear. By requiring very steady arcs in all cases and comparing all photographs with each other, quantitative dimensions of the luminous region were obtained.

The boundary of this region represents an isotherm and temperature gradient combination because the path length changes with transverse distance. ** Since the temperature gradients appear to be steep

---

*Exposure = (intensity) (exposure time or shutter speed).

**The effect of path length on the luminosity will be discussed in more detail in Section 5. 6.

in this region it will be assumed that the luminous boundary is an isotherm. At this time, the temperature corresponding to this boundary is not known. Estimates are 6000 to 7200°K (Ref. 19 and Section 5. 5). These dimensions, however, are relative to all the arc data and provide an appropriate characteristic dimension for the arc data taken at Mach 2. 5, 3. 0, and 3. 5. Using this characteristic dimension, a characteristic or mean temperature can be determined for each set of arc data.

The measurements of the arc column indicated clearly that the arc cross-section is not circular but that the transverse dimension, d_T, is about one and one half times as large as the free-stream dimension, d_S. It was assumed that the cross-section was elliptical in shape. Measurements were made on arcs at electrode gaps of 1. 0 in. and 0. 6 in. and with copper and carbon electrodes. In all cases the dimensions of the column were the same, being dependent only on current and Mach number. These observed dimensions are shown on Fig. 8.

For one sequence of five identical runs, the lens opening was set at f/8, f/11, f/16, f/22, and f/32. Figure 10 shows photographs of 3 of the 5 runs. The developing was held constant as mentioned earlier. The dimensions of the luminous region did not change. Since the radiative power received by the film was different for each

lens setting, the invariance of the luminous dimension indicated that the dimensions represented isotherm boundaries in a region of steep temperature gradients. This observation was also reported by Harvey (Ref. 31). Figure 10 also indicates the repeatability of the balanced arc obtained with the test set-up.

2.5 ELECTRIC CHARACTERISTICS FOR THE CONVECTED BALANCED ARC IN A SUPERSONIC STREAM

The electric field strength E (or voltage gradient) of the column was determined by measuring the potential across the electrodes at gaps of 1.0 and 0.6 in. Suits reported in Ref. 40 that determining the E field by changing the gap from run to run is very difficult. Therefore, great care and patience was taken in making the voltage and current measurements. The arcs were required to be very steady with very little voltage fluctuation (the voltage trace was required to resemble that of Fig. 3). The photographs of each run were required to show that the arc configurations were comparable. After much effort, a set of consistent data was obtained and the resulting E versus current (characteristic curve) is shown in Fig. 9. An interesting feature of the characteristic curves for convected balanced arcs is the flat portion starting at about 250 amps. This flat portion begins at 50 to 100 amps for free-burning arcs as shown in Appendix D and by King (Ref. 57). The free-burning arc characteristic for $P_\infty = 14.5$ mm Hg is shown in Fig. 9 for comparison with the Mach 3.0 curve.

2.6 EFFECTIVE TEMPERATURES

Effective temperatures T_σ for the balanced convected arcs were determined by first calculating a mean electrical conductivity

$$\bar{\sigma} = \frac{I}{\left(\frac{\pi}{4} d_T d_s\right) E} \tag{2-1}$$

and then using Ref. 47 to provide $T_\sigma = f(\bar{\sigma}, P_\infty)$. These temperatures are shown in Fig. 11. The quantity determined is an effective temperature which, were it constant across the section of the arc, would provide the proper constant electron density for the observed electric gradient. This effective temperature is not the peak temperature of the convected balanced arc. It is, however, a temperature that characterizes the behavior of the arc.

The interesting observation from Fig. 11 is that the effective temperatures for a given M_∞ are nearly constant over the current range of 250 to 600 amps. Free-burning and convected arcs are able to increase their cross-sectional area to accommodate increases in current, thereby maintaining a fairly constant mean current density. Suits (Ref. 42) observed that this mean current density for free burning arcs in air, nitrogen and hydrogen was nearly constant over a great range of current. If E were fairly constant, as indicated in Fig. 9, the effective temperature would be constant for varying current and constant P_∞.

2.7 ENERGY TRANSFER FROM THE ARC

In the uniform column of the convected balanced arc, the input power gradient is balanced by two-dimensional radiation, forced convection and mass transfer at the boundary. It is useful to examine these mechanisms of energy transfer to determine which ones are dominant.

Because of the low pressures used in this investigation, the radiation corresponding to the temperatures of Fig. 11 is negligible compared to the power input gradient of the convected balanced arc column. Harvey (Ref. 31, p. 45) estimated the ratio of power radiated to joule heating to be 10^{-3} for a 300 amp convected balanced arc at $M_\infty = 2.5$.

An estimate of the energy transfer across the arc boundary by mass transfer can be made as follows:

Q_{MT} = energy transfer across boundary by mass transfer

$= 2\pi r_b \rho h u_b$ watt/cm

We assume a boundary temperature T_b of 6000°K and consider the following typical values:

$P_\infty = 14.5$ mm Hg

$E = 18$ volt/in. $= 7.1$ volt/cm

$I = 300$ amp

$Q_{input} = 5400$ watt/in. $= 2130$ watt/cm

$r_b = 0.5$ cm

$h = 29,600$ watt-sec/gm (Ref. 49)

$\rho = 6.14 \times 10^{-7}$ gm/cm^3

The value of the radial velocity u_b at the boundary in order for $Q_{MT} = 0.1\ Q_{input}$ is 3730 cm/sec or 121 ft/sec. This value of u_b would require extremely large axial velocities. Harvey (Ref. 31) observed flow velocities along the column of about 35 ft/sec. Thus the required radial velocities for Q_{MT} to be 10% of the input energy are unrealistic. The energy transfer across the boundary by mass transfer can therefore be considered negligible compared to the joule heating. Estimates made of Q_{MT} using Roman's experimental data (Ref. 19) indicate that the neglect of Q_{MT} is equally valid for high current arcs at one atmosphere.

Thus, we can assume that the primary energy transfer mechanism balancing the input power will be forced convection at the arc boundary.

2.8 CHARACTERISTICS OF FREE-BURNING ARCS

The free-burning arc can be considered as the limiting case of a convected balanced arc as $u_{\infty_n} \rightarrow 0$. The transition from a free-burning arc to a convected balanced arc was considered (discussed in Section IV) and it was of interest to know the E-I curve for high current, low pressure free-burning arcs.

For this reason an experimental investigation of free-burning arcs in air at pressures of 1.0 to .0191 atm* and currents of 190 to

*P_∞ = .0191 atm is 14.5 mm Hg and is the same free stream static pressure for the M_∞ = 3.0 runs.

400 amps was carried out and is discussed in detail in Appendix D. The interesting observation to note here is that the characteristic curves are flat over this pressure and current range. The curve for $P_\infty = .0191$ is shown in Fig. 9. Also, at this lowest pressure the arc was natural convection stabilized for column lengths greater than 2.0 in.

TABLE I. RANGE OF EXPERIMENTAL CONDITIONS

Item	$M_\infty = 2.5$	$M_\infty = 3.0$	$M_\infty = 3.5$
Average free stream temperature, T_∞, ^oK	126	101	84
Free stream pressure, P_∞, mm Hg	19.3	14.5	9.6
Average value of magnetic field, gauss	1730	1430	1100
Current range, amps	175-500	175-500	175-500
Slant angle range, degrees	22-27	17 1/2-24	16-21
Range of free stream normal velocities, fps	705-845	642-800	615-745
Free stream velocity, fps	1840	1970	2110
Range of free-stream normal Reynold's number		See Figure 22	
Range of Lorentz number		See Figure 22	

Note: All values are for the reference station defined in Section 2.3.

III. THEORY OF CONVECTED BALANCED ARCS

3.1 PHYSICAL MODEL

The convected balanced arc is defined here as a vertical D. C. electric arc immersed in a moving fluid and an external magnetic field. The moving fluid and magnetic field are at right angles to each other such that the Lorentz force ($\vec{j} \times \vec{B}$) on the arc balances the momentum loss of the fluid (fluid dynamic drag) as it flows around the arc. Experimentally this is the problem considered by Bond (Ref. 17), Myers et al (Ref. 18), Roman (Ref. 19), and Harvey (Ref. 31). Malliaris (Ref. 26), Bond and Potillo (Ref. 21) and many others have considered the moving convected arc where the transverse magnetic field accelerates or retards the motion of the arc through the fluid.

Experimentally it is observed that the arc is impervious to the external flow, that is, that there is no flow through the arc. The external flow interacts with the periphery of the arc and probably "strips off" heated fluid from the arc boundary, but there is a region of the arc, interior to this interaction layer, where the external flow does not penetrate and which remains as an entity. This interior region is denoted as the arc core.

This impervious body behavior has been observed by several investigators. Kuethe et al. (Ref. 29 and 30) and Harvey (Ref. 31) observed and measured flow along the arc column of a balanced convected arc in a supersonic stream. Harvey introduced magnesium particles into the column at the anode and was able to follow their trajectory up the column. The presence of the jet interaction region shown in Fig. 3 and discussed in Section 2. 3 is further evidence that there is an axial flow along the column. If the external stream flowed through the arc column the axial flow could not exist. Thus its presence indicates a region of the arc column which is impervious to the external stream.

Roman in Ref. 19 studied the wake behind a convected balanced arc in a low speed flow and concluded that the arc was "similar"*to a heated solid cylinder. He observed a flow separation at about 90^{o} from the stagnation point and a very well defined wake formation. The region behind the arc was stagnant. The arc wake was about twice as wide as the wake from a solid cylinder having a diameter comparable to the transverse luminous dimension of the arc. These observations can not be consistent with the concept of a flow-through arc.

---

*The use of the term "similar" here and elsewhere in the thesis does not imply fluid dynamic similarity, but rather it is used in the sense that a convected balanced arc and a heated solid cylinder have certain features in common such as a boundary layer, flow separation and a wake.

Based upon the impervious body behavior the following physical model, shown in Fig. 14, will be used to study the plasma column of the convected balanced arc:

(1) Arc core or interior region

a. The gas is a high temperature conducting fluid. Generally the degree of ionization for arcs is less than 10% (i. e. weakly ionized).

b. The column is steady and uniform.

c. The arc configuration is such that buoyancy forces are small compared to the Lorentz force in the cross-section.

d. Electrons, ions and neutral particles are in equilibrium at the same temperature T. This is an assumption which will be valid provided the electric field is not too strong (i. e. drift speed of electrons $\ll$ mean thermal speed of electrons) and the gas pressure is not too low. This is the thermal arc assumption mentioned in Section 1. 3 and as before there is not a clearly defined pressure above which the arc is thermal (Ref. 4). This assumption will permit the use of continuum fluid ideas, i. e. the MHD approach.

e. The arc shape is not necessarily circular. From experiment (Fig. 8) we observe that this is indeed the case.

f. The self magnetic field is negligible compared to the external uniform field (Ref. 20, p. 25).

(2) Free stream or exterior region

a. The gas is a cold non-conducting fluid at ambient flow conditions.

b. The gas is a continuum fluid and the flow is steady and uniform.

(3) Interaction region or boundary layer

a. This is the flow region between the free stream and the arc core. The transition from the velocity and temperature field at the boundary of the arc core to free stream conditions takes place over this region. This region is not necessarily thin everywhere as observed by Roman on the wake formation of arcs and solid cylinders of comparable dimensions.

b. The gas in this region is a steady continuum fluid.

The physical model consists of three distinct and separate regions: the arc core, the interaction region and the free stream. The free stream influences the arc core by boundary conditions applied through the boundary layer. The important point is that we can independently consider the flow in the arc core and represent the influence of the surroundings by appropriate boundary conditions. These surroundings might be a cross flow or a tube wall. Thus the problem of an arc burning in a tube with a transverse magnetic field is much the same as the convected balanced arc, except of course, for different boundary conditions.

It is misleading to label a convected balanced arc as "similar" to a heated solid cylinder in a cross flow. The two are similar only in the respect that they are impervious to the free stream and hence the free stream must flow around the arc or cylinder and suffer a momentum loss, which is reflected as a drag force on the cylinder or arc. Thus the convected balanced arc and the heated solid cylinder have similar velocity and temperature fields at the outer edge of their boundary layers. If the two had similar flow separation points* one would expect their pressure drag coefficients to be similar.

Velocity and temperature conditions, however, at the arc boundary (inner edge of the boundary layer) and the solid cylinder surface are very much different, implying that forced convection heat transfer coefficients would also be different. Therefore the application of forced convection heat transfer ideas (see Appendix B) to convected balanced arcs would be valid, but the use of heated cylinder experimental results (i.e. Hilpert's curve, Fig. B-1) would not.

The boundary layer is a complicated interaction region. Here the cold external stream penetrates into the arc periphery as far as it can against the increasing Lorentz force of the arc fluid elements. This region will probably be characterized by large velocity and temperature gradients.

---

*Roman (Ref. 19) has shown that balanced convected arcs in low speed flow have flow separation points and wake formations similar to subcritical heated cylinders.

3.2 GOVERNING EQUATIONS FOR FLOW INSIDE ARC CORE

Here we consider the general formulation of the governing equations for the balanced convected arc. Because of the physical model selected we need only to consider the flow inside the arc core. Then by appropriate boundary conditions we include the influence of the external flow and complete the statement of the problem. The simultaneous set of governing equations can be solved by numerical integration on a high speed computer, but the specification of boundary conditions that realistically represent the actual problem is indeed difficult. The primary difficulty is the delineation of the boundary layer. The question of boundary conditions will be delayed until later in this section.

The equations governing the conducting continuum fluid inside the arc core are the usual MHD equations (see, for example, Ref. 25, p. 295). Assuming steady, two-dimensional flow and the flow arrangement of Fig. 14, the formulation of the governing equations is as follows:

Conservation of Mass:

$$\frac{\partial}{\partial x}(\rho u) + \frac{\partial}{\partial y}(\rho v) = \epsilon \qquad (3\text{-}1)$$

where ϵ = source strength term (mass drawn per second from the axial flow to balance the mass transfer to the boundary).

Conservation of Momentum:

$$u\frac{\partial u}{\partial x} + v\frac{\partial u}{\partial y} = -\frac{1}{\rho}\frac{\partial P}{\partial x} + \frac{1}{\rho} j B_y + \frac{1}{\rho}\rho_e E + \frac{1}{\rho}\left[\frac{\partial \tau_{xx}}{\partial x} + \frac{\partial \tau_{xy}}{\partial y}\right] \tag{3-2}$$

$$u\frac{\partial v}{\partial x} + v\frac{\partial v}{\partial y} = -\frac{1}{\rho}\frac{\partial P}{\partial y} + \frac{1}{\rho}\left[\frac{\partial \tau_{yx}}{\partial x} + \frac{\partial \tau_{yy}}{\partial y}\right] \tag{3-3}$$

where τ_{ij} = stress tensor (see Ref. 25)

ρ_e = net free charge density = $\sum_s n_s e Z_s$, and

Z_s = charge number of particle ($Z_s = -1$ for electrons). This term is usually small in a plasma owing to the tendency for quasineutrality. Thus the term will be neglected (Ref. 25, p. 115).

Conservation of Energy:

$$\rho u\frac{\partial h}{\partial x} + \rho v\frac{\partial h}{\partial y} = \vec{V}\cdot\nabla P + \text{div}\,(k\nabla T) + \sigma E^2 + \Phi + Q_R + Q_{MT} \tag{3-4}$$

where Φ = viscous dissipation = $\tau_{ij}\,(\partial u_j/\partial x_i)$

Q_R = energy transfer by radiation, $Q_R(P, T)$ watts/(volume) (3-5)

Q_{MT} = energy transfer by mass transfer to the boundary, $Q_{MT}(\epsilon, T)$

Caloric Equation:

$$h = \int_{T_b}^{T} C_p\, dT', \text{ static enthalpy of fluid element} \tag{3-6}$$

Equation of State:

$$P = Z\rho RT \tag{3-7}$$

where Z = compressibility factor, Z(P, T). (3-8)

Heat Flux Potential:

The heat flux potential ϕ is defined as

$$\phi = \int_0^T k dT' \quad , \quad \text{thus div } (k\nabla T) = \nabla^2\phi \tag{3-9}$$

Ohms Law:

The general Ohms law, neglecting ion slip, pressure diffusion and currents due to curvature and gradients of the magnetic field lines (see Appendix C) can be expressed as:

$$\vec{j} = \frac{\sigma}{1 + (\omega_e\tau_e)^2}\left[\vec{E} + \vec{V} \times \vec{B} - \omega_e\tau_e\,(\vec{E} + \vec{V} \times \vec{B}) \times (\vec{B}/B)\right] \tag{3-10a}$$

where $\omega_e = (Be/m_e)$, electron cyclotron frequency

τ_e = electron-neutral collision time, Ref. 24

$\omega_e\tau_e$ = Hall parameter, number of gyrations (in radians) about the field lines that an electron makes between collisions

$$\sigma = (n_e e^2 \tau_e/m_e), \text{ electrical conductivity} \tag{3-11}$$

The last term in Eq. (3-10a) is the Hall current. It is shown in Appendix C that for arcs the Hall current is zero. Thus the Ohms law becomes:

$$\vec{j} = \sigma (\vec{E} + \vec{V} \times \vec{B}) \qquad (3\text{-}10b)$$

Maxwell's Equations:

We assume that the fields are fairly steady such that $\partial\vec{E}/\partial t$ and $\partial\vec{B}/\partial t$ are very small. Thus we can neglect the displacement current compared to the conduction current and the induced EMF compared to the applied electric field. We have already assumed that the self magnetic field is small compared to the externally applied uniform field.

Essentially we are assuming that the induced fields are small compared to the applied fields and hence the fluid dynamic equations are uncoupled from Maxwell's equations.

Physical and Transport Properties:

These properties are estimated from a blend of kinetic theory and experiment (see, for example, Ref. 34 and 35).

$$\mu = \mu(P, T) \qquad (3\text{-}12)$$

Note: μ is sometimes considered constant since its variation is small compared with φ and h.

$$k = k(P, T) \qquad (3\text{-}13)$$

$$C_p = C_p(P, T) \qquad (3\text{-}14)$$

$$Q_R = Q_R(P, T) \qquad (3\text{-}5)$$

$$\sigma = \sigma(P, T) \qquad (3\text{-}11)$$

Our unknowns are $\rho, u, v, P, T, \vec{j}$, and ϵ. We observe that we have a set of six simultaneous equations to solve for the seven unknowns. The unknown precluding completeness is the source term ϵ and its associated mass transfer energy term Q_{MT}. The source term ϵ represents the mass drawn per second from the axial flow to balance the mass transfer to the boundary. In the general three-dimensional problem, this ϵ is accounted for by the axial mass flow and the problem is specified completely. It seems wise at this point to consider the simpler problem obtained when ϵ and Q_{MT} are set equal to zero. A great deal more must be learned about the simpler problem before realistic assessment of ϵ and Q_{MT} can be made. Thus the above formulation with ϵ and Q_{MT} equal to zero, along with appropriate boundary conditions, is sufficient to specify the problem of the balanced convected arc. From the discussion in Section 2.7, the assumption of $Q_{MT} = 0$ is reasonable.

3.3 SIMILARITY PARAMETERS

We choose to non-dimensionalize the governing equations by considering certain reference or characteristic quantities. The basic reference quantity is the temperature T_1. This reference temperature must be some temperature that characterizes the problem, i.e. the peak temperature, mean temperature, effective temperature, etc.

Since the arc is a gaseous cloud and cannot support large pressure gradients, the internal pressure will not be much different from the free stream static pressure. Thus the reference pressure can be P_∞.

A characteristic dimension would be the streamwise dimension of the arc boundary or of a particular isotherm. The latter will be more meaningful since this dimension can be obtained from photographs. Other characteristic dimensions such as a viscous length or the length used by Han and Kihara (Ref. 36) are appropriate and depend upon the initial information of the problem.

Our search for a reference velocity which characterizes the internal flow of the arc core is aided by the analogy with the natural convection problem (see Appendix A). We can determine a reference velocity u_1 from the effective kinetic energy increase of a fluid element due to the work done by the Lorentz force over the distance d. Once u_1 is defined in this manner we observe experimentally that u_1/u_∞ is constant over a wide range of conditions (Ref. 31). The reason for this is discussed in Section 4. 4.

Our reference quantities will be denoted by the subscript 1 and are determined at the reference temperature and pressure T_1 and P_1. The reference quantities are

$$T_1,\ P_1,\ d_1,\ k_1,\ C_{p_1},\ \mu_1,\ \rho_1,\ \sigma_1,\ h_1,\ \phi_1$$

J_1 = reference current density = $\sigma_1 E$

u_1 = reference velocity = $\sqrt{J_1 Bd_1/\rho_1}$

Because of the analogy between the buoyancy force in the problem of natural convection in a horizontal tube and the Lorentz force in the convected balanced arc problem, it follows that a parameter analogous to the Grashoff number will be important in our problem.

We replace the buoyancy force in the Grashoff number (Eq. (A-1) in Appendix A) by the Lorentz force and obtain a parameter called the Lorentz number.

$$L_c = \text{Lorentz number} = (\rho_1 J_1 Bd_1^{\,3}/\mu_1^{\,2})$$

The Lorentz number indicates the ratio between the Lorentz force and viscous force on a fluid element.

We can form an interior Reynolds number $Re_1 = (\rho_1 u_1 d_1/\mu_1)$ and show that $Re_1 = \sqrt{L_c}$.

The nondimensional quantities are:

$$j' = \frac{j}{J_1}\ ,\quad u' = \frac{\vec{V}}{u_1}\ ,\quad P' = \frac{P}{P_1}\ ,\quad \phi' = \frac{\phi}{\phi_1}$$

$$\rho' = \frac{\rho}{\rho_1}\ ,\quad x' = \frac{x}{d_1}\ ,\quad y' = \frac{y}{d_1}\ ,\quad T' = \frac{T}{T_1}\ ,\quad h' = \frac{h}{h_1}$$

The non-dimensional governing equations for steady, two dimensional flow (neglecting mass transfer and radiation, assuming μ constant and discarding the prime notation) are as follows:

$$\text{div}\,(\rho\vec{u}) = 0 \tag{3-17}$$

$$\rho(\vec{u}\cdot\nabla)\,\vec{u} = -\nabla P + j\,\vec{e}_x + \frac{1}{Re_1}\nabla^2\vec{u} + \frac{1}{3Re_1}\nabla(\nabla\cdot\vec{u}) \tag{3-18}$$

$$\rho\vec{u}\cdot\nabla h = K_1\,\vec{u}\cdot\nabla P + \frac{1}{Pr_1\,Re_1}\nabla^2\phi + K_{JH}\,j + \frac{K_1}{Re_1}\Phi \tag{3-19}$$

where $K_1 = (u_1^2/h_1)$, Eckert number (3-20)

Φ = viscous dissipation

$$Pr_1 = (\mu_1 h_1/\phi_1) = \mu \int_0^{T_1} C_p dT' \Big/ \int_0^{T_1} k dT' \ ,$$

Prandtl number

$$Re_1 = \rho_1 u_1 d_1/\mu_1 = \sqrt{L_c}$$

$K_{JH} = J_1 E d_1/\rho_1 u_1 h_1$, the ratio of joule heating to energy transfer by convection (3-21a)

We can express K_{JH} as follows:

$$K_{JH} = \frac{EI_1/\phi_1}{Pr_1\sqrt{L_c}} \tag{3-21b}$$

where $I_1 = J_1 d_1^2 = \sigma_1 E d_1^2$, reference current and $P_L = EI_1/\phi_1$ is termed the power gradient parameter and expresses the ratio of joule heating to energy transfer by conduction.

Thus the governing similarity parameters for the motion in the arc core appear to be the Lorentz number (L_c), the Prandtl number (Pr_1), the Eckert number (K_1), and the power gradient parameter ($P_L = EI_1/\phi_1$). Note that in the power gradient parameter either E or I is known initially and the other is determined from Ohm's law using the electrical conductivity σ_1 evaluated at T_1 and the reference dimension d_1. Thus the power gradient parameter P_L is expressed either as

$$P_L = \frac{E(\sigma_1 E d_1^2)}{\int_0^{T_1} k dT} = \frac{EI_1}{\phi_1}$$

or

$$P_L = \frac{I^2/\sigma_1 d_1^2}{\phi_1} = \frac{E_1 I}{\phi_1}$$

3.4 POWER GRADIENT RELATION

It is now useful to examine the governing equations for the case of large and small Lorentz number.

Case I: Small Lorentz number, $\sqrt{L_c} \ll 1$

This is the case of vanishingly small free stream velocity or the free-burning arc. Here there is no fluid dynamic drag force for the Lorentz force to balance so that $B \to 0$.

Thus:

$$u_\infty \to 0$$

$$B \to 0 \qquad \text{and} \qquad \sqrt{L_c} = Re_1 \to 0$$

$$K_1 \to 0 \qquad \text{such that} \quad K_1/Re_1 \to 0$$

The fluid is stagnant in the arc core so that the continuity and momentum equations cease to govern the motion. The energy equation (3-19) becomes

$$\frac{EI_1}{\phi_1} j = \nabla^2 \phi$$

or dimensionally

$$\sigma E^2 = \nabla \cdot (k \nabla T) \tag{3-22a}$$

the Elenbaas-Heller equation. The arc is conduction dominated and the governing similarity parameter is EI_1/ϕ_1, with L_c not appearing in the problem.

Case II: Large Lorentz number

This is the case of a large B due to a large free stream dynamic pressure. We assume here that $Pr_1 = O(1)$ and that $K_1 \leq O(1) \ll \sqrt{L_c}$.

As L_c becomes large we observe that the heat conduction and viscous dissipation terms become negligible in the energy equation. Also, there must be some functional dependence of EI_1/ϕ_1 on $\sqrt{L_c}$, otherwise the joule heating term is negligible compared to the convection term. Since joule heating must be a significant term in our problem we consider for large L_c that

$$EI_1/\phi_1 = \beta (L_c)^n$$

where β is a constant coefficient and n a real exponent. We examine the three cases of $n < (1/2)$, $n > (1/2)$, and $n = (1/2)$ in Eq. (3-19).

$n < (1/2)$:

Here joule heating is small compared to convection for large L_c. For this case the governing equations reduce to an inviscid set identical with the natural convection problem for large Gr in Appendix A.

$n > (1/2)$:

Here the convection would be negligible compared to the joule heating term and the energy equation would be balanced only for $\vec{j} = 0$. This is the non-conducting fluid case and is not of interest here.

$n = (1/2)$:

Here the joule heating and convection would be of the same magnitude and the non-dimensional energy equation for large L_c would be:

$$\frac{DH}{Dt} = \frac{\beta}{Pr} j$$

where H = nondimensional total enthalpy per mass.

The only realistic value for n is (1/2). Therefore, for large L_c we must have

$$\frac{EI_1}{\phi_1} = \beta\sqrt{L_c}$$

This is not consistent, however, with the small L_c case, where joule heating must also remain in the problem. Thus the general form of the power gradient relation is expressed by

$$EI_1/\phi_1 = f(L_c)$$

At this point we do not know the functional form for f, however we do know the behavior of f at limiting values of L_c:

$$\frac{EI_1}{\phi_1} = \begin{cases} \alpha & \text{as} \quad L_c \ll 1 \\ \beta\sqrt{L_c} & \text{as} \quad L_c \gg 1 \end{cases} \tag{3-23}$$

where α and β are constant coefficients determined by the imposed conditions.

Essentially the governing parameter for $L_c \gg 1$ is

$$K_{JH} = \frac{EI_1/\phi_1}{Pr_1\sqrt{L_c}} = \frac{J_1 E d_1}{\rho_1 u_1 h_1}$$

which is the ratio of joule heating to energy transfer by convection. As $L_c \to \infty$ we must have $K_{JH} = (\beta/Pr) \approx \beta = O(1)$ since the coefficient of the energy equation convection term (LHS of equation (3-19)) is O(1). Equation (3-23) is a statement of the fact that

(a) for $L_c \ll 1$, the joule heating is balanced by conduction;

(b) for intermediate L_c, the joule heating is balanced by conduction and convection; and

(c) for $L_c \gg 1$, the joule heating is balanced entirely by convection.

As before, values for α and β are not known, nor the magnitude of L_c when L_c is "large." it appears that Eq. (3-23) indicates the transition from a free-burning arc to a highly convected arc.

3.5 SIMPLIFIED MODEL

Here we consider the general steady two-dimensional equations with the following simplifications:

(1) Incompressible

(2) Electrical conductivity σ can be approximated by $\sigma = C(T - T_s)$, where C = constant coefficient and T_s is the temperature where $\sigma(P, T) \approx 0$. For air this is approximately $5000^{\circ}K$ and the linear approximation is fairly good up to about $15000^{\circ}K$.

(3) The Mach number of the interior flow is small such that $M^2 \ll 1$. Another way of saying this is that the kinetic energy of a fluid element is small compared to its internal energy, i.e.:

$$\int_{T_o}^{T} C_p \, dT' + \frac{1}{2} u^2 \approx \int_{T_o}^{T} C_p \, dT' = h = \text{static enthalpy/mass}$$

(4) The temperature of the arc is low enough so that energy transfer by radiation can be neglected.

(5) C_p, μ, and k (or at least μ and C_p/k) are constant such that Pr ≈ constant.

Now we let

$$\Delta T = T_o - T_s$$

$$\Theta = (T_o - T)/\Delta T$$

$$T(r, \theta) = T_o - \Delta T\, \Theta(r, \theta)$$

where the subscripts o and s denote conditions at the origin and boundary respectively. Thus

$$\sigma = C(T - T_s) = C\Delta T(1 - \Theta)$$

$$\vec{j} = C\Delta T(1 - \Theta)\, \vec{E}$$

$$\vec{j} \times \vec{B} = - j B \vec{e}_x$$

The characteristic quantities are:

$T_1 = T_o$ reference temperature is temperature at the origin

$$P_1 = \rho_1 u_1^2$$

$$J_1 = \sigma_1 E = C\Delta T E$$

$$u_1 = \sqrt{J_1 B d_1/\rho_1}$$

$$d_1 = 2r_s$$

The non-dimensional quantities are:

$$T' = T/T_1 \quad , \quad u' = u/u_1 \quad , \quad \rho' = \rho/\rho_1 \quad , \quad j = j/J_1$$

$$r' = r/d_1 \quad , \quad P' = P/P_1 \quad , \quad \text{etc.}$$

The non-dimensional equations are (discarding the prime notation):

$$\operatorname{div} \vec{u} = 0 \tag{3-24a}$$

$$(\vec{u} \cdot \nabla)\, \vec{u} = -\nabla P - (1 - \Theta)\, \vec{e}_x + \frac{1}{\sqrt{L_c}} \nabla^2 \vec{u} \tag{3-24b}$$

$$-(u \cdot \nabla\Theta) = K_1 (u \cdot \nabla P) - \frac{1}{Pr_1 \sqrt{L_c}} \nabla^2 \Theta$$

$$+ K_{JH} (1 - \Theta) + \frac{K_1}{\sqrt{L_c}} \Phi \tag{3-24c}$$

where

$$L_c = (\rho_1 J_1 B d_1^{\,3})/\mu_1^{\,2}$$

$$K_{JH} = E J_1 d_1/\rho_1 C_{p_1} T_1 u_1 = (E I_1/k_1 T_1)/Pr_1 \sqrt{L_c}$$

$$I_1 = J_1 d_1^{\,2}$$

$$K_1 = u_1^{\,2}/C_{p_1} T_1 \approx M_1^{\,2} \ll 1$$

$$Pr_1 = \mu_1 C_{p_1}/k_1 = O(1)$$

$$Re_1 = \rho_1 u_1 d_1/\mu_1 = \sqrt{L_c}$$

As a consequence of Eq. (3-24a) we can introduce the non-dimensional stream function $\psi(r, \theta)$ as

$$u_r = \frac{1}{r}\frac{\partial \psi}{\partial \theta} \quad , \quad u_\theta = -\frac{\partial \psi}{\partial r} \tag{3-25}$$

where r is the non-dimensional radius vector with respect to d_1.

We can rewrite the momentum equation, by taking the curl of Eq. (3-24b) as:

$$\frac{1}{r}\left(\frac{\partial \psi}{\partial r}\frac{\partial}{\partial \theta} - \frac{\partial \psi}{\partial \theta}\frac{\partial}{\partial r}\right)\nabla^2 \psi = -\left(\sin\theta \frac{\partial \Theta}{\partial r} + \frac{\cos\theta}{r}\frac{\partial \Theta}{\partial \theta}\right) + \frac{1}{\sqrt{L_c}}\nabla^4 \psi \tag{3-26}$$

Now we consider the case for large L_c. Using the form of the power gradient relation developed in the last section, our non-dimensional equations governing the flow for our simplified model are:

$$\frac{1}{r}\left(\frac{\partial \psi}{\partial r}\frac{\partial}{\partial \theta} - \frac{\partial \psi}{\partial \theta}\frac{\partial}{\partial r}\right)\nabla^2 \psi = -\left(\sin\theta \frac{\partial \Theta}{\partial r} + \frac{\cos\theta}{r}\frac{\partial \Theta}{\partial \theta}\right) \tag{3-27}$$

$$\frac{\partial \psi}{\partial r}\frac{\partial \Theta}{\partial \theta} - \frac{\partial \psi}{\partial \theta}\frac{\partial \Theta}{\partial r} = -\frac{\beta}{Pr_1}(1 - \Theta) \tag{3-28}$$

We observe that the convected balanced arc is convection dominated for large L_c whereas the small L_c case was conduction dominated. These equations are very similar to the equations governing the natural convection of heat in a horizontal tube for large Gr (the difference in the sine and cosine terms in the body force term of

Eq. (3-27) and (A-10) is due to the angle θ being referenced differently in the two problems). The difference between the two problems is the joule heating term in the case of the convected balanced arc whereby a fluid element is continually heated.

For large L_c our problem is of the boundary layer type since the terms of highest order in the momentum and energy equations are negligible in the interior region of the arc core where the gradients are small. If we reduce the order of our set of differential equations we must give up some boundary conditions. These lost boundary conditions are the conditions at r = 1 and thus our Eq. (3-27) and (3-28) are valid only in the interior of the arc. It is clear that the boundary layer (region at r = 1 where the gradients are large) must become thinner as L_c gets large since the gradients must steepen.

We point out that the boundary layer of interest here is not the interaction region outside the arc core mentioned in Section 3.1, but rather the boundary layer interior to the arc boundary and influenced solely by the interior Reynold s number Re_1. We will discuss later, however, the connection between Re_1 and the free stream Reynold's number Re_∞.

Physically, the Lorentz force on a fluid element inside the arc core is balanced by the inertial force and the joule heating is balanced by the convection. Since heat conduction is negligible in the core

(for large L_c) a fluid element which is continually heated by the joule heating is convected along a closed streamline and there is no mechanism for the heat to be transferred across to another streamline. Hence a fluid element on an interior streamline, i.e. $\psi = 2$ in Fig. 15, has no way of transferring its heat to the core boundary. This is inconsistent and the streamline pattern of Fig. 15 must not be appropriate.

If we hold to the requirement of closed streamlines (i.e. div $\vec{u} = 0$) we can remove this inconsistency by considering the more realistic streamline pattern shown in Fig. 16. Here the streamlines crowd together near the boundary layer in the forward portion of the arc. As the streamlines crowd together, the temperature and velocity gradients can become large enough such that heat conduction and viscous dissipation are again significant and heat is transferred to the boundary and out of the arc. Since all closed streamlines of the arc core will pass through these regions of large gradients, an equilibrium can be established whereby the heat input (joule heating) to the interior is convected and then conducted to the arc boundary. The streamline pattern of Fig. 16 indicates a shift in the peak temperature region from the arc origin or centerline to the forward portions of the arc. This temperature shift was observed in numerical computations by Fischer and Uhlenbusch (Ref. 39) and Harvey (Ref. 31) and will be discussed in Section V.

Another way of removing the heat from the arc core without the mechanism of heat conduction in the interior is to assume that there is mass transfer at the arc boundary. Here we would consider an axial flow or source flow (div $\vec{u} = \epsilon$) to balance the mass lost at the boundary. In this case there would not be a stream function ψ and the streamlines would not be closed, but rather would appear as in Fig. 17.

Physically, the most satisfying flow pattern would be a combination of Fig. 16 and 17, where there would be mass transfer at the boundary and the fluid element path lines would crowd together in the forward portion of the arc. The argument for this is that experimentally an axial flow is observed and the external flow appears to be stripping off the outer portions of the arc boundary. Also, theoretically and experimentally we observe this shifting of the peak temperature region from the arc centerline to the forward portion of the arc.

3.6 BOUNDARY CONDITIONS

Wall Stabilized (B = 0)

For the steady electric arc burning in a vertical tube without an externally applied magnetic field, the governing equation is the Elenbaas-Heller equation

$$\sigma E^2 = - \nabla \cdot (k \nabla T) + Q_R \qquad (3\text{-}22b)$$

If the temperature at the boundary is uniform, the solution T(r) is axially symmetric. It is also necessary for the tube to be vertical for the solution to be symmetric. A horizontal tube would result in a non-symmetric distribution due to the natural convection currents that would be generated by the buoyancy forces.

The solution to Eq. (3-22b) is made unique with the two boundary conditions:

$$\begin{aligned} T(r) &= T_w \quad \text{at} \quad r = R_w \\ dT/dr &= 0 \quad \text{at} \quad r = 0 \end{aligned} \tag{3-29}$$

This condition at r = 0 comes from the symmetry of the problem and is equivalent to the requirement that the temperature be finite at r = 0. If the temperature at r = 0 is specified (or equivalently the total current is specified) then the electric field E is determined. However, since I is not a single valued function of E, due to the falling and rising branch of the characteristic curve (see Fig. 25), the specifying of E leaves the problem indeterminate (Ref. 9).

Free-Burning (B = 0)

We assume first of all that convection is small in the interior of the free-burning arc (Ref. 56, 61, 62, and 63) and we solve for the temperature distribution out to the boundary r_b where convection (driven by the buoyancy forces) will be the primary mechanism for

removing heat from the arc. The governing equation in the interior is the Elenbaas-Heller equation:

$$\sigma E^2 = Q_R - \frac{1}{r}\frac{\partial}{\partial r}\left(rk\frac{\partial T}{\partial r}\right) \tag{3-22b}$$

The temperature distribution is still symmetric about the column axis, thus one boundary condition is $dT/dr = 0$ at $r = 0$. Since the interior of the free-burning arc is very much influenced by the external surroundings, a boundary condition at $r = r_b$ must be specified. Information about the capability of the surroundings to transfer heat across the arc boundary must be brought into the problem.

Integrating Eq. (3-22b) over r from 0 to r_b (the radius where some boundary temperature T_b exists) gives

$$2\pi E^2 \int_0^{r_b} \sigma r\, dr = U_R - 2\pi\, r_b\, k\left(\frac{dT}{dr}\right)_{r=r_b} \tag{3-30a}$$

where U_R = total energy transfer by radiation/unit length.

The conduction across the boundary can be expressed as

$$-2\pi\, r_b\, k\left(\frac{dT}{dr}\right)_{r=r_b} = 2\pi r_b\, h_{NC}\,(T_b - T_\infty)$$

where h_{NC} = natural convection heat transfer coefficient. We define (from Appendix B):

Nu_{NC} = Nusselt number for natural convection

$$h_{NC}\, r_b/k_f = f(Gr\ Pr)$$

where k_f = thermal conductivity evaluated at T_f

$T_f = (T_b + T_\infty)/2$, film temperature

T_b = boundary temperature at $r = r_b$

Because of the oscillatory behavior of thermal conductivity and specific heat, it is better to express $k_f(T_b - T_\infty)$ as $\phi_b = \int_{T_\infty}^{T_b} k\,dT$ and Prandtl number as $Pr = \mu \int_{T_\infty}^{T_b} C_p\, dT/\phi_b$.

The energy balance at the boundary, Eq. (3-30a), is rewritten as (using Ohm's law):

$$EI = U_R + 2\pi\, Nu_{NC}\, \phi_b \qquad (3\text{-}30b)$$

The values of Nu_{NC} would be derived from the experimental data of free-burning arcs in the manner carried out in Appendix D.

The problem would be solved by having available experimental information about Nu_{NC}. The values for E, P_∞, T_∞, and T_b would be specified initially. Then we would pick a value for r_b and solve for T(r) using Eq. (3-22b) with the boundary and auxiliary conditions:

$$\frac{dT}{dr} = 0 \quad \text{at} \quad r = 0$$

$$\left.\begin{aligned} T &= T_b \\ \left(\frac{dT}{dr}\right) &= -\frac{Nu_{NC}\, \phi_b}{k\,(T_b)\, r_b} \end{aligned}\right\} \text{at } r = r_b$$

Krinberg (Ref. 56) solves the free-burning arc problem using a scheme very similar to the one mentioned above. He uses the Nu_{NC} for vertical solid cylinders (Fig. B-2) which, as will be shown in Appendix D, underestimates the convection heat transfer from free-burning arcs.

Wall Stabilized ($B \neq 0$)

Let us consider the wall stabilized arc with a transverse magnetic field. The appropriate set of equations are equations (3-17), (3-18), and (3-19). The boundary of the arc coincides with the tube wall and is specified (and is usually taken as circular). The boundary conditions specified at the boundary $r = R_w$ are:

$$\left.\begin{aligned} &\rho(r, \theta) = \rho_w \\ &u_r(r, \theta) = \text{radial velocity} = 0 \\ &u_\theta(r, \theta) = \text{tangential velocity} = 0 \\ &T(r, \theta) = T_w \end{aligned}\right\} \quad \text{at } r = R_w \qquad (3\text{-}31)$$

Also u_r and u_θ are finite everywhere.

Since the temperature distribution is not radially symmetric due to the convection currents generated by the Lorentz force, we cannot use $dT/dr = 0$ at $r = 0$. Thus we require temperatures to be finite in the region and our conditions are complete.

The incompressible form of this problem was considered by Harvey (Ref. 31) and Fischer and Uhlenbusch (Ref. 39).

It is interesting to point out that the steady arc burning in a horizontal tube without a magnetic field would be a similar problem with identical boundary conditions as above. The governing equations would have the Lorentz force replaced by the buoyancy force and the Lorentz number would be replaced by the Grashoff number.

Balanced Convected Arc ($B \neq 0$)

Finally we consider the boundary conditions for the case which is the subject of this investigation, i.e. the balanced convected arc. The boundary is not known a priori and from experiment (Fig. 8) we observe that the boundary is non-circular (assumed to be elliptical). Thus there must be sufficient boundary conditions prescribed to determine not only the size but the shape as well. The temperature and velocity fields are not symmetric about the z axis but are symmetric about the xz plane (Fig. 14).

Since the arc is balanced the Lorentz force must balance the fluid dynamic drag force. The external fluid flows around the arc core which is simulating a solid body of some shape. The fluid undergoes a momentum loss as evidenced by the drag on the arc. Thus, for a given set of conditions, this drag force can be represented as a pressure distribution about the arc boundary. The integrated Lorentz force must balance this integrated pressure distribution, i.e.

$$BI = C_D\, q_\infty\, d_T \quad , \qquad \text{force/unit length} \tag{3-32}$$

where C_D is the effective drag coefficient of the arc based upon the transverse dimension.

Let $\Delta P = P_F - P_B$, difference in pressure between front and back along an arc slice in the x direction (see Fig. 18). Then

dF_o = incremental force due to pressure in x direction

$= \Delta P(y)\, ds \cos\theta' = \Delta P(y)\, dy$

where the arrangement is shown in Fig. 18.

Then

$$C_D\, q_\infty\, d_T = 2\int_0^{d_T/2} \Delta P\, dy = 2q_\infty \int_0^{d_T/2} \left(\frac{\Delta P}{q_\infty}\right) dy$$

and $(\Delta P/q_\infty)$ is the differential pressure coefficient.

Our force balance can be expressed as

$$2B \int_0^{d_T/2} \int_{-d_s/2}^{+d_s/2} j(x, y)\, dx\, dy = 2q_\infty \int_0^{d_T/2} \left(\frac{\Delta P}{q_\infty}\right) dy$$

$$\int_0^{d_T/2} \left[B \int_{-d_s/2}^{d_s/2} j(x, y)\, dx - q_\infty \left(\frac{\Delta P}{q_\infty}\right) \right] dy = 0$$

or

$$B \int_{-d_s/2}^{d_s/2} j(x,y)\, dx = q_\infty \left(\frac{\Delta P}{q_\infty}\right) \tag{3-33}$$

Equation (3-33) is the force balance requirement that must be satisfied at every y station in the arc core. The $(\Delta P/q_\infty)$ is a function of y, the shape of the arc boundary, and, very important, the assumed flow separation pattern. Equation (3-33) is the relation between the required value of the magnetic field B and the specified free stream conditions.

The energy balance is a statement of the fact that all the energy put into the arc cross-section (per second per unit length) by joule heating must be equal to the energy transported out of the arc core by radiation and forced convection at the boundary. The energy balance equation is the same as for the free-burning arc (Eq. (3-30)).

$$E^2 \int_{-d_s/2}^{d_s/2} \int_{-d_T/2}^{d_T/2} \sigma(x,y)\, dx\, dy$$

$$= \int_{-d_s/2}^{d_s/2} \int_{-d_T/2}^{d_T/2} Q_R\,(x,y)\, dx\, dy + \pi\, Nu_{FC}\, \phi_b \tag{3-34}$$

where Nu_{FC} = Nusselt number for forced convection, $f(Re_f)$, see Appendix B

d_{eff} = effective diameter, diameter of circular cylinder having the same surface area as the elliptical cylinder

$$\approx (d_T + d_s)/2 \text{ for shapes having } d_T/d_s < 2 \tag{3-35}$$

$$Re_f = \rho_f u_{\infty_n} d_{eff} / \mu_f \text{ , fluid Reynold s number} \tag{3-36}$$

and ρ_f and μ_f are density and viscosity evaluated at the film temperature $T_f = (T_b + T_\infty)/2$.

As mentioned earlier in this section, the Nu_{FC} for the convected balanced arc should be different than for heated solid cylinders in a cross flow.

The boundary conditions on the momentum equation would be that the normal velocity vanish (no mass transfer across the boundary) at the boundary and the tangential velocity u_θ is some fraction of the free stream velocity at the outer edge of the interaction region. Here we are assuming that u_θ will have a distribution influenced by the velocity in the free stream.

By the nature of the problem and associated boundary conditions (boundary not known initially) the method of solution would most likely be an iterative scheme. An initial boundary shape and size would be

guessed and the temperature and velocity fields determined. Equations (3-33) and (3-34) would then be used to check the initial boundary estimate for force and energy balance. The information from this check would be used to make subsequent estimates of the boundary location. With this scheme the temperature on the estimated boundary would probably be specified instead of the peak temperature T_{max}.

IV. DISCUSSION OF EXPERIMENTAL RESULTS AND COMPARISON WITH THEORY

4. 1 INTRODUCTION

The experimental results from the present investigation (Chapter II) and from Roman's work (Ref. 19) were used to test and extend the theory of Chapter III. It will be shown that the general behavior of the convected balanced arc is to follow the relation $EI \sim L_c$ at low L_c and to tend toward the relation $EI \sim \sqrt{L_c}$ for large L_c. Criteria for determining whether an L_c value is low or large is discussed. The variables which are controllable during an experiment and thus chosen as the independent variables are I, u_∞, P_∞, and T_∞. The functional forms for the dependent variables E, d_{eff} and B in terms of the independent variables are determined for the low and large L_c regions.

4. 2 OHM'S LAW FOR CONSTANT CHARACTERISTIC TEMPERATURE

For a constant free stream pressure P_∞ and temperature T_∞ the arc effective temperature T_σ is fairly constant with changing current (Ref. 41) and u_{∞_n}. This behavior of T_σ is shown in Fig. 11 for the present investigation (see also Section 2. 6). Also, assuming Roman's arc to be an argon arc burning in a 1 atm cross flow of air (Ref. 19, Appendix E) effective temperatures based on the luminous dimensions shown in Fig. 13a (and using Ref. 76 and 77) are about 13, 500°K and fairly constant over the current and

velocity range considered. This constant T_σ gives us a constant mean electrical conductivity, i. e.

$$\bar{\sigma} = \frac{8\pi}{\pi D^2} \int_0^{D/2} \sigma r \, dr \approx \text{constant for constant } P_\infty \text{ and } T_\infty$$

Thus Ohm's Law becomes

$$I = \left(\frac{\pi D^2}{4}\right) \bar{\sigma} \, E = C_2 D^2 E \tag{4-1}$$

where $D = d_{eff}$ (Eq. 3-35) and $C_2 = \pi \bar{\sigma}/4$ for constant P_∞ and T_∞.

The experimental measurements of this investigation for a constant M_∞, are in agreement with the above assumption. The effective temperatures (Fig. 11) are fairly constant for currents greater than 250 amperes, so that $\bar{\sigma}$ is constant. Also, as observed from Fig. 9, E is fairly constant for $I > 250$ amps. Thus, for this current range, Eq. (4-1) becomes for a given P_∞ and T_∞

$$D = \sqrt{\frac{I}{C_2 E}} = \text{constant} \sqrt{I} \tag{4-2}$$

The observed arc dimensions for constant M_∞ shown in Fig. 8 agree extremely well with Eq. (4-2).

Roman (Ref. 19) reports that his dimensions shown in Fig. 13a are linear with current. This is not the case because his dimensions (for a constant u_∞) plotted versus $\sqrt{I}$ lie on a straight line through the origin as shown on Fig. 13c.

4. 3 APPLICATION OF HEAT TRANSFER TO ARC COLUMN IN FORCED CONVECTION

As mentioned earlier we might expect the forced convection heat transfer approach of Appendix B to apply to balance convected arcs. The functional form of $Nu_{FC} = f(Re)$ would be determined from experimental information on balanced convected arcs.

Consider initially that energy transfer by radiation and mass transfer from the uniform column is negligible such that the forced convection heat transfer must equal the power gradient input of the arc. Thus using Eq. (3-34)

$$EI = \pi \; Nu_{FC} \; \phi_b \tag{4-3}$$

we shall assume that (from Eq. (B-3))

$$Nu_{FC} = f(Re_f) = \text{const } (Re_f)^n \tag{4-4}$$

where the fluid Reynolds number is

$$Re_f = \frac{\rho_f u_{\infty_n} D}{\mu_f} \tag{3-36}$$

and

$$D = d_{eff} \tag{3-35}$$

Hopefully the value for the exponent n can be determined from experimental results.

The effective temperature T_σ will be used for the characteristic or reference temperature T_1. Thus, the T_1 is constant for constant P_∞ and T_∞.

Let us again consider that P_∞ and T_∞ are constant and that Ohm's Law is given by Eq. (4-1). We assume that over the modest current range of 200 to 600 amperes the arc boundary temperature T_b is fairly constant such that ϕ_b , ρ_f and μ_f are constant. We can express the energy balance Eq. (4-3) as

$$EI = \text{const } u_{\infty_n}^n D^n \tag{4-5}$$

If we eliminate D between Eq. (4-1) and (4-5) we get

$$E = \text{const}' \; u_{\infty_n}^{2n/(n+2)} \; I^{(n-2)/(n+2)} \tag{4-6}$$

We want to use the experimental information that $dE/dI = 0$ over a portion of the characteristic curve. Thus

$$\frac{dE}{dI} = \frac{\partial E}{\partial I} + \frac{\partial E}{\partial u_{\infty_n}} \frac{d u_{\infty_n}}{dI} + \frac{\partial E}{\partial P_\infty} \frac{dP_\infty}{dI}$$

For Roman's data $d u_{\infty_n}/dI$ and dP_∞/dI are zero, thus $dE/dI = 0$ implies $\partial E/\partial I = 0$. For the present investigation, $dE/dI = 0$ for a constant M_∞ (Fig. 9) and $dP_\infty/dI = 0$ but $d u_{\infty_n}/dI > 0$ as observed on Fig. 7b. Although u_∞ is independent of I, u_{∞_n} is not since the arc slant is dependent upon I and this dependence is not known at present. Thus $\partial E/\partial I < 0$ and is not known. We will put aside the present data for the moment and proceed using Roman's data.

Taking the derivative of Eq. (4-6) with respect to I gives

$$\frac{dE}{dI} = \frac{\partial E}{\partial I} = \left(\frac{n-2}{n+2}\right) \text{const}'' \; u_{\infty_n}^{2n/(2+n)} \; I^{-4/(n+2)} \qquad (4\text{-}7)$$

For that portion of the characteristic curve (Fig. 13b) where $\partial E/\partial I = 0$, Eq. (4-7) indicates that we must have $n = 2$. Therefore

$$Nu_{FC} = C_3 (Re_f)^2 \qquad (4\text{-}8)$$

where C_3 would be an experimental constant, and

$$EI = C_3 \pi \left(\frac{\rho_f u_{\infty_n} D}{\mu_f}\right)^2 \int_{T_\infty}^{T_b} k dT \qquad (4\text{-}9)$$

or

$$EI = C_4 \; u_{\infty_n}^2 D^2 \qquad (4\text{-}10)$$

where $C_4 = \rho_f^2 \; \pi \; \phi_b \; C_3/\mu_f^2$ = constant for constant P_∞, T_∞ and T_b.

Roman's data displays a flat characteristic for flow velocities less than 51 fps. If radiation was negligible compared to forced convection, or if radiation were approximately a constant fraction of the input power gradient, then we would expect Roman's data to agree with Eq. (4-9). The measured power input gradients from his experiment are plotted against the square of the fluid Reynolds number on Fig. 19 and the agreement with Eq. (4-9) is excellent.

Roman estimated his arc boundary temperature to be $6000^{o}K$ $\pm$ $1000^{o}K$. A value of $T_b = 6000^{o}K$ was chosen for his data on Fig. 19. The choice of T_b does not alter the significant behavior of Fig. 19 which is that EI (for $\partial E/\partial I = 0$ and constant P_∞ and T_∞) is proportional to Re_f^2. As mentioned earlier, the data from the present investigation should not agree with Eq. (4-9) since $\partial E/\partial I \neq 0$.

The result that $Nu_{FC} = \text{const}\, Re_f^2$ for the convected balanced arc is very interesting when compared with the heated solid cylinder data of Appendix B. For the heated solid cylinder $Nu_{FC} = \text{const}\, Re^n$ where n is 0. 6 to 0. 8 for a comparable free stream Reynold s number range. The mere fact that the convected balanced arc has a boundary temperature 6 to 8 times as large as the maximum surface temperature considered in the solid cylinder tests does not explain this significant difference in the value of the exponent for Re_f. Rather, the forced convection heat transfer processes for the convected balanced arc are very much different than those for the heated solid cylinder. This same observation was reported by Lord and Broadbent (Ref. 50) when they tried to correlate Adams' (Ref. 54) experimental data with the Hilpert curve (Fig. B-1).

Equation (4-9) is not valid as $u_{\infty_n} \rightarrow 0$ since the dominant heat transfer mechanism becomes natural convection and natural convection was considered negligible in the development of Eq. (4-9) (i. e. the highly convected case). We can generalize the expression for EI as follows:

$$EI = E_o I + C_4 u_{\infty_n}^2 D^2 \tag{4-11}$$

for constant P_∞, T_∞, T_b and $\partial E/\partial I = 0$. E_o is the free-burning value of the electric field and is only a function of P_∞ and the gas (see Appendix D). Roman's data (for I = constant) on Fig. 19 shows that the transition from natural convection dominated (i. e. $u_{\infty_n} = 0$ or free-burning) to forced convection dominated flow is nearly linear. Hence Eq. (4-11) is a realistic generalization for the power input gradient.

If we consider P_∞, T_∞ and T_b constant and $\partial E/\partial I = 0$ the form for $E = E(u_{\infty_n})$ can be determined. Eliminating D between Eq. (4-1) and (4-10) gives

$$E^2 = E_o E + C_5 u_{\infty_n}^2$$

where $$C_5 = C_4/C_2 = \rho_f^2 \, 4\phi_b \, C_3/\bar{\sigma} \, \mu_f^2$$

Finally

$$E = \frac{E_o}{2} + \sqrt{\frac{E_o^2}{4} + C_5 u_{\infty_n}^2} \tag{4-12}$$

The expression for D, Eq. (4-2), can be generalized to show the influence of changing u_{∞_n}, i. e.

$$D = \frac{\sqrt{I}}{\sqrt{C_2}\left\{\frac{E_o}{2} + \sqrt{\frac{E_o^2}{4} + C_5 u_{\infty_n}^2}\right\}^{1/2}} \qquad (4\text{-}13)$$

Equation (4-13) indicates that as the convection velocity increases for constant I and P_∞, the dimensions of the convected arc must decrease to maintain the energy balance. In this regard, Roman's data shown in Fig. 13a displays a curious behavior. His transverse dimension d_T increases with increasing u_{∞_n} for P_∞ = 1 atm and constant current. However his streamwise dimension d_S decreases faster with increasing u_{∞_n} so that the effective dimension d_{eff} (Eq. (3-35)) does behave according to Eq. (4-13).

4.4 NORMAL FORCE COEFFICIENTS

From the earlier descussion in Section 3.1 we suspect that the normal force coefficient for the balanced convected arc will be similar to the pressure drag coefficient of a solid cylinder. We would not expect the values of the coefficient to be the same for the arc and solid cylinder because for one reason we have not established what is an equivalent dimension for the two cases. However we would expect similar behavior, i.e. fairly constant value of C_D for comparable Re_{∞_n} intervals.

We express the balance between the cross-sectional Lorentz force (force per unit length) and the two-dimensional fluid dynamic drag force as

$$BI = C_D \, q_{\infty_n} \, d_T \tag{3-32}$$

where C_D = pressure drag coefficient or normal force coefficient referenced to the transverse dimension d_T.

The measured values of the magnetic field B for this investigation are fairly constant with Mach number (Table I). However u_{∞_n} increases with increasing I as indicated in Fig. 7b so that the value of C_D is fairly constant. The value of C_D is about 1.75 for all three Mach numbers and is shown in Fig. 21 with values determined by Roman. The C_D's for circular and elliptical cylinders are also shown on Fig. 21 for comparison.

If we assume that C_D is constant we have the relation

$$\frac{B}{q_{\infty_n}} \sim \frac{D}{I}$$

Using Eq. (4-13) and considering the two cases of small u_{∞_n} ($E_o \approx E$) and large u_{∞_n} ($E_o < E$) we obtain

$$\frac{B}{u_{\infty_n}^2} \sim \frac{1}{\sqrt{I}} \qquad \text{for small } u_{\infty_n} \tag{4-14}$$

and

$$\frac{B}{u_{\infty_n}^{3/2}} \sim \frac{1}{\sqrt{I}} \qquad \text{for large } u_{\infty_n} \tag{4-15a}$$

or

$$u_{\infty_n} \sim I^{.33}\, B^{.67} \tag{4-15b}$$

Roman's data displays the $B/q_{\infty_n} \sim 1/\sqrt{I}$ behavior except for the data at I = 400 amperes as shown on Fig. 12. There is a suspicion that Roman's data might be affected by wall interference due to the close proximity of the magnets. Roman did report that the wake formation behind solid cylinders was different when the magnets were in place than when they were withdrawn. This wall interference could explain the behavior of Roman's data on Fig. 12 and Fig. 21; the effect of wall interference being to lower the fluid dynamic drag force (hence a lower required value of B).

If Roman's drag coefficients are referenced to d_{eff} instead of d_T, the values of C_D increase in magnitude and are more nearly constant with increasing Re_{∞_n}; also the curves for 200 and 300 amps overlap each other. The 400 ampere curve is still below the other two as before.

The fact that the C_D values reported by Roman and the present investigation are different is not important here because the C_D is

so dependent upon the reference dimension used and different investigators measure this dimension in different ways. The comparison of arc dimensions between different experiments is not appropriate at the present time since the temperatures corresponding to the dimensions have not been firmly established. What is important and what Fig. 21 does show is that for a given experiment with measured dimensions consistent with the other measured data, the C_D will be fairly constant over the range of Re_{∞_n} considered.

The relation $B \sim \sqrt{u_{\infty_n}^3/I}$ of Eq. (4-15a) for large u_{∞_n} is interesting in that other investigators have reported (Ref. 20) a similar relation for travelling arcs between parallel rail electrodes. As the velocity of the travelling arc increases the effects of the root constraints on the arc motion lessen significantly (Ref. 20, page 40). Thus one might conjecture that as the velocity and length of the travelling arc increase, the arc motion would be limited primarily by the fluid dynamic drag on the column. In that event the column behavior of the travelling arc would be comparable to the column of the convected balanced arc. Roman reported in Ref. 74 that for travelling arc velocities of about 450 fps and electrode spacings of about one inch, the relation between u_∞, B and I could be empirically expressed as

$$u_\infty = \text{const } I^{0.33} B^{0.61}$$

This relation is nearly identical with Eq. (4-15).

4.5 RELATIONS BETWEEN INTERIOR AND EXTERIOR CHARACTERISTIC PARAMETERS

The interior characteristic velocity u_1 is defined as

$$u_1 = \sqrt{\frac{J_1 B d_s}{\rho_1}} = \sqrt{\frac{4BI}{\rho_1 \pi d_T}} \tag{4-16}$$

Using the force balance equation

$$BI = C_D \frac{1}{2} \rho_\infty u_{\infty_n}^2 d_T \tag{3-32}$$

we can relate the interior characteristic velocity u_1 to the exterior characteristic velocity u_{∞_n} as

$$u_{\infty_n} = \sqrt{\frac{2BI}{C_D \rho_\infty d_T}} = u_1 \sqrt{\frac{\rho_1 \pi}{\rho_\infty 2 C_D}} \tag{4-17a}$$

or

$$\frac{u_1}{u_{\infty_n}} = \sqrt{\frac{\rho_\infty}{\rho_1} \frac{2 C_D}{\pi}} \tag{4-17b}$$

Harvey (Ref. 31) reported that u_1/u_{∞_n} was constant over a wide range of test conditions. This is a consequence of the fact that C_D and T_1 are fairly constant over a wide range.

In wall stabilized arcs with a transverse magnetic field, L_c is an independent parameter with B being specified with the initial data. In

balanced convected arcs the free stream velocity u_{∞_n} must be specified initially. Then because of the force balance equation and the constancy of C_D the value of B is determined. Hence L_c is a function of the free stream Reynolds number. This relation between the external and internal similarity parameters is:

$$Re_{\infty_n} = \sqrt{L_c}\left(\frac{\rho_\infty}{\rho_1}\right)^{1/2}\left(\frac{\mu_1}{\mu_\infty}\right)\sqrt{\frac{\pi}{2C_D}} \tag{4-18}$$

and if T_1 is constant over a range of currents, then

$$Re_{\infty_n} = \text{const}\sqrt{L_c} \tag{4-19}$$

for constant P_∞ and T_∞.

Also

$$Re_f = \sqrt{L_c}\left(\frac{\mu_1}{\mu_f}\right)\frac{\rho_f}{\sqrt{\rho_1\,\rho_\infty}}\sqrt{\frac{\pi}{2C_D}} \tag{4-20}$$

4.5 POWER GRADIENT RELATION

Primarily as a result of the $\partial E/\partial I = 0$ for convected balanced arcs the energy balance can be expressed as

$$EI = E_o I + \text{const}\, Re_f^2 \tag{4-21}$$

By using the force balance requirement this can be rewritten as

$$EI = E_o I + \text{const}'\, L_c \tag{4-22}$$

From our discussion in Section 3.4, for large L_c we concluded that

$$EI = \beta \sqrt{L_c} \qquad \text{for} \qquad L_c \gg 1 \tag{3-23}$$

The behavior of the convected balanced arc as it changes from being governed by Eq. (4-22) to Eq. (3-23) is very significant. Also, the question of "when is L_c large?" must be considered.

By the same procedure which led to Eq. (4-8), we can determine the slope of the characteristic curve in order to have n = 1 (i. e. $EI \sim \sqrt{L_c}$). We find that we must have $E \sim I^{-1/3}$ for the characteristic curve. Thus at large L_c where Eq. (3-23) is valid the characteristic is not flat (for constant u_{∞_n} and P_∞), but rather has the form

$$E = \text{const } I^{-1/3} \tag{4-23}$$

We observe from Roman's data, Fig. 13b, that for I = 200 amps as u_∞ increases (i. e. L_c increases) the value of E increases (as we expect) and the slope of the characteristic changes from zero to a negative value. The experimental data are not complete enough to determine whether the characteristic curves are tending towards Eq. (4-23).

Kookekov (Ref. 67) investigated the motion of an electric arc in a cross-flow under the influence of an external, transverse magnetic

field. He made a semi-empirical analysis based on the conservation of energy, Ohm's law and the minimum principle and reports the relation

$$E = \text{const}' \, I^{-1/3}$$

for a constant velocity cross-flow. Kookekov does not give a description of the experimental set-up, measurement techniques or range of parameters investigated. His characteristic relation is very interesting and agrees with the results of this investigation for large L_c.

From this discussion we might conclude that for a "low" L_c and $I > 100$ amps the characteristic curve for constant u_{∞_n} is flat and the power input gradient of the balanced convected arc behaves according to Eq. (4-22). For "large" L_c the characteristic curve has a negative slope (i. e. $\partial \log E / \partial \log I = -1/3$), and the power input gradient behaves according to Eq. (3-23). Thus we have

$$\frac{EI}{\phi_1} \begin{cases} \alpha & \text{for} \quad L_c = 0 \\ \alpha + \beta' L_c & \text{for low} \quad L_c \\ \alpha + \beta \sqrt{L_c} & \text{for large} \quad L_c \end{cases} \qquad (4\text{-}24)$$

We can examine the question of "when is L_c large?" by studying the behavior of the coefficients of the terms in the energy equation as L_c becomes large. Consider the non-dimensional energy equation of Section 3. 3:

$$\rho\vec{u}\cdot\nabla h = K_1\,\vec{u}\cdot\nabla P + \frac{1}{Pr_1\sqrt{L_c}}\,\nabla^2\phi + K_{JH}\,j + \frac{K_1}{\sqrt{L_c}}\,\Phi \qquad (3\text{-}19)$$

where again the joule heating parameter is $K_{JH} = (EI_1/\phi_1)/Pr_1\sqrt{L_c}$. We observe that the coefficient of the convection term (LHS of 3-19) is O(1). Hence the parameter K_{JH} is always greater than or equal to a quantity of O(1) and for the case of $L_c \to 0$ we have $K_{JH} \to \infty$.

As K_{JH} decreases to O(1), the pressure work, heat conduction and viscous dissipation terms decrease to $O(\epsilon)$ where $\epsilon < 1$. Once $K_{JH} = O(1)$ it remains constant at this value and we have $EI_1/\phi_1 = \beta\sqrt{L_c}$ and $K_{JH} = \beta/Pr_1$. Thus L_c is "large" when $K_{JH} = O(1)$. For $K_{JH} > O(1)$ we have shown that $EI_1/\phi_1 \sim L_c$, and L_c is "low".

We can express the joule heating parameter as

$$K_{JH} = \frac{EI/\phi_1}{Pr_1\sqrt{L_c}} = \text{const}\,\frac{E^{3/2}\sqrt{I}}{u_{\infty_n}} \qquad (4\text{-}25)$$

where we have assumed constant P_∞, T_∞ and C_D and used the relations $D \sim \sqrt{I/E}$ and $BI \sim \rho_\infty u_{\infty_n}^2 D$.

When L_c is large, K_{JH} = constant. Thus using Eq. (4-25) we obtain the relation

$$E \sim \frac{u_{\infty_n}^{2/3}}{I^{1/3}} \qquad (4\text{-}26)$$

Using Ohm's law and Eq. (4-26) we obtain the relation for the effective dimension D

$$D \sim \frac{I^{2/3}}{u_{\infty_n}^{1/3}} \tag{4-27}$$

Finally, the expression for B (assuming constant C_D) is

$$B \sim \frac{u_{\infty_n}^{5/3}}{I^{1/3}} \tag{4-28a}$$

or

$$u_{\infty_n} = \text{const } I^{0.2} B^{0.6} \tag{4-28b}$$

which is also similar to the empirical travelling arc relation discussed in Section 4. 4.

For constant B, the relation between u_{∞_n} and I is

$$u_{\infty_n}^{3} \sim I \quad , \qquad \text{low } L_c \text{ but } E_o < E$$

and

$$u_{\infty_n}^{5} \sim I \quad , \qquad \text{large } L_c$$

The u_{∞_n} versus I data for the present investigation shown in Fig. 7b best fits the relation $u_{\infty_n}^4 \sim I$ as shown on Fig. 12 which is an intermediate relation to the low and large L_c relations above.

The behavior of K_{JH} is shown in Fig. 23 for Roman's data. As L_c increases we observe K_{JH} decreasing to a constant value of O (1). The interesting point here is that L_c does not have to approach infinity in order that K_{JH} become constant. In Fig. 23, K_{JH} for I = 200 amps appears to be near a constant O (1) value at L_c = 5600. The O (1) value for K_{JH} is about 4.5 for the 200 amp curve and this first occurs at a u_∞ of about 40 fps. We see from Fig. 13b that at u_∞ = 40 fps the characteristic curve at I = 200 amps in changing from a zero slope to a slightly negative slope.

The behavior of K_{JH} for the data of the present investigation is shown in Fig. 24. The K_{JH} is at a constant value for increasing L_c at all three Mach numbers. Also, the characteristic curve for constant u_{∞_n} (i. e. $\partial E/\partial I$) is negative as was pointed out in Section 4.3. Thus the UM data is at least in an intermediate L_c range (between low L_c and large L_c) and possibly the large L_c.

We are interested here in the effect of the forced convection on the convected balanced arc. That is to say, the influence of L_c or Re_{f_n} on the contribution of the forced convection to the total power

input gradient. Thus we should examine $(E - E_o)I$ as it changes with L_c. When $L_c \gg 1$ the free-burning contribution to the total power input gradient is negligible compared to the contribution from forced convection, i. e. $E_o \ll E$.

Using Fig. D-3 we determine E_o to be 3. 0, 2. 5, 2. 0 volts/inch for the Mach numbers 2. 5, 3. 0 and 3. 5 respectively. The parameter $(E - E_o)I/P_{r_1}\phi_1$ versus L_c is plotted on Fig. 20 for the data from Roman and the present investigation. The reference Prandtl number P_{r_1} is constant for a given gas and constant P_∞. The P_{r_1} is necessary in Fig. 20 to collapse the data since different pressures and gases are involved. Fig. 20 indicates that the data collapses (with some scatter) to a single curve which has a slope of 1. 0 at low L_c and tends toward a slope of 0. 5 at large L_c in accordance with Eq. (4-24).

Figure 20 indicates the general behavior of a convected balanced arc as the L_c or Re_{f_n} is increased. The slope of the curve m at any L_c gives us the input power relation $EI \sim L_c^m \sim Re_{f_n}^n$ where $n = 2m$. If P_∞, T_∞ and C_D are assumed constant the value for n can be used in Eq. (4-6) to determine the $E = E(I, u_{\infty_n})$ relation. The relations for D and B follow using Eq. (4-1) and (3-23) as was done in Section 4. 3. Thus the general macroscopic features of the convected balanced arc are determined for any L_c.

If we start with a free-burning arc having a flat characteristic (i. e. $I > 100$ amps) and begin blowing on it holding I and P_∞ constant, the $\partial E/\partial I$ will remain zero and the input power gradient will behave as $EI = E_o I + \text{const } L_c$. This behavior will prevail until K_{JH} approaches a constant O (1) value. At this point a further increase in u_{∞_n} will result in $\partial E/\partial I$ becoming negative and a change from $EI \sim L_c$ to $EI \sim \sqrt{L_c}$.

4. 6 GENERAL BEHAVIOR OF THE CONVECTED BALANCED ARC

From the development of the theory thus far and the observations of experimental data we can now discuss the general behavior of a convected balanced arc.

Let us assume that P_∞, T_∞, and I are held constant while u_{∞_n} increases. The value of the applied external magnetic field B increases, keeping the Lorentz force equal to the drag force, otherwise the arc would be blown downstream. As u_{∞_n} increases there is initially an energyimbalance as the forced convection heat transfer at the boundary will be greater than the power input. The arc begins to adjust itself to again have an energy balance. The size of the arc (as represented by d_{eff}) decreases which decreases the forced convection heat transfer. At the same time the value of E increases until there is a balance between the power input EI and the forced convection at the boundary. Arc radiation would play a minor role in the adjustment process.

The effective temperature T_σ would remain fairly constant. This was observed in Roman's experiment as the u_∞ was increased from 20 ft/sec to about 50 ft/sec for constant current.

This same general behavior has been observed for free-burning arcs where the natural convection heat transfer has been augmented by forced mass influx into the column. Nikolay Khvostov considered the arc heater design shown in Fig. 27 and determined the temperature distributions theoretically and E-I characteristics experimentally for different values of mass influx q. His results, indicated in Fig. 27. show that as I is held constant and q increased the arc adjusts to the new conditions by increasing E and decreasing r_b. Similar observations can be made using the data of Weber (Ref. 65) and Baum and Cann (Ref. 66).

Noeske (Ref. 68) analytically considered the problem of an arc in a low speed cross-flow and no magnetic field. His model was a flow-through arc in an incompressible and inviscid flow. Noeske reports that the voltage gradient increases with increasing cross-flow and the diameter decreases with decreasing current and increasing cross-flow.

V. TEMPERATURE DISTRIBUTION

5. 1 INTRODUCTION

The purpose of the work described in this section was to study the temperature distribution of the convected balanced arc. The governing equations were solved numerically on an IBM 7090 computer and the theoretical temperature distribution was determined. The equations were examined in their unsteady form and solved as initial value problems by iterating to a steady solution. Both one- and two-dimensional models were studied. The one-dimensional model was found to give a satisfactory approximation and it required a shorter computer time to converge to a near steady solution. The influence of T_b and K_{JH} on the peak temperature and peak temperature shift was determined. Finally, the radiance distribution, calculated from the theoretical temperature distribution, was compared with measured results.

5. 2 TWO-DIMENSIONAL PROBLEM

The two-dimensional model was the physical model of Section 3. 1 with a circular boundary. The interaction region influenced the arc core only by the imposed conditions on the arc boundary. The equations considered were the unsteady form of equations (3-17), (3-18) and (3-19) in cylindrical coordinates. The unsteady equations in finite difference form were iterated with respect to time until a near steady solution was obtained. The physical significance of this numerical

scheme is discussed by Crocco in Ref. 55. The two-dimensional model required at least 30 minutes of machine time to converge to a near steady solution.

Since the arc is symmetric about the xz plane only the half plane $\theta = 0$ to π radians (Fig. 18) was considered. The spatial variables were $r = i\Delta r$ ($i = 0, \ldots, 10$) and $\theta = j\Delta\theta$ ($j = 0, \ldots, 12$). This mesh size appeared about optimum. A smaller mesh size did not improve the accuracy, however a larger mesh size (i. e. $i = 0, \ldots, 5$) produced significant differences.

The boundary conditions were: 1) the temperature and density were constant values specified around the boundary , 2) the radial velocity was zero at the boundary (i. e. no mass transfer) and 3) the tangential velocity at the boundary was some fraction of the velocity outside the arc core. The velocity distribution outside the arc core was assumed to be that of a potential flow about a cylinder up to $\theta = \pi/2$ and then zero from $\pi/2$ to π. The tangential velocity at the boundary was assumed to be zero or ten per cent of the velocity just outside the are core. The assumed tangential velocity distribution at the boundary had little influence on the velocity and temperature fields inside the arc core near the x axis.

The other details of the two-dimensional problem are common to the one-dimensional problem and will be discussed in the next section.

5. 3 ONE-DIMENSIONAL PROBLEM

The convected balanced arc is symmetric about the xz plane, therefore the x axis is a dividing streamline. The normal velocity and gradients of density, velocity and temperature normal to this dividing streamline are zero. Thus the one-dimensional equations should provide a realistic estimate of the velocity and temperature distribution along the x axis inside the arc core.

The model assumed for the one-dimensional problem was the physical model of Section 3. 1 with uniform temperature and velocity gradients in the y direction. The governing equations were the one-dimensional unsteady forms of Eq. (3-17), (3-18), and (3-19)

$$\frac{\partial \rho}{\partial t} = - u\frac{\partial \rho}{\partial x} - \rho \frac{\partial u}{\partial x} \tag{5-1}$$

$$\rho \frac{\partial u}{\partial t} = - \rho u\frac{\partial u}{\partial x} - \frac{\partial P}{\partial x} + j + \frac{4}{3}\frac{1}{\sqrt{L_c}}\frac{\partial^2 u}{\partial x^2} \tag{5-2}$$

$$\rho \frac{\partial h}{\partial t} = - \rho u \frac{\partial h}{\partial x} + K_1 u \frac{\partial P}{\partial x} + \frac{1}{Pr_1 \sqrt{L_c}} \frac{\partial^2 \phi}{\partial x^2} + K_{JH}\, j + \frac{K_1}{\sqrt{L_c}}\left(\frac{\partial u}{\partial x}\right)^2 \tag{5-3}$$

The density, temperature and velocity (u = 0) were specified at the front and back of the arc, i. e. the boundaries. Equations (5-1), (5-2) and (5-3) along with Eq. (3-6), (3-7), (3-9) and (3-10) for h, P, ϕ and $\vec{j}$ respectively, were sufficient to determine the non-dimensional variables (referenced to the quantities in Section 3. 3) density, velocity and temperature.

The fluid physical and transport properties were read into the machine in tabular form as functions of temperature. The properties (i. e. σ, Z, ϕ and h) were brought into the machine calculations by a table look-up routine. The coefficient of viscosity μ was assumed constant at a mean temperature value. The actual value of μ varied from the mean value by at most a factor of two over the temperature ranges considered. It was of interest to compare the calculated results with experimental results, thus most of the numerical work was for P_∞ = . 0191 atm (i. e. Mach 3. 0). The air data was taken from References 25, 47, 49, and 75. The curves used for σ, h, and ϕ are shown on Fig. 30 and 31. The data for nitrogen was taken from References 34, 35, and 48.

Equations (5-1), (5-2), and (5-3) were formulated in explicit form using central finite differences according to the scheme discussed in the next section. Because of the explicit form the momentum and energy equations were unstable under some conditions and stability criteria had to be considered (Section 5. 4). Twenty stations along the x axis (from the back of the arc to the front) appeared about optimum for accuracy. The one-dimensional problem converged to a steady solution in 3 to 5 minutes for most cases.

The reference temperature T_1 was usually the boundary temperature T_b, except in cases where T_b was so low that $\sigma_1 = 0$. In these cases using $T_1 = T_b$ would result in a singularity in the problem,

thus T_1 was taken as the peak temperature. Since the peak temperature was not known a priori, it was first guessed and then the guess was improved on the succeeding one or two runs. One observation of the numerical work is that for constant P_∞ the peak temperature is fairly constant for data consistent with the physical behavior of convected balanced arcs.

5.4 STABILITY CRITERIA

Consider the partial differential equation

$$\frac{\partial u}{\partial t} = a_0 \frac{\partial^2 u}{\partial x^2} + a_1 \frac{\partial u}{\partial x} \tag{5-4}$$

where a_0 and a_1 are constant coeffiecients. An explicit central finite difference form of Eq. (5-4) and the scheme used in this investigation is

$$\frac{u_i^{n+1} - u_i^n}{\Delta t} = a_0 \left[\frac{u_{i+1}^n - 2u_i^n + u_{i-1}^n}{(\Delta x)^2} \right] + a_1 \left(\frac{u_{i+1}^n - u_{i-1}^n}{2\Delta x} \right) \tag{5-5}$$

where $n = 0, 1, \ldots$ and $i = 1, 2, \ldots, M$.

If $u(x, t)$ is the exact solution of Eq. (5-4) and u_i^n is the solution of the finite difference equation (5-5), the error of the approximation is $|u_i^n - u(i\Delta x, n\Delta t)|$. The basic notion of such an approximation is that the error can be made as small as one pleases by letting Δt, $\Delta x \to 0$ for a fixed $n\Delta t$. If we hold Δx constant and continue the solution

of Eq. (5-5) for smaller values of Δt there is a value of Δt where we will begin to accumulate errors of some sort which will be amplified to an unacceptable degree after a relatively small number of cycles (Ref. 43, p. 9). This behavior is a property of the difference equation (5-5) and is called instability. If we are to reduce the error of the approximation by refining our mesh size, we cannot reduce Δx and Δt in an arbitrary manner.

For the finite difference equation (5-5) the requirement on Δx and Δt to insure stability is (from Ref. 43)

$$\frac{2a_0 \Delta t}{(\Delta x)^2} \leq 1 \tag{5-6}$$

We assume that locally for a given time increment, u = constant such that the momentum equation (5-3) is quasi-linear of the form

$$\frac{\partial u}{\partial t} = a_0 \frac{\partial^2 u}{\partial x^2} + a_1 \frac{\partial u}{\partial x} + a_2 u + a_3 \tag{5-7}$$

where

$$a_K = a_K(x, t) \quad , \quad K = 0,\ 1,\ 2,\ 3$$

$$a_0 = 4/3 \sqrt{L_c}\, \rho$$

$$a_1 = -u$$

$$a_2 = 0$$

$$a_3 = \frac{1}{\rho} \left(j - \frac{\partial P}{\partial x} \right)$$

The criterion for stability of the explicit finite difference form of Eq. (5-7) is

$$\frac{8}{3}\frac{1}{\rho_i^n\sqrt{L_c}}\frac{\Delta t}{(\Delta x)^2}\leq 1 \tag{5-8}$$

The stability criterion for the energy equation (5-4) was less stringent on the required value of Δt than Eq. (5-8) so that Eq. (5-8) was the criterion for the system. The actual criterion used was

$$\frac{8}{3}\frac{1}{\rho_i^n\sqrt{L_c}}\frac{\Delta t}{(\Delta x)^2}\leq \frac{1}{2} \tag{5-9}$$

The computation started with a constant Δt and Δx. At each station and time increment Eq. (5-9) was checked. If Eq. (5-9) was violated at any station, the Δt was adjusted so that Eq. (5-9) was satisfied. The solution was then backed up one time increment and the computation continued using the adjusted value of Δt. There were several cases where the required Δt from Eq. (5-9) was so small that the computation was essentially stalled. These cases occurred when there was some question about the inputs E, B, and D being realistic. For realistic data inputs the above stability scheme worked very well and the one-dimensional problem iterated to a near steady solution in 3 to 5 minutes.

5. 5 NUMERICAL RESULTS

The Lorentz force acting on the conducting fluid elements and (to a lesser extent) the pressure distribution and viscous stresses on the front half of the arc boundary will generate a circulation inside the arc core. This convection interior to the arc will displace and distort the isotherms from their cylindrically symmetric pattern of a free-burning arc. A typical two-dimensional result for a large isotherm displacement is shown on Fig. 32. The peak temperature is displaced in the $\vec{j} \times \vec{B}$ direction to about 70 per cent of the radius. This severe distortion of the isotherm pattern is in agreement with results reported by Harvey in Ref. 31.

Figure 32 is the near steady two-dimensional solution for a zero slip condition at the arc boundary. A solution was also determined assuming the same inputs as Fig. 32 but a ten per cent slip at the arc boundary. The influence of this change in the tangential velocity boundary condition extended in from the arc boundary about 30 per cent of the radial distance for the velocity field and about 20 per cent for the temperature field. At the x axis the temperature and velocity fields were the same for these two cases. From this limited study it appears that the external flow (in regard to pressure distribution and viscous stresses at the boundary) does not have a significant influence on the fields inside the arc core. This study did not consider

mass transfer at the boundary; further work should include this effect as it may influence the internal motion significantly.

Figure 33 shows the comparison of the temperature distribution along the x axis for the one- and two-dimensional models. The agreement is quite good and thus we assume that the one-dimensional model will give realistic temperature distributions along the x axis even for arcs with non-circular cross-sections but symmetric about the xz plane. Based upon the comparison in Fig. 33 and the much shorter machine time required by the one-dimensional model, the one-dimensional model was used to determine the effects of the governing parameters.

Figure 34 shows a comparison of results from the present one-dimensional numerical program with measured and numerical results of other investigators for a wall stabilized nitrogen arc at one atmosphere. The one-dimensional results agree quite well, thus we conclude that the present one-dimensional numerical program gives reliable results for low magnetic fields. It was assumed that the program also gave reliable results for large magnetic fields. Later comparisons with measured results indicated that the assumption was valid.

The effect of boundary temperature T_b on the peak temperature and displacement of the peak temperature is shown on Fig. 35. A qualitatively similar behavior was observed by Harvey (Ref. 31) for a wall stabilized arc in air at one atmosphere. The initial conditions

specified on Fig. 35 correspond to RUN 657 (Fig. 10). The T_b is determined by specifying q_{∞_n} and requiring the one-dimensional force balance condition, i. e.

$$BE \int_{\frac{-d_s}{2}}^{\frac{d_s}{2}} \sigma dx = \left(\frac{\Delta P}{q_{\infty_n}}\right) q_{\infty_n} \qquad (3\text{-}33)$$

to be satisfied. The stagnation point pressure coefficient ($\Delta P/q_{\infty_n}$) has a constant value of 2. 05 for blunt shapes with separated flow and flow Mach numbers up to 0. 9 (Ref. 71, Chapter 12).

If we specify q_{∞_n} = 0. 196 psi (i. e. the value for RUN 657) and the initial conditions on Fig. 35, Eq. (3-33) is satisfied for T_b = 7200 ^{o}K. This estimated temperature distribution for RUN 657 is shown in Fig. 36 and we observe the peak temperature to be well forward. The densitometer trace for RUN 657 shown in Fig. 26 indicates a similar shift in the peak temperature. This comparison between measured and calculated results for RUN 657 will be continued in Section 5. 6.

The effect of varying u_{∞_n}, while maintaining constant P_∞ and I, on the temperature distribution along the x axis is shown in Fig. 36 and 37. The measured data for RUN 657 with u_{∞_n} = 655 fps was used as a base point. The values for E, B, and D at lower velocities but I = 216 amperes and P_∞ = . 0191 atmospheres were determined

as follows. From Fig. 20, RUN 657 appears to be in a transition region between low and large L_c. It was assumed that RUN 657 was in the L_c region where $(E - E_o)\, I \sim L_c^{2/3}$ (i. e. the slope m = 2/3). From the discussion in Section 4. 6 the relations for E, B, and D become

$$E \sim \frac{u_{\infty_n}^{4/5}}{I^{1/5}} \quad , \quad D \sim \frac{I^{3/5}}{u_{\infty_n}^{2/5}} \quad \text{and} \quad B \sim \frac{u_{\infty_n}^{8/5}}{I^{2/5}} \qquad (5\text{-}10)$$

Using the base point and the relations above, new values for E, B and D at constant P_∞ and I were determined. Examples of the estimated data are given in Fig. 36. The result was sets of data at constant I and P_∞ but varying u_{∞_n} which were consistent with the physical behavior of convected balanced arcs. If new values for E, B, and D had been estimated using the relations for low L_c and large L_c, the difference between the values would have been less than 25 per cent at $u_{\infty n}$ = 100 fps.

Figure 37 shows the influence of the joule heating parameter K_{JH} on the peak temperature displacement. This investigation indicates that K_{JH} is the significant parameter for the displacement, rather than simply L_c. The displacement of the peak temperature to its most forward position appears to be related to the decrease of K_{JH} to its constant 0 (1) value.

For all conditions represented by the curve on Fig. 37 the velocity along the x axis was always less than the local sonic speed and the induced electric field $\vec{u} \times \vec{B}$ was less than ten per cent of the applied $\vec{E}$. The peak temperature was fairly constant at 12, 600 ^{o}K for all the u_{∞_n} considered. The result that the peak temperature was fairly constant is consistent with the travelling arc results of Slovetskiy (Ref. 72). Slovetskiy measured the peak temperature of a travelling arc in air at one atmosphere. For the current range of 320 to 1800 amperes and velocities of 80 to 128 m/sec the peak temperature was fairly constant at 12, 400 ^{o}K.

The cross-sectional temperature distribution for RUN 657 was estimated as follows. The temperature distribution in the x direction but at different y stations (see Fig. 18) was assumed to be similar to the temperature distribution along the x axis (Fig. 36). This assumption appeared reasonable in view of the two-dimensional distribution of Fig. 32 and the two-dimensional numerical results reported by Harvey (Ref. 31). The cross-section was assumed elliptical with dimensions corresponding to RUN 657. A distribution of pressure coefficients around the boundary was assumed such that the total fluid dynamic drag coefficient was 1. 75. Finally, the peak temperature at each y station was adjusted so that the temperature dis-

tribution in the x direction satisfied the force balance Eq. (3-33). The result was a cross-sectional temperature distribution which balanced the fluid dynamic drag on the arc. This temperature distribution is shown in Fig. 38. Because of the manner in which the cross-sectional temperature distribution was determined, it must be made clear that the distribution is not unique, but rather a possible temperature distribution.

5.6 RADIANCE DISTRIBUTION FOR RUN 657

The characteristic response curve (optical density versus log exposure) for the Kodak Panatomic - X film developed in D-76 (diluted 1 to 4) for 5 minutes at 68 ^{O}F was determined using the Edgerton, Germeshausen and Grier Mark VI sensitometer. The sensitometer was calibrated by comparing the characteristic response curves for film developed by standard processes with Kodak published data (Ref. 73). The light source for the sensitometer was a Xenon flashtube (GE type FT-118) which has a spectral radiance similar to a black body at 7000 ^{O}K. The film and lens combination is sensitive to radiation from 3800 to 6500 ^{O}A (Ref. 73). The characteristic response curve had a $\gamma = 0.225$ (i.e. tangent of the slope of the response curve). The above developing process was used to insure that the film had sufficient contrast over the exposure range of interest to preserve the arc detail.

The optical densities from Fig. 26b were converted to film exposures E_x (in meter - candle - seconds) using the film response curve. We assume that the Xenon flashtube radiates like a black body at 7000 ^{o}K. Therefore the radiant effectiveness is approximately 90 lumens per watt over the entire spectral band. The fraction of the black body radiation at 7000 ^{o}K between . 38 and . 65 microns is . 38 so that we define a "film" watt as

$$1 \text{ watt} = .38 \text{ "film" watt}$$

Thus 1 lumen corresponds to $.38/90 = 4.2 \times 10^{-3}$ "film" watt and finally

$$1 \text{ mcs} \approx 4.2 \times 10^{-7} \text{ "film" watt-sec/cm}^2$$

The radiance N in watt/cm^2 was determined from

$$E_x = N \Omega \tau_{sys} t_{ex}$$

where Ω = solid angle for f/11 lens opening, 6.48×10^{-3} steradians

τ_{sys} = transmission factor for viewing system, assumed to be 1/3

t_{ex} = exposure time or shutter speed, 1/1000 sec.

The measured radiance distribution for the side-on view of RUN 657 is shown in Fig. 39. Assessing all the uncertainties involved, the accuracy for the measured radiances should be within one order of magnitude.

The angular data for the visual observation of RUN 657 is presented in Table II. The angle between the normal of the microdensitometer scan plane for the side-on view and the arc column axis (i. e. the normal to the arc cross-section plane) is 32^{o}. The projection of the side-on look vector in the cross-section plane is about 6^{o} from the major axis as shown in Fig. 38.

The calculated radiance distribution for RUN 657 was determined assuming an optically thin gas in local thermodynamic equilibrium (LTE) at T_g (i. e. the assumed equilibrium is among the gas molecules rather than between the gas and the radiation) and using the temperature distribution of Fig. 38. The total spectral radiation emission coefficient ε_ν (from Ref. 78) in watt/cm^3-steradian - hertz was integrated over the spectral band . 38 to . 65 microns to obtain the visible range emission coefficient ε. The calculated radiances were determined from

$$N = \int_{-\infty}^{\infty} \varepsilon \, d\ell \approx \sum_{i=0}^{L} \varepsilon \, \Delta\ell_i \quad , \quad \frac{\text{watt}}{\text{cm}^2\text{-ster}}$$

where the integration paths were along lines 6^{o} from the major axis. The path lengths (see Fig. 38) were increased by a factor $1/\cos 32^{o}$ to account for the fact that the scan plane sliced up through the cross-section plane at an angle of 32^{o}. The calculated radiances are shown in Fig. 39.

The large difference (approximately three orders of magnitude) between the measured and calculated radiance distributions shown on Fig. 39 is not understood. If the peak temperature on Fig. 38 was increased to 16000 ^{o}K the increase in the radiance would only be about a factor of three. If we assessed all of the possible uncertainties (short of possible non-equilibrium effects) we could account for at most one and a half order of magnitude error. At this point there is not enough information to account for the difference between the measured and calculated results. Radiative non-equilibrium effects might be the reason for the discrepancy.

The measured and calculated radiance distributions have similar shapes which suggests that the kinetic temperature distributions are approximately similar. The distributions show that the peak temperature is forward of the arc axis since these radiance distributions could not be the result of a cylindrically symmetric temperature distribution.

Station 0 on Fig. 39 is in a region of steep temperature gradients as it represents the summation of intensities along line 0 on Fig. 38. Thus station 0 essentially represents a temperature of 7200 ^{o}K since the contribution to N from temperatures other than 7200 ^{o}K is negligible because their path lengths along line 0 are small. On the other hand, station 21 is in a region of shallow temperature gradients and

the contribution to N from temperatures other than 7200 ^{o}K along line 21 is significant. Thus the boundary of a luminous region represents a temperature and temperature gradient combination, and a temperature can be assigned to this boundary only if the temperature gradients are steep.

TABLE II. ANGLE DATA FOR VISUAL OBSERVATIONS OF RUN 657

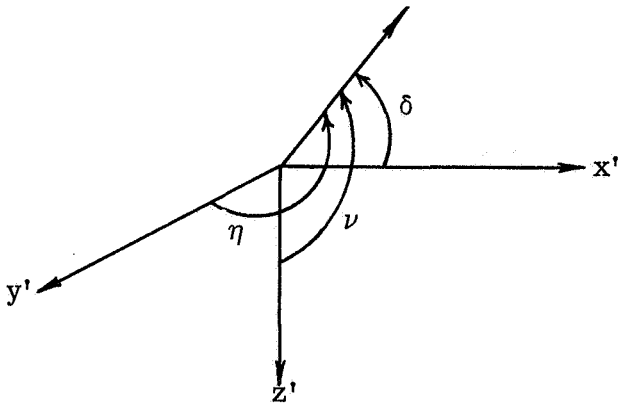

Angles in degrees

	δ	η	ν
Arc axis (normal to cross-section plane)	19	90	109
Side-on View:			
Look vector	127	-38	96
Normal to scan plane	42	59	116
Head-on View:			
Look vector	-16	106	79
Normal to scan plane	79	90	169

Notes:

1. x' is positive downstream along the electrode.
2. The Look vector is along the line of sight.
3. The scan plane is the plane for the microdensitometer scan shown on Fig. 26.

VI. CONCLUSIONS

This investigation was an experimental and theoretical analysis of the convected balanced arc. The experimental part of the investigation was carried out on high current arcs (175 to 500 amperes) immersed in a supersonic airstream at Mach numbers of 2. 5, 3. 0 and 3. 5. Based upon the experimental results the following conclusions are made:

1. For cone cylinder electrodes and a supersonic airstream the arc always slanted with the anode spot upstream of the cathode spot. The angle of slant at a reference station one-third of the distance from the anode to the cathode was near the free stream Mach angle. The slant angle at a constant Mach number increased slightly with increasing current. The velocity normal to the arc leading edge varied approximately as $u_{\infty_n} \sim I^{1/4}$.

2. The electric field was constant for a given Mach number (i. e. constant P_∞ and T_∞) and currents greater than about 250 amperes.

3. The transverse d_T and streamwise d_S dimensions of the arc increased with increasing current for a given M_∞ according to $d \sim \sqrt{I}$.

4. The value of the magnetic field B at the reference station was nearly constant for a given Mach number.

5. The normal force coefficient C_D based upon d_T and the normal free stream dynamic pressure q_{∞_n} was nearly constant at 1.75 for all three Mach numbers.

6. The arc effective temperature T_σ (temperature corresponding to a mean conductance $\bar{\sigma}$ or current density) for a given M_∞ was nearly constant.

7. The rate of energy transfer per unit length from the arc column by radiation and mass transfer at the boundary was small compared to the input energy gradient EI. Thus the joule heating was balanced primarily by forced convection heat transfer at the boundary.

8. Microdensitometer scans of the arc photographs showed the peak temperature to be located well forward of the arc axis. Results from the numerical solution of the governing equations showed the same feature. A microdensitometer scan (optical density distribution) of the side-on view from a typical run was converted to a radiance distribution. This measured radiance distribution was three orders of magnitude higher than the calculated distribution (gas assumed optically thin and in LTE). The measured and calculated radiance distributions had similar shapes, however, suggesting similar kinetic temperature distributions.

The theoretical analysis was based upon a continuum fluid in LTE and the experimental observation that the convected balanced arc is impervious to the free stream. The physical model chosen for the arc column consists of 1) an arc core or interior region, 2) an external region of free stream flow and 3) an interaction region separating the interior and exterior regions. The interaction region has the features of a boundary layer but it is not necessarily thin everywhere. The model assumes that μ is constant at a mean value, and that the energy transfer from the arc column by radiation and mass transfer is small compared with EI. This model permitted the study of the arc core independent of the external flow and interaction region. The theoretical analysis of the uniform column based upon the above model indicated the following conclusions:

1. A characteristic velocity for the arc core is $u_1=\sqrt{\sigma_1 \, E B \, d_S/\rho_1}$ in agreement with Harvey. This velocity represents the effective increase in the kinetic energy of a fluid element due to the work done by the Lorentz force over the distance d_S. Based upon u_1 and a characteristic dimension and temperature the significant similarity parameters for the arc core are the Lorentz number $L_c = \rho_1 BI d_1/\mu_1^2$ (analogous to the Grashof number in natural convection problems), the power gradient parameter $P_L = EI_1/\phi_1$, the Prandtl

number $Pr_1 = \mu_1 h_1/\phi_1$ and the Eckert number $K_1 = u_1^2/h_1$. Since the arc is balanced in the moving stream with nearly constant C_D, $L_c \sim Re_{\infty_n}$.

2. As L_c becomes large (i. e. increasing u_{∞_n}) the heat conduction, viscous dissipation and pressure work terms in the energy equation become negligible compared to the joule heating and convection terms. At large L_c the coefficient of the joule heating term $K_{JH} = EI/\phi_1 Pr_1 \sqrt{L_c}$ becomes constant. Thus at large L_c we must have $EI/\phi_1 \sim \sqrt{L_c}$. The characteristic relation for constant P_∞ becomes $E \sim u_{\infty_n}^{2/3}/I^{1/3}$.

3. For large L_c and T_1 and C_D constant, the theory predicts $D \sim I^{2/3}/u_\infty^{1/3}$ and $B \sim u_\infty^{5/3}/I^{1/3}$. Thus, as u_{∞_n} increases for constant I, the size of the arc (as represented by D) decreases and E increases. At the same time B would increase to keep the Lorentz force equal to the drag force. This behavior is observed experimentally.

4. The numerical solution of the governing equations for the arc core indicates that the one-dimensional equations give a satisfactory approximation for the temperature distribution along the x axis. As K_{JH} decreases to its constant value for large L_c the calculated peak temperature shifts to

its most forward position. If L_c is increased further (for constant I and P_∞) the temperature isotherms distort around the periphery of the front half of the arc and the temperature distribution along the x axis becomes more flat.

The experimental results from Roman (Ref. 19) and the present investigation were used to test the theoretical model. Based upon this comparison the following significant conclusions are made:

1. For large L_c the present theory simplifies the energy equation considerably and predicts $EI/\phi_1 \sim \sqrt{L_c}$ which is in close agreement with UM data. Roman's data, however, displays an $EI/\phi_1 \sim L_c$ behavior and is in the low L_c region where the effects of heat conduction, viscous dissipation, pressure work, self-field, etc. are significant.
2. If the data from Roman and the present study is expressed as $\log \left\{ (E - E_o)I/Pr_1 \phi_1 \right\}$ versus $\log L_c$, Roman's data collapses about a curve having a slope of 1.0 and the present data collapses about a curve having a slope near 1/2. A continuous curve drawn through the two sets of data appears to describe the macroscopic behavior of the convected balanced arc from low L_c to large L_c.
3. The results are consistent with the hypothesis of a uniform impervious slanted arc column.

LIST OF REFERENCES

1. Finkelnburg, W. and Maecker, H., "Electric Arcs and Thermal Plasma", Handbuck Des Physik, Vol. XXII,(1956), pp. 254-444.

2. Von Engel, A., "Ionized Gases", Oxford, Clarendon Press, (1965).

3. Ecker, G., "Electrode Components of the Arc Discharge", Ergebn. d. exakt. Naturw XXXIII, (1963), pp. 1-104.

4. Cobine, J.D., "Gaseous Conductors", Dover, (1958), pp. 290-348.

5. Lee, T.H., "A Closer Look at an Arc Cathode", Sixth International Symposium on Ionization Phenomena in Gases, Paris, France, July 1963.

6. Lee. T.H., Greenwood, A., Breingan, W.D., and Fullerton, H.P., "An Analytical Study of the Physical Processes in the Cathode Region of an Arc", ARL 66-0065, April 1966.

7. Hoh, F.C., "Low Temperature Plasma Diffusion in a Magnetic Field", Rev. of Modern Physics, 34, (1962), p. 267.

8. Thompson, W.B., "An Introduction to Plasma Physics", Pergamon Press, (1962), pp. 25-42.

9. Uhlenbusch, J., "Theory and Calculation of Stationary and Quasistationary Cylindrical Arcs", ARL 65-109, May 1965.

10. Krizhanskii, S.M., "Theory of the Positive Column in an Arc Discharge", Soviet Physics-Technical Physics, Vol. 7, No. 2, August 1962, p. 129.

11. Champion, K.S.W., "The Theory of Gaseous Arcs: I. The Fundamental Relations for the Positive Column", Proc. Physical Society, LSV, 5-B, 1952.

12. Tonks, L. and Langmuir, I., Phys. Rev. 34, (1929), p. 876.

13. Edels, H., "Properties and Theory of the Electric Arc", The Institution of Electrical Engineers, Paper No. 3498, February 1961.

14. Stine, H. and Watson, V., "The Theoretical Enthalpy Distribution of Air in Steady Flow Along the Axis of a Direct Current Arc", NASA TN D-1331, (1962).

15. Maecker, H., Z. Physik, 157, (1959), p. 1.

16. Thiene, P. G., Chambers, J. B., and Von Jaskowsky, W., "An Experimental Investigation of the Behavior of an Arc Positive Column in the Presence of Forced Convection", Plasmadyne Report 682 (1961).

17. Bond, C. E., "The Magnetic Stabilization of an Electric Arc in Transverse Supersonic Flow", ARL Report 65-185, Wright-Patterson AFB, Ohio, October 1965.

18. Myers, T. W., McKinnon, C. N., and Lysen, J. C., "Experimental Investigation of a Magnetically Balanced Arc in a Transverse Argon Flow", J. of Engr. for Power, 88-1, January 1966, pp. 27-30.

19. Roman, W. C., "Investigation of Electric Arc Interaction with Aerodynamic and Magnetic Fields", Ph. D. Dissertation, Ohio State University, (1966).

20. Meyers, T. W. and Roman, W. C., "Survey of Investigations of Electric Arc Interactions with Magnetic and Aerodynamic Fields", ARL 66-184, September 1966.

21. Bond, C. E. and Potillo, R. W., "Stability and Slanting of the Convective Electric Arc in a Thermionic Rail Accelerator", AIAA Electric Propulsion and Plasmadynamics Conference, AIAA Paper No. 67-674, September 11-13, 1967.

22. Zauderer, B., "Discharge Structure and Stability of a Linear, Non-Equilibrium MHD Channel", AIAA Electric Propulsion and Plasmadynamics Conference, AIAA Paper No. 67-718, September 11-13, 1967.

23. Edels, H. and Craggs, J.D., "The Coefficients of Thermal and Electrical Conductivity in High Temperature Gases", Progress in Dielectrics - 5, 1962.

24. Shkarofsky, Bachynski, and Johnston, "The Particle Kinetics of Plasmas", Addison-Wesley, 1966.

25. Sutton, G.W. and Sherman, A., "Engineering Magneto-hydrodynamics", McGraw-Hill, 1965.

26. Malliaris, A.C., "Experimental and Analytical Study of the Fundamental Interaction and Energy Exchange Processes Between Electric Arc Discharges and Cross-Flow Fields of Pre-Ionized Gases with and without the Presence of Transverse Magnetic Fields", ARL 64-216, December 1964.

27. Anderson, J.M., "Hall Effect and Electron Drift Velocities in the Plasma of the Positive Column", Physics of Fluids, 7, (1964), p. 9.

28. Somerville, J.M., "The Electric Arc", Meuthen and Co., Ltd., 1959.

29. Progress Report, February 28, 1965, Contract AF 33(657)-8819 and Final Report, June 1, 1965, monitored by Thermomechanics Branch, ARL, Wright-Patterson AFB, Ohio.

30. Kuethe, A.M., Harvey, R.L., and Nicolai, L.M., "Model of an Electric Arc Balanced Magnetically in a Gas Flow", AIAA Paper No. 67-96, (1967).

31. Harvey, R.L., "An Experimental and Theoretical Investigation of Magnetically Balanced Arcs", Ph.D. Dissertation, Univ. of Michigan, (1968).

32. Weinbaum, S., "Natural Convection in a Horizontal Circular Cylinder", J. of Fluid Mechanics, 18, Part 3, (1964).

33. Ostrach, S. and Menald, E.R., "Natural Convection in a Horizontal Cylinder at Large Prandtl Numbers", AFOSR TR 65-2239, November 1965.

34. Yos, J., "Transport Properties of Nitrogen, Hydrogen, Oxygen and Air to 30,000°K", RAD-TM-63-7, March 1963.

35. Burhorn, F. and Wienecke, R., Zeitschrift für Physikalische Chemie, Vol. 215, (1960), pp. 269-284.

36. Han, L.S. and Kihara, D.H., "An Analytical Study of the Heat Transfer from an Electric Arc in Cross-Flow", ARL 66-0193, October 1966.

37. Jakob, M., "Heat Transfer", Vol. I, Wiley and Sons, Inc., New York, 1949.

38. McAdams, W.H., "Heat Transmission", McGraw-Hill Book Co., New York, 1954.

39. Fischer, E. and Uhlenbusch, J., "Interactions of Free Burning Arcs with Transverse Gas Flows in Magnetic Fields", Tech. Univ. of Aachen, Report HMP 111, West Germany, January 1967.

40. Suits, C.G., "High Pressure Arcs in Common Gases in Free Convection", Physical Review, 55, (1939), pp. 561-567.

41. Suits, C.G. and Poritsky, H., "Application of Heat Transfer Data to Arc Characteristics", Physical Review, 55, (1939), pp. 1184-1191.

42. Suits, C.G., "The Temperature of High Pressure Arcs", J. of Applied Physics, 10, (1939), p. 728.

43. Richtmyer, R.D. and Morton, K.W., "Difference Methods for Initial-Value Problems", 2nd edition, Interscience Publishers, (1967).

44. Rieder, W., "Power Balance of the Electrodes and Characteristics of Free Burning Low Current Arcs", Z. für Physik, 146, (1956), pp. 629-643.

45. Busz-Peuckert and Finkelnburg, W., Z. für Physik, 146, (1956), p. 655.

46. Haydon (editor), "Discharge & Plasma Physics", Univ. of New England, Armidale, Australia, (1964).

47. Meyer, R.X., "The Electrical Conductivity of Air Up to 24000°K", U.S. Dept. of Commerce, Office of Technical Services, AD 607 701, June 1958.

48. Bade, W.L. and Yos, J.M., "Theoretical and Experimental Investigation of Arc Plasma Generation Technology", ASD-TDR-62-729, Vol. 2, Part II, September 1963.

49. Hilsenrath, J. and Klein, M., "Tables of Thermodynamic Properties of Air in Chemical Equilibrium Including Second Virial Corrections from 1500°K to 15000°K," AEDC TR-65-58, March 1965.

50. Lord, W.T. and Broadbent, E.G., "An Electric Arc Across an Air Stream", RAE Tech. Report 65055, (1965).

51. Broadbent, W.G., "Electric Arc in Cross-Flow", RAE Tech. Memo 897, (1965).

52. Lord, W.T., "An Electric Arc in a Transverse Magnetic Field: A Theory for an Arc of Low Power", RAE Tech. Report 67086, (1967).

53. Lord, W.T., "Correlation of Voltage-Current Characteristics of Wall Stabilized, Free-Burning and Cross-Flow Arcs", RAE Tech. Report 67087, (1967).

54. Adams, V.W., "The Influence of Gas Streams and Magnetic Fields on Electric Discharges, Part I: Arcs at Atmospheric Pressure in Annular Gaps", RAE Tech. Note 2896, (1963).

55. Crocco, L., "A Suggestion for the Numerical Solution of the Steady Navier-Stokes Equations", AIAA Journal, Vol. 3, No. 10, October 1965, pp. 1824-1832.

56. Krinberg, I.A., "On the Theory of an Electric Columnar Arc Burning Under Conditions of Natural Convection", Soviet Physics-Technical Physics, Vol. 9, November 1964, pp. 684-689.

57. King, L.A., "The Voltage Gradient of the Free-Burning Arc in Air or Nitrogen", Proc. Vth International Conference on Ionization Phenomena in Gases, 1961, Vol. I, North-Holland Pub. Co., Amsterdam, (1962).

58. Rowe, R.D., "The Theory of Free-Convection Arc Columns", Univ. of Oxford, Dept. of Engineering Science, Report No. 1, 045, (1968), p. 68.

59. Ragent, B. and Nobel, C.E., "High-Temperature Transport Coefficients of Selected Gases", ARL Report 62-328, April 1962.

60. Pelzer, H., Technical Report ERA Reference G/XT 164, (1958).

61. Hagenah, W., Z. Physik, 128, (1950), p. 279.

62. Maecker, H., Z. Physik, 136, (1953), p. 119.

63. Wienecke, R., Z. Physik, 143, (1955), p. 128.

64. Khvostov, Nikolay, Moscow Institute of Energy, USSR, Oral communication on 29 March 1968, Univ. of Michigan, Ann Arbor, Michigan.

65. Weber, H.E., "Growth of an Arc Column in Flow and Pressure Fields", AGARDograph 84, Part 2, September 1964.

66. Baum, E. and Cann, G.L., "Interaction Between Electric Arcs and Gas Flows", ARL Report 63-151, Wright-Patterson AFB, Ohio, September 1963.

67. Kookekov, G.A., "Mechanism of Heat Transfer in Transverse Blown Arcs", Engineering and Physics Journal, 9, (1965).

68. Noeske, H., "Interaction of an Electrical Discharge with a Cross-Flow", AF Contract 33(657)-11310, AVCO-Rad Corp., (1965).

69. Morse, F. H. Mitchner, M. and Kruger, C. H., "Microwave Measurement of the Non-equilibrium Electron Density in a Supersonic Plasma Nozzle Flow", AIAA Paper 67-704, September 1967.

70. Podolsky, B. and Sherman, A., "Influence of Tensor Conductivity on End Currents in Crossed Field MHD Channels with Skewed Electrodes", Journal of Applied Physics, Vol. 33, No. 4, (1962), pp. 1414-1418.

71. Howarth, L., "Modern Developments in Fluid Dynamics", Oxford Press, 1953.

72. Slovetskiy, D. I., "Investigation of the Temperature and Cross-Sectional Shape of an Electric Arc Column Moving Along Parallel Electrodes in a Magnetic Field", NASA Technical Translation F-11, 445, November 1967.

73. Kodak Data Handbook for Roll Film, Eastman-Kodak Co., 1968.

74. Roman, W. C., "Some Observations on the Motion of Electric Arcs in Transverse Magnetic Fields", ARL Report 63-151, 1962.

75. Peng, T. and Pindroh, A. L., "An Improved Calculation of Gas Properties at High Temperatures", ARS Preprint No. 1995-61, August 1961.

76. DeVoto, R. S., "Argon Plasma Transport Properties", SUDAER No, 217, Stanford University, February 1965.

77. Drellishak, K. S., Knopp, C. F. and Cambel, A. B, "Partition Functions and Thermodynamic Properties of Argon Plasma", AEDC-TDR-63-146, August 1963.

78. Aroeste, H. and Magee, J. L., "Thermal Radiation Phenomena, Vol. III, Tables of Radiative Properties of Air", Lockheed Report 3-27-67-1, May 1967.

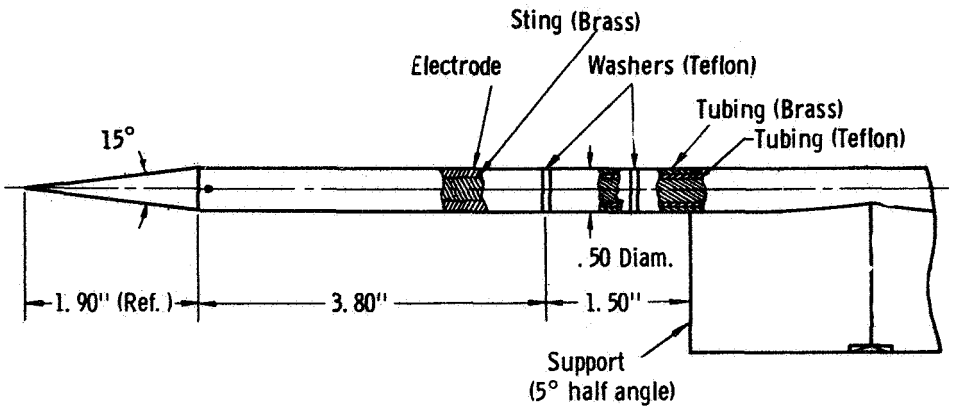

FIGURE 1 Details of electrode and electrode assembly

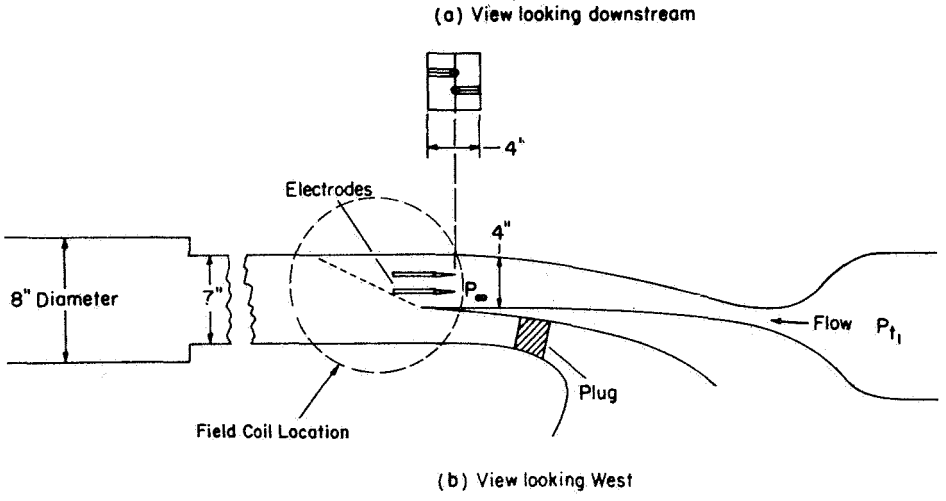

FIGURE 2 Experimental apparatus for convected balanced arcs in a supersonic stream

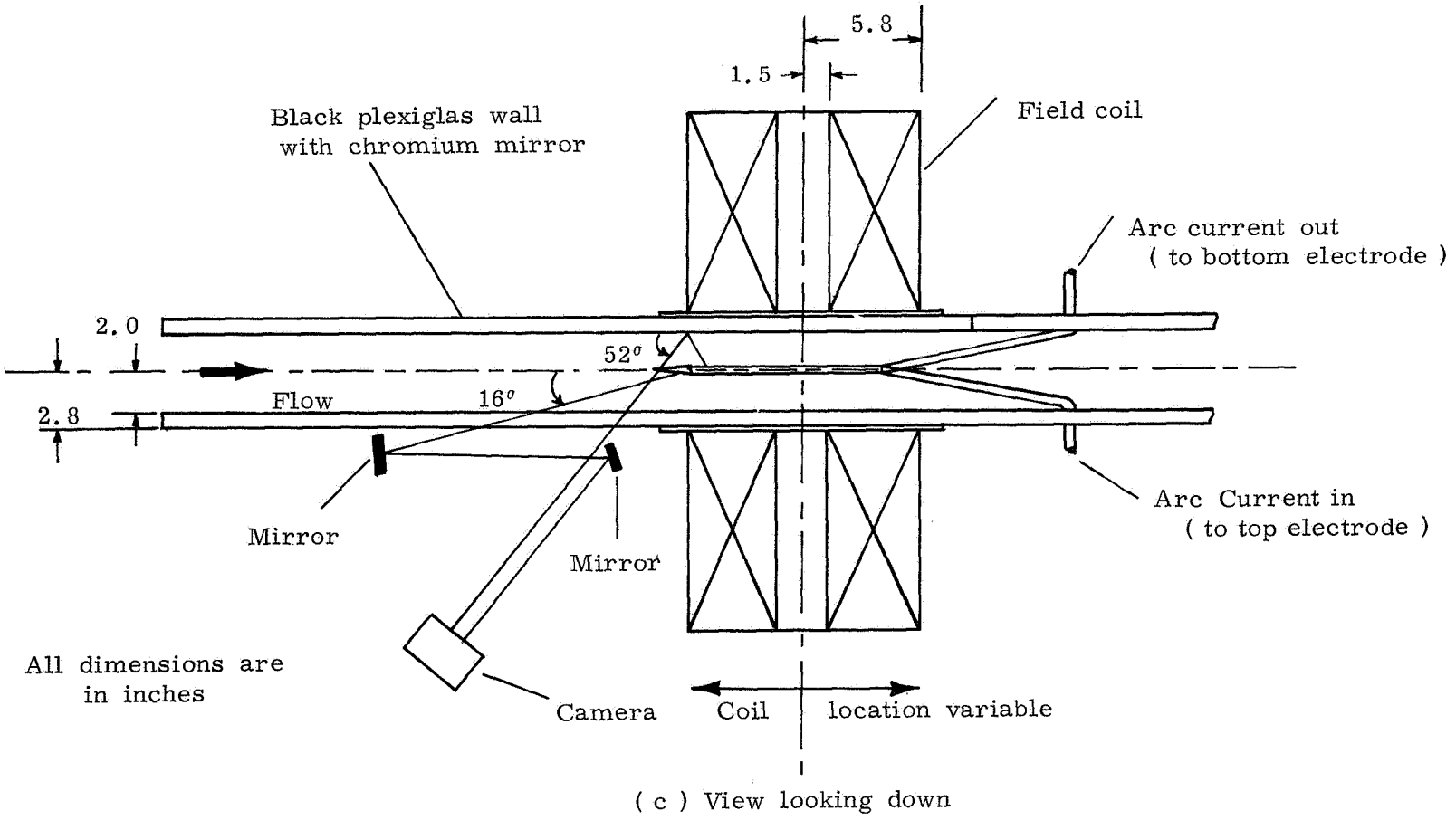

Fig. 2 (cont.) Experimental apparatus for convected balanced arcs in a supersonic stream

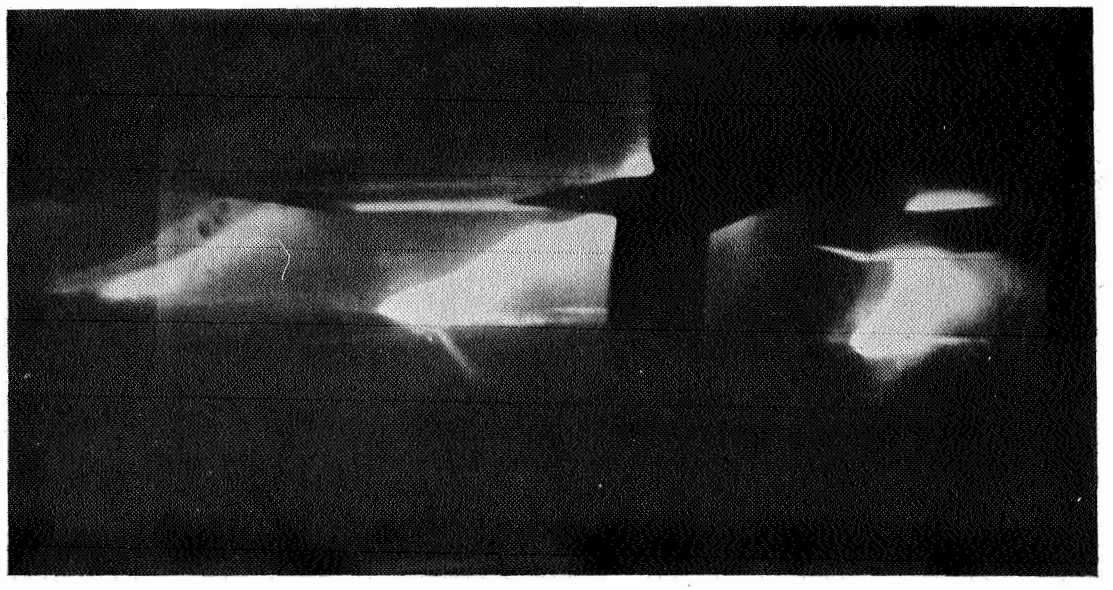

(a) Photograph of steady arc

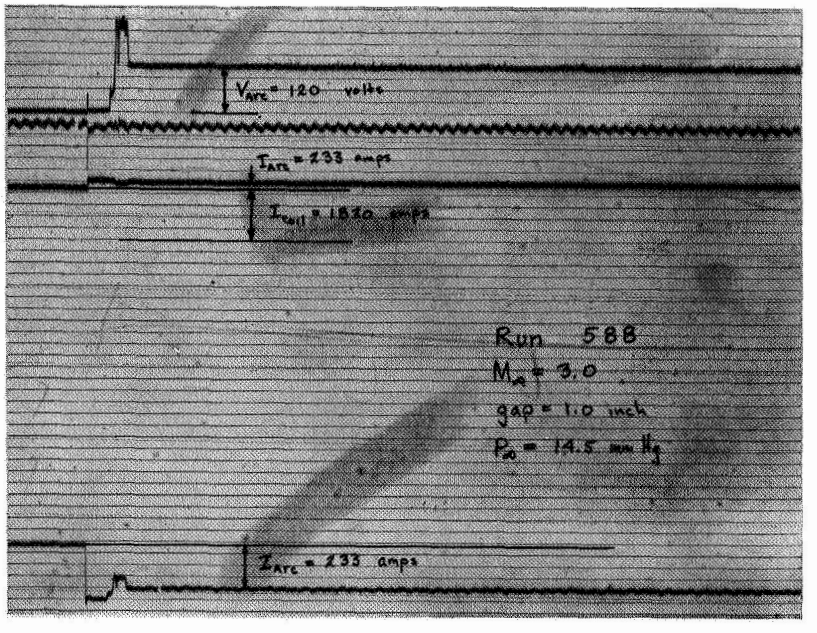

(b) Viscicorder trace of steady arc

FIGURE 3 RUN 588, M_∞ = 3.0, I = 233 amps, gap = 1.0 inch, V_{arc} = 120 volts, copper electrodes

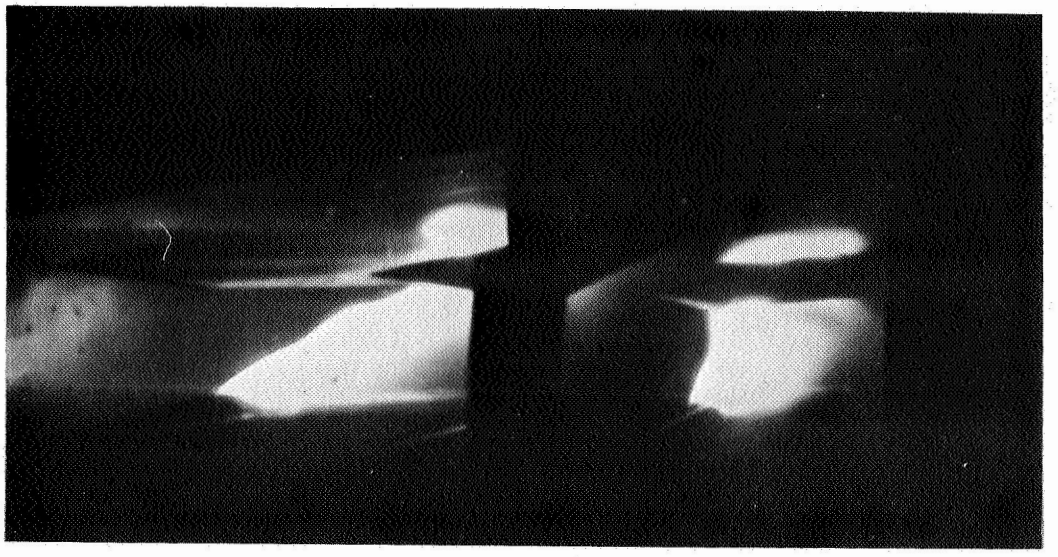

(a) Photograph of a steady arc

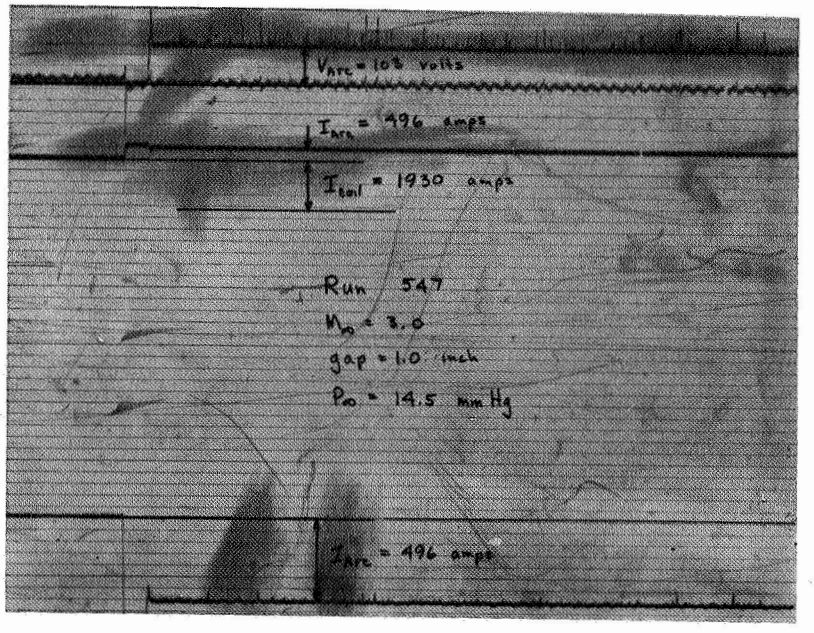

(b) Viscicorder trace of a steady arc

FIGURE 4 RUN 547, $M_\infty = 3.0$, I = 496 amps, gap = 1.0 inch, $V_{arc} = 103$ volts, copper electrodes

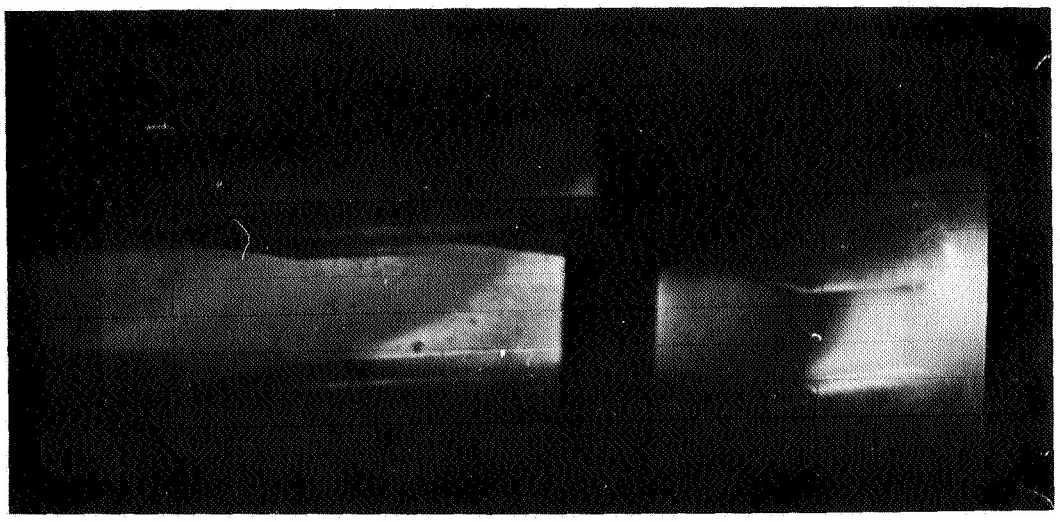

(a) Photograph of an unsteady arc

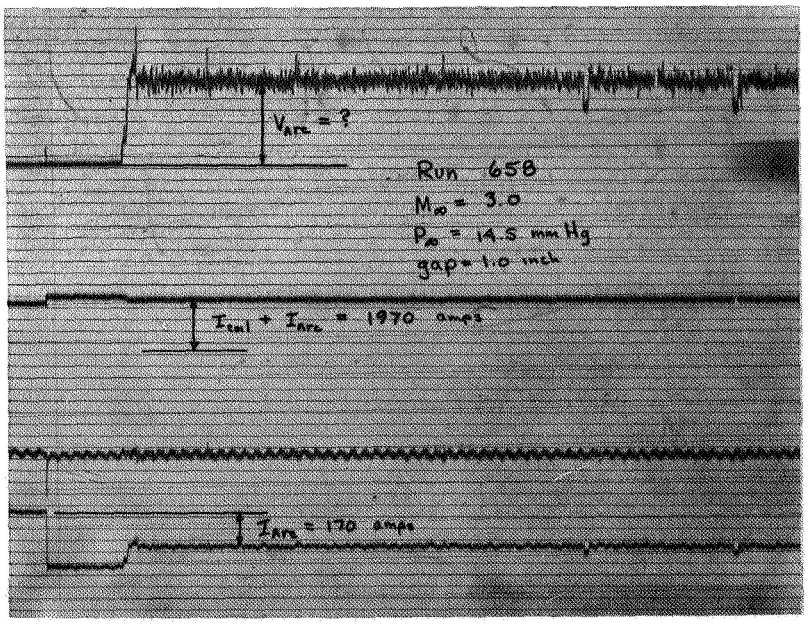

(b) Viscicorder trace of an unsteady arc

FIGURE 5 RUN 658, M_∞ = 3.0, I = 170 amps, gap = 1.0 inch, V_{arc} = ?, copper electrodes

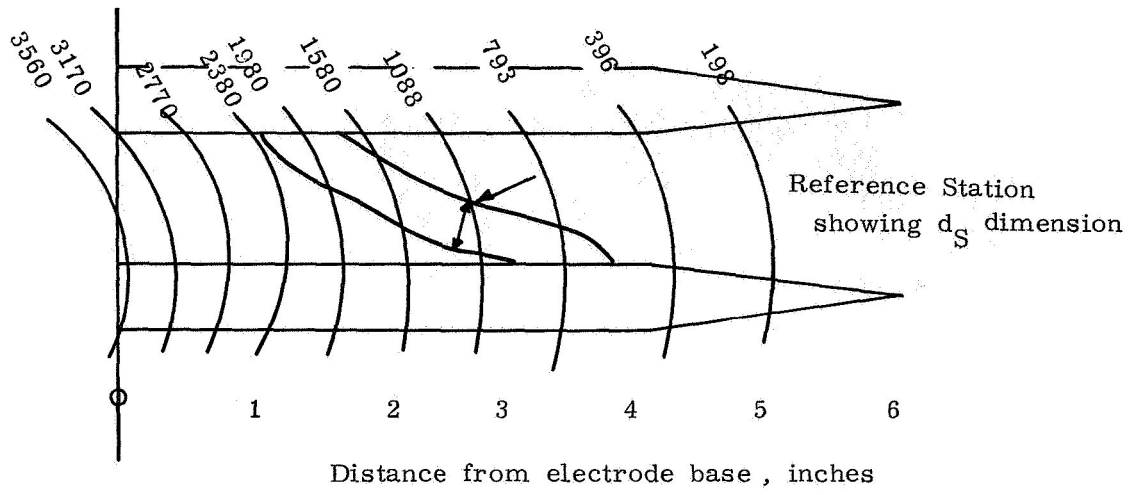

(a) Side view schematic showing magnetic field lines

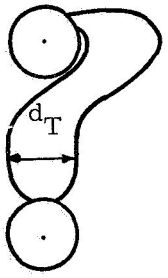

(b) Head-on Schematic

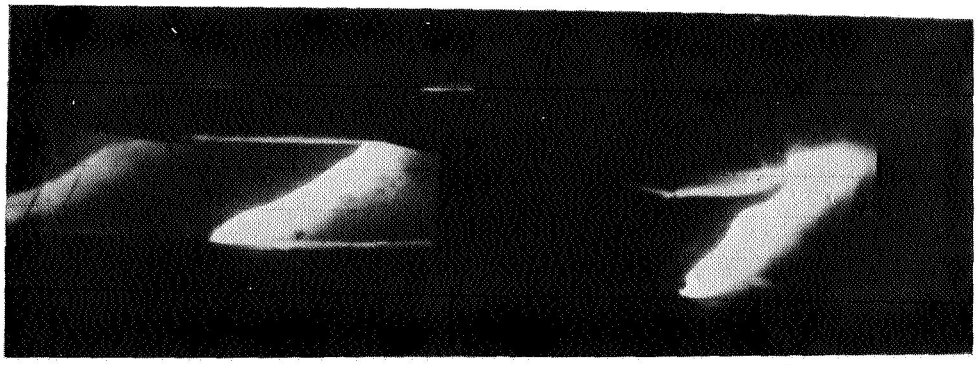

(c) Near side-on and head-on photographs

Fig. 6 RUN 562 , $M_\infty = 3.5$, I = 180 amps , gap = 1.0 inch , V_a = 129 volts, P_∞ = 9.6 mmHg , copper electrode

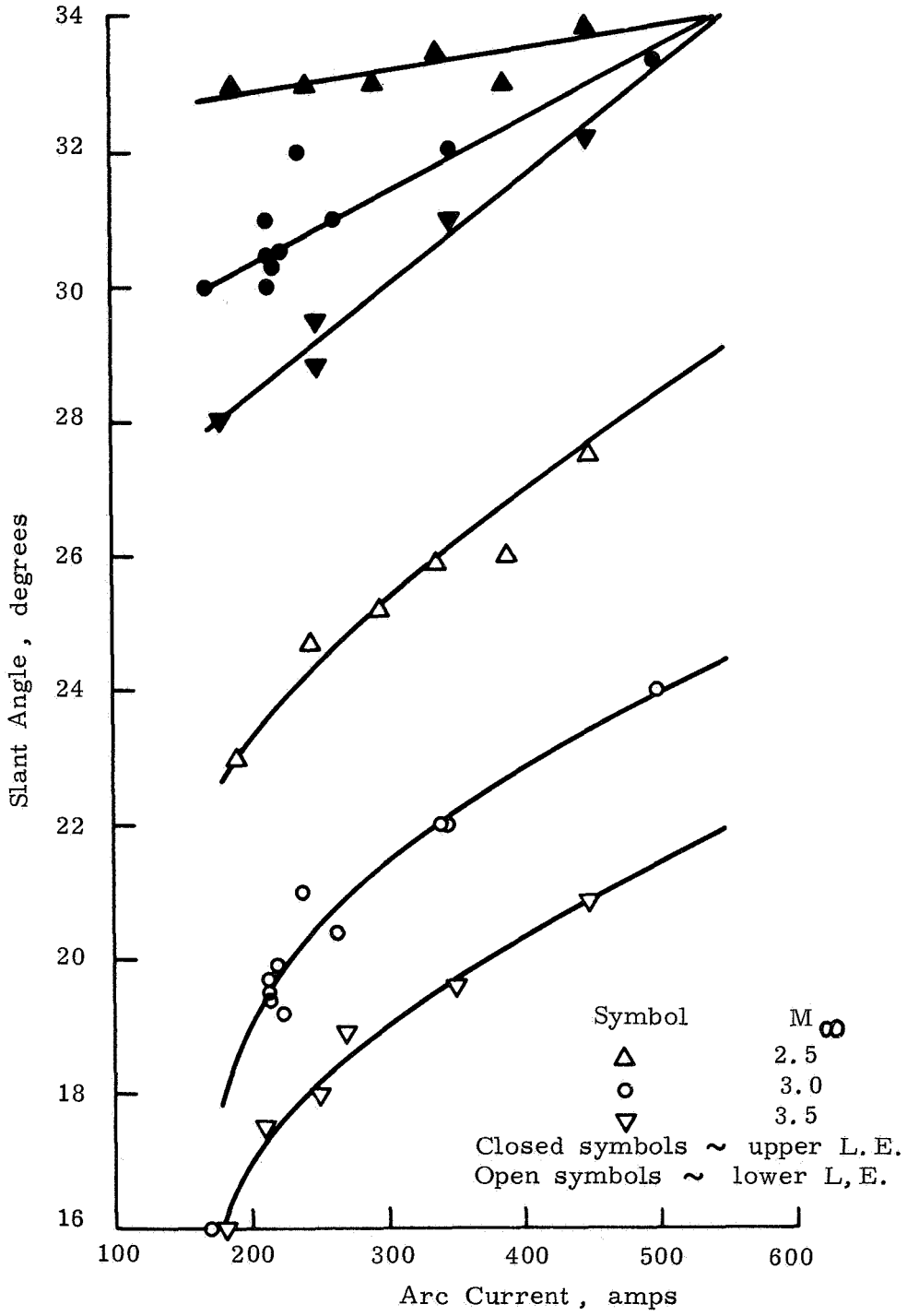

Fig. 7 Observed leading edge slant angles for balanced convected arc in a supersonic stream

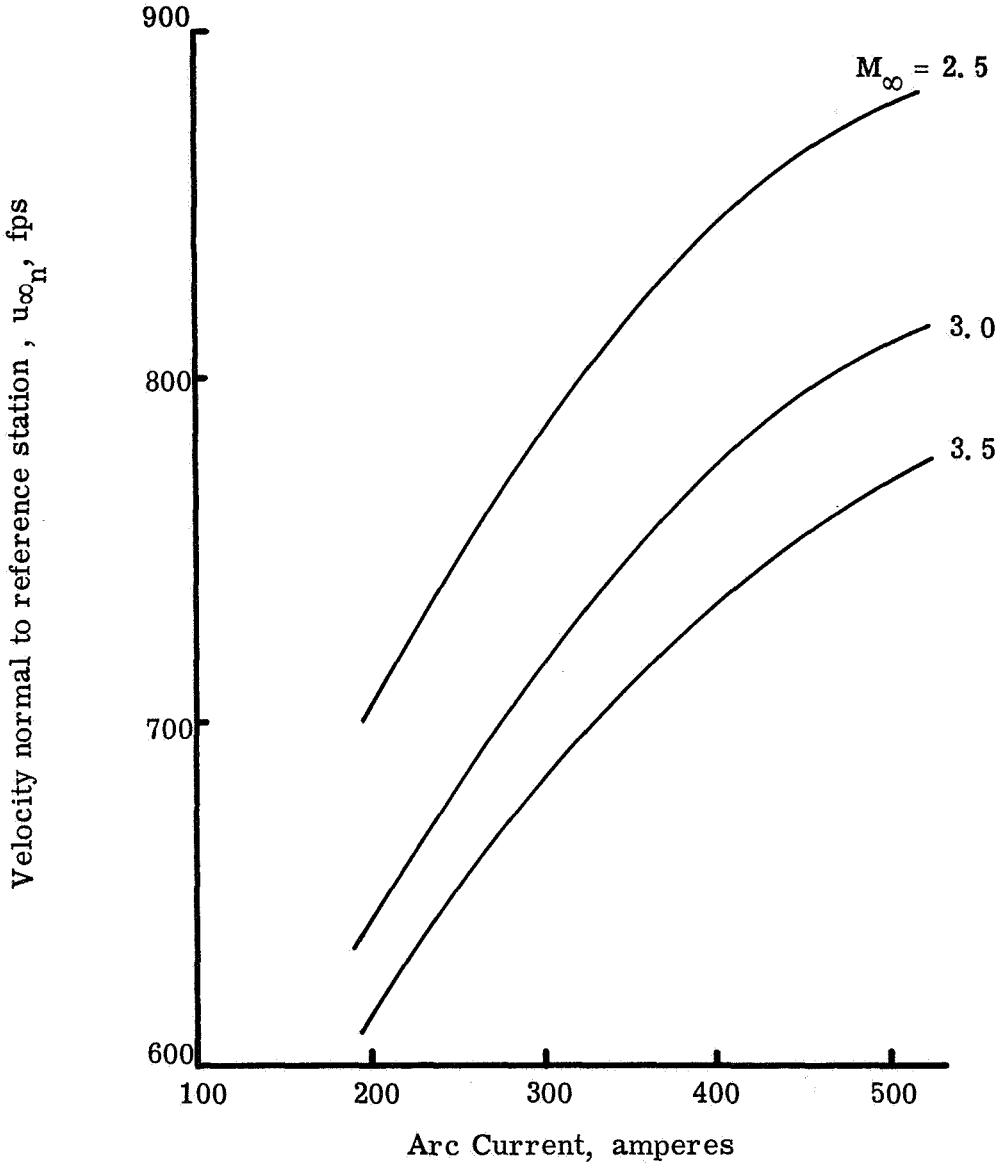

Fig. 7b. Variation of u_{∞_n} with arc current for convected balanced arc in a supersonic stream.

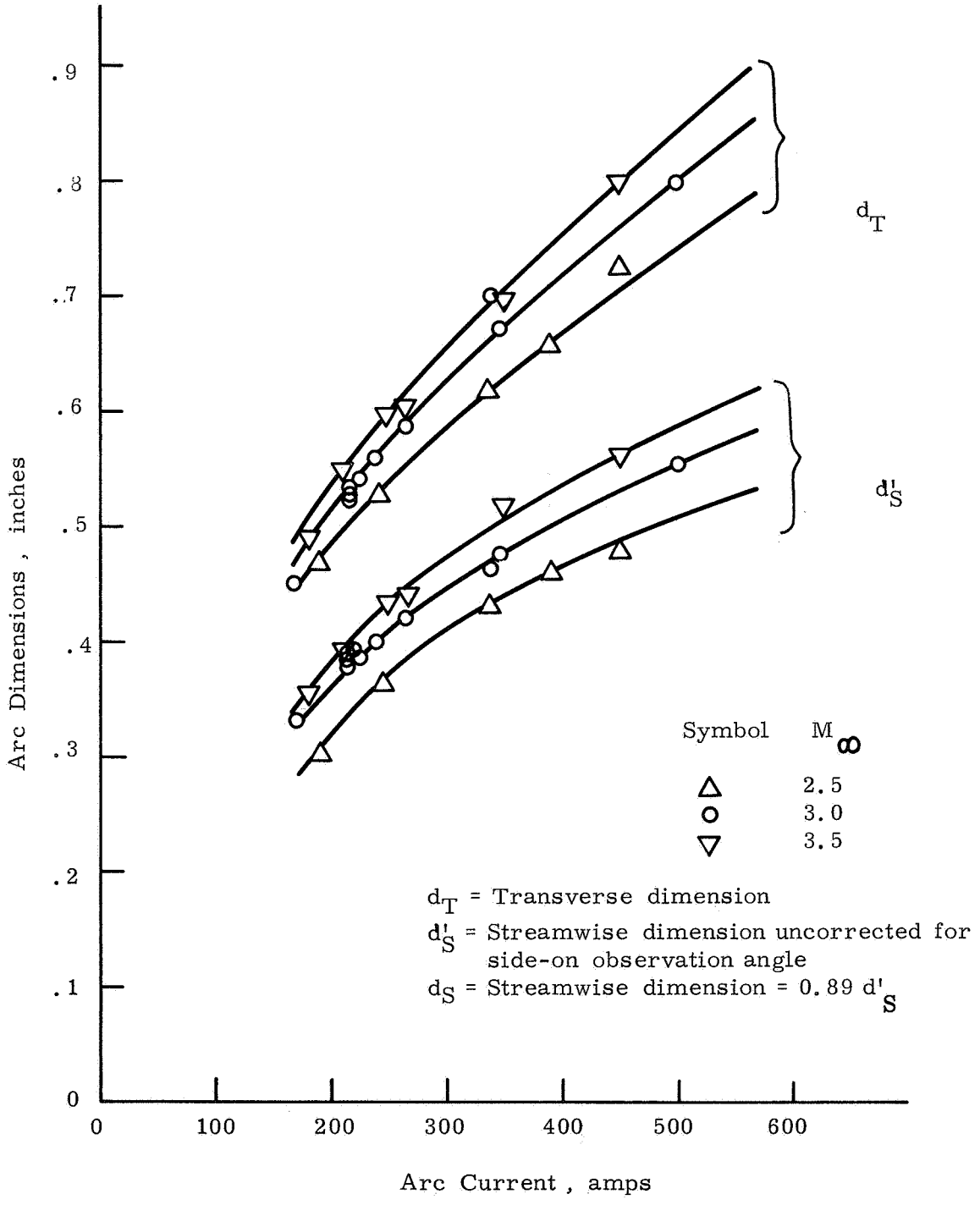

Fig. 8 Observed dimensions of arc luminous region

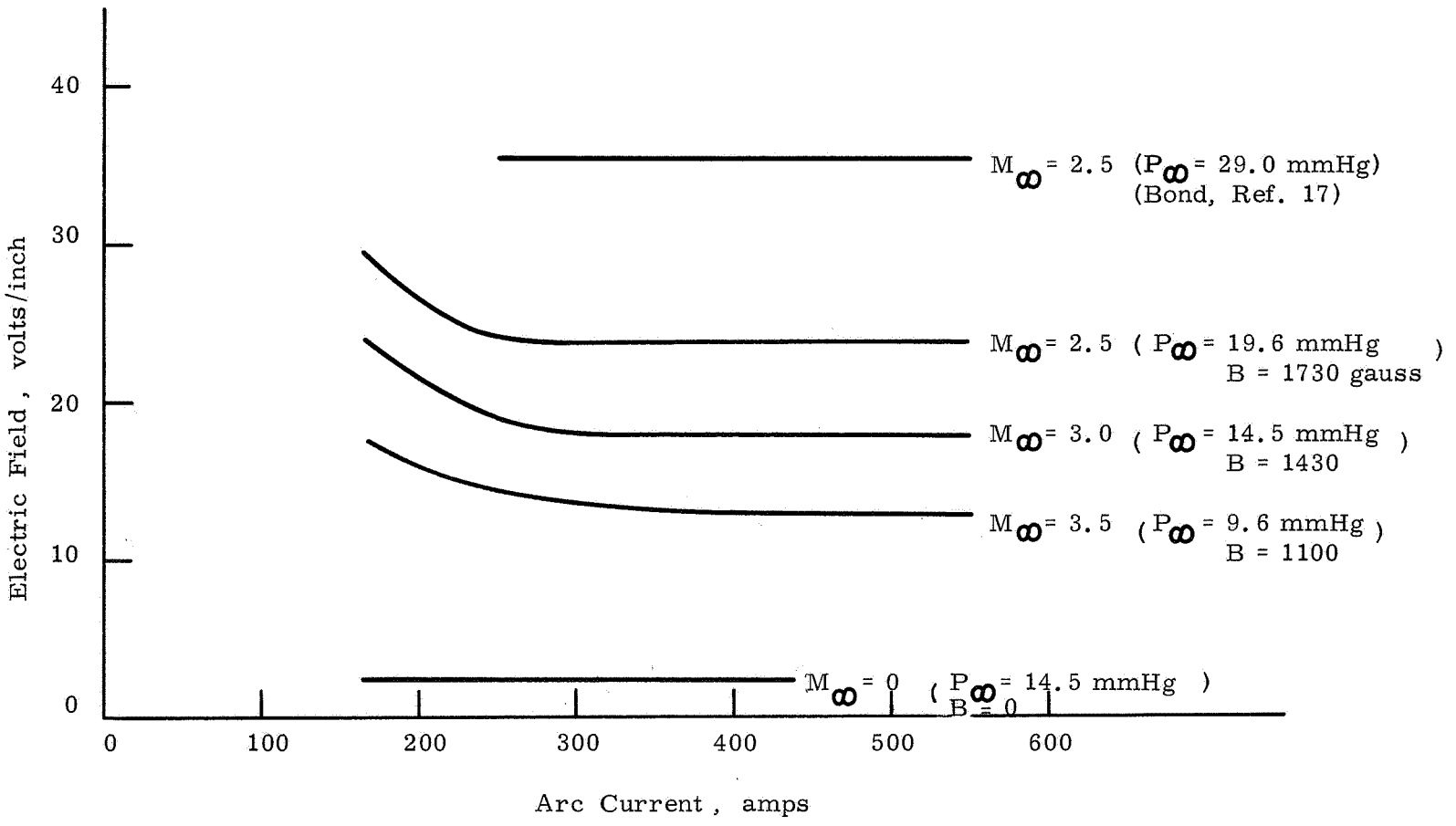

Fig. 9 Electric characteristics for balanced convected arcs in a supersonic stream

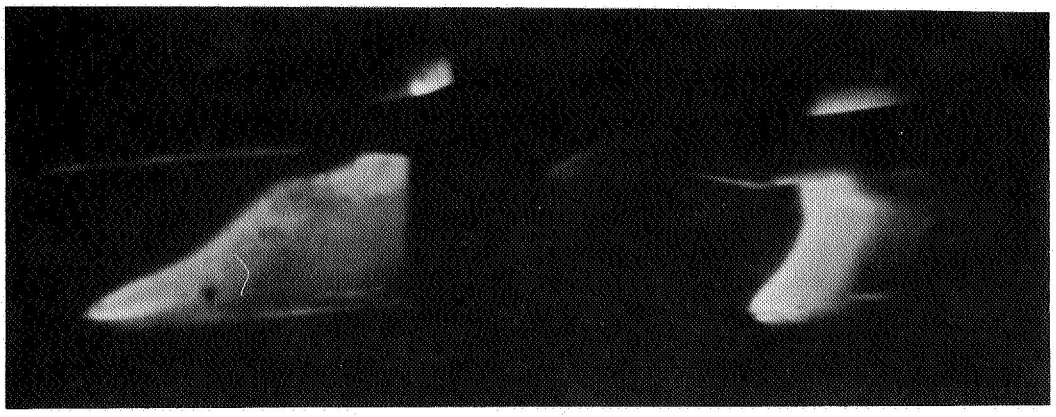

(a) RUN 657 , f/11 at 1/1000 , I = 216 amps

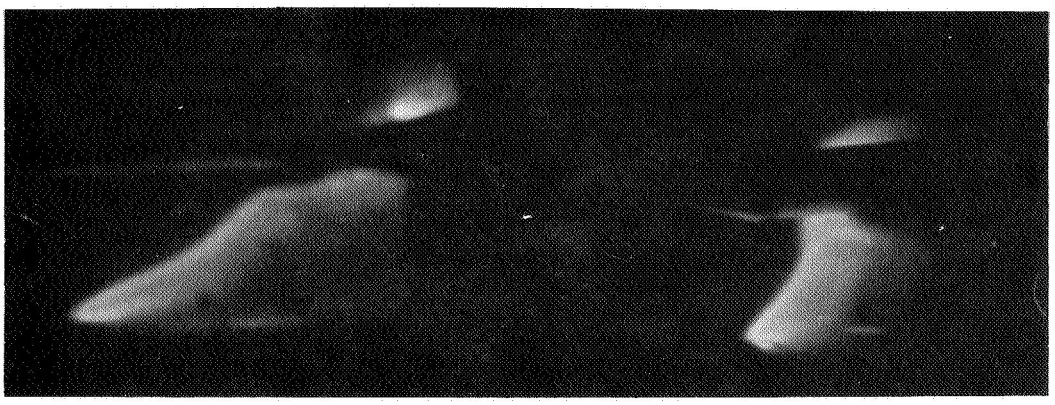

(b) RUN 663 , f/22 at 1/1000 , I = 216 amps

(c) RUN 665 , f/32 at 1/1000 , I = 216 amps

FIGURE 10 Variation of Lens Opening for Mach 3.0

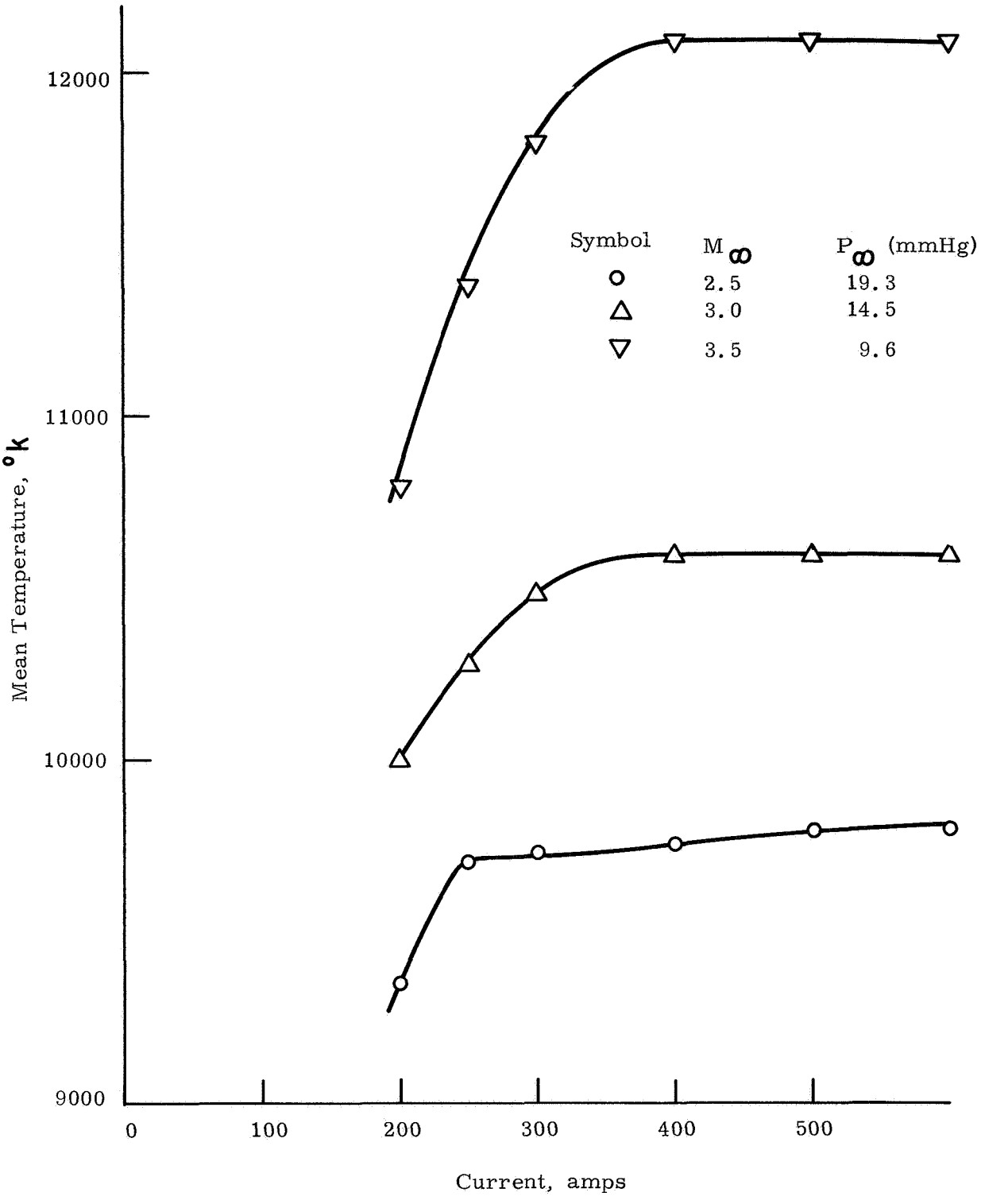

Fig. 11. Calculated effective temperatures T_σ using measured electrical characteristics and dimensions.

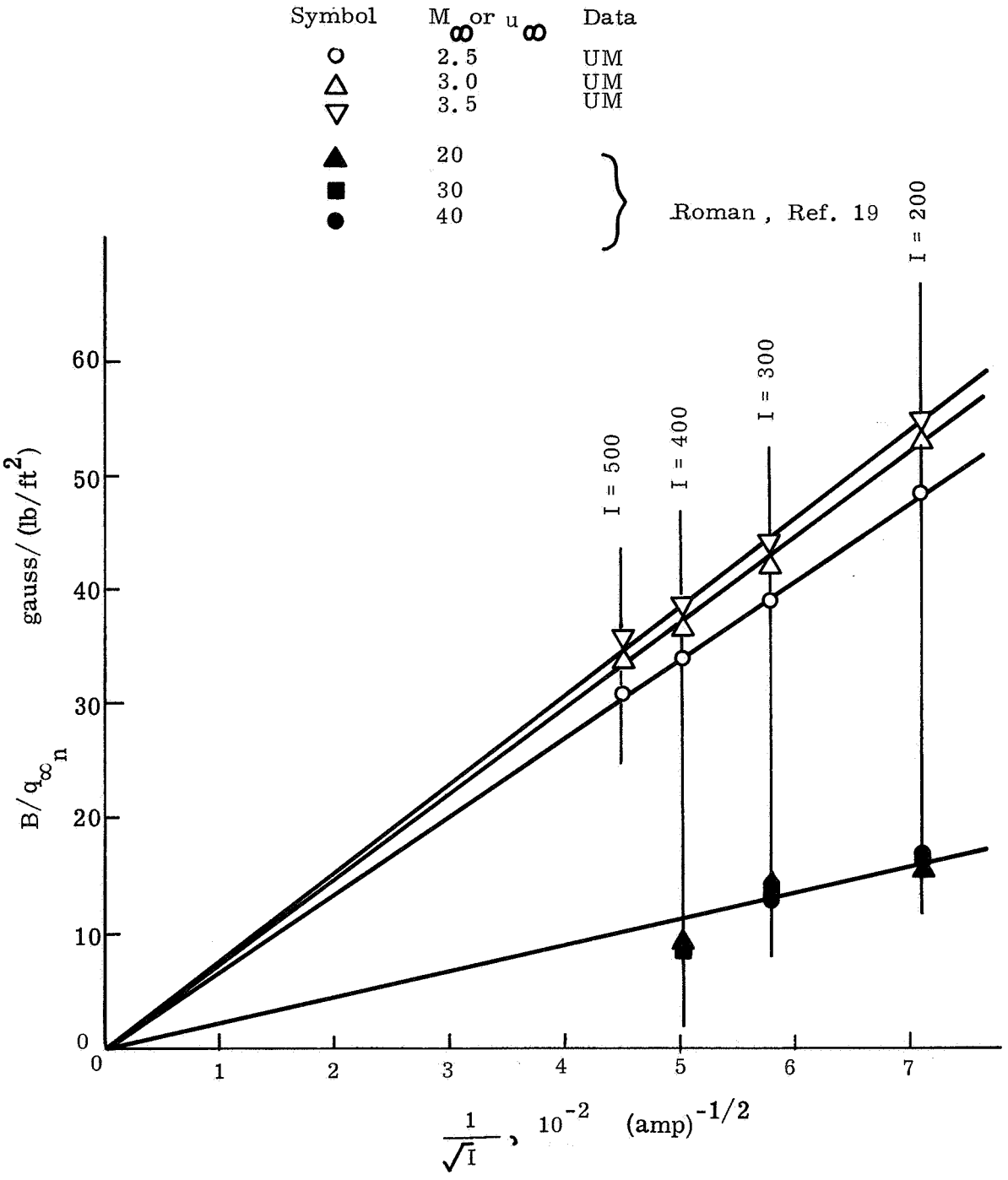

Fig. 12. B/q_{∞_n} variation with $1/\sqrt{I}$ for balanced convected arcs

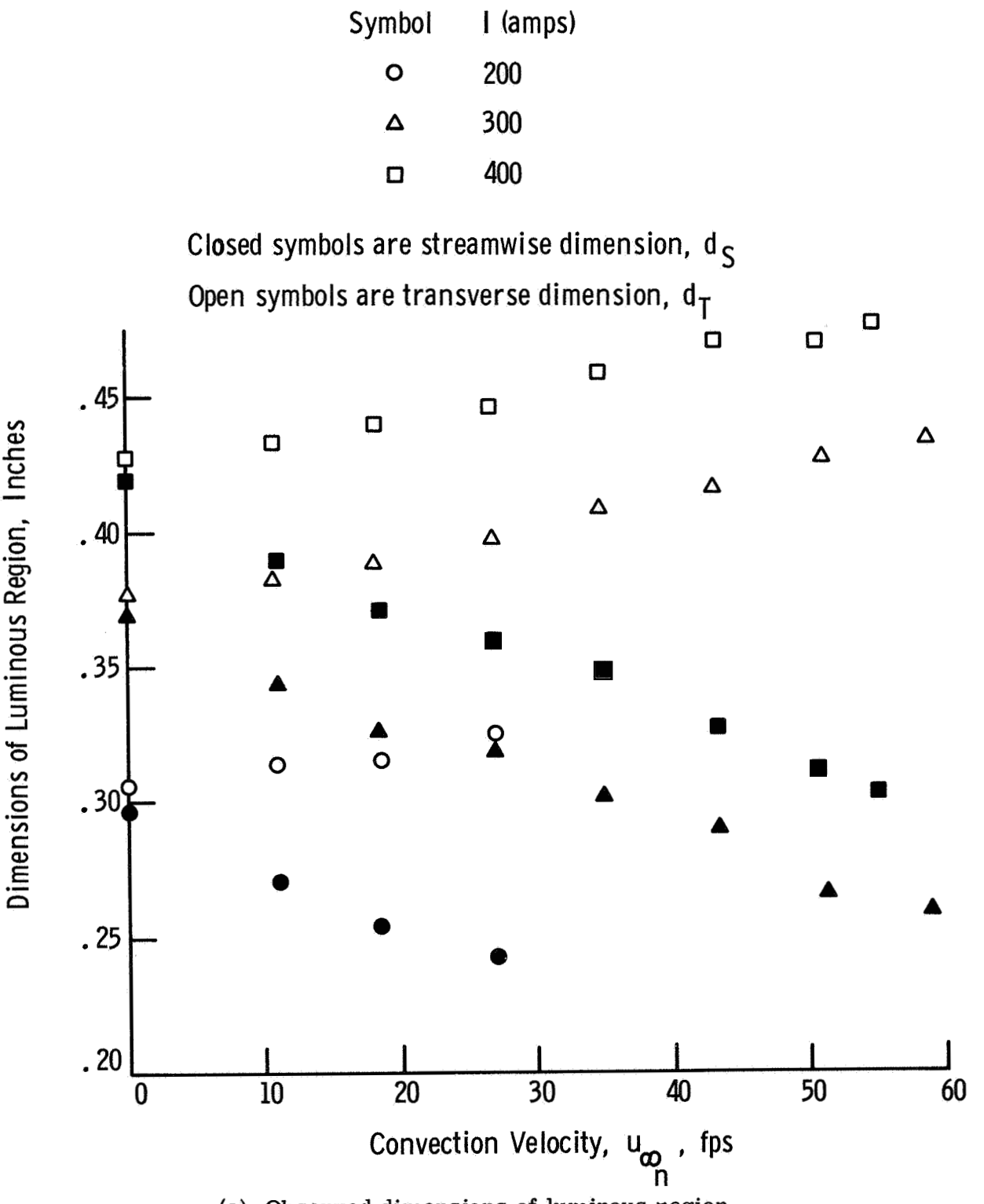

(a) Observed dimensions of luminous region

Fig. 13. Roman's experimental data for an Argon arc burning in air at 1 atm and low speed cross-flow (Ref. 19).

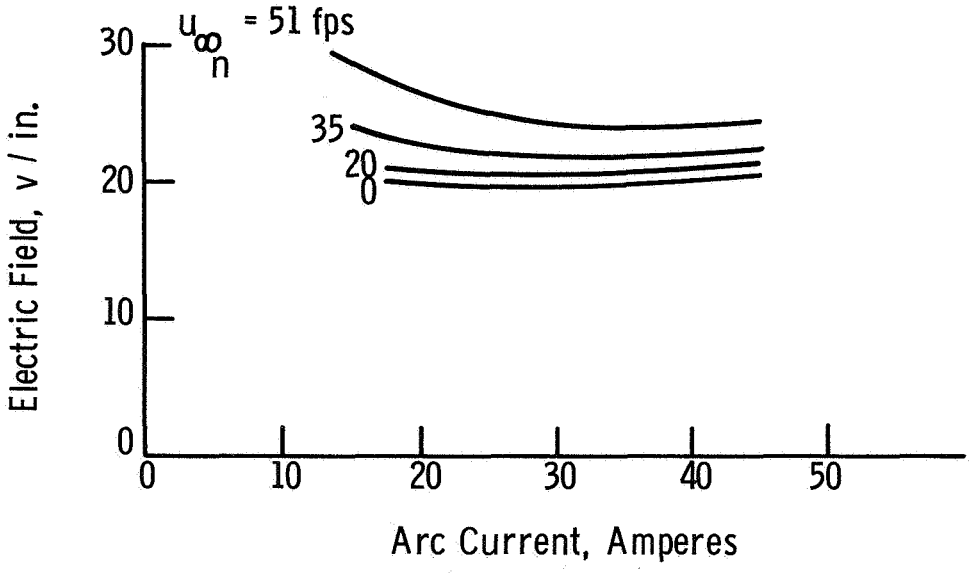

(b) Electric Characteristics

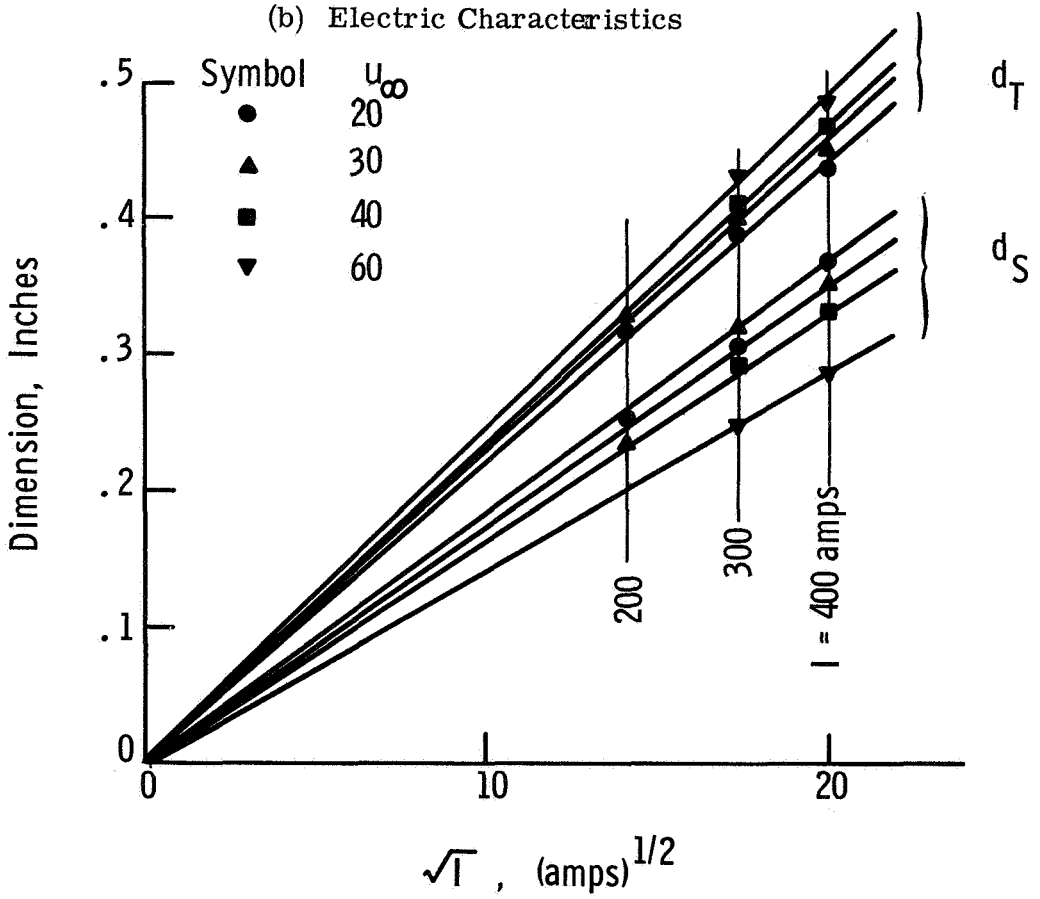

(c) Behavior of d_S and d_T versus $\sqrt{I}$

Fig. 13 (cont.)

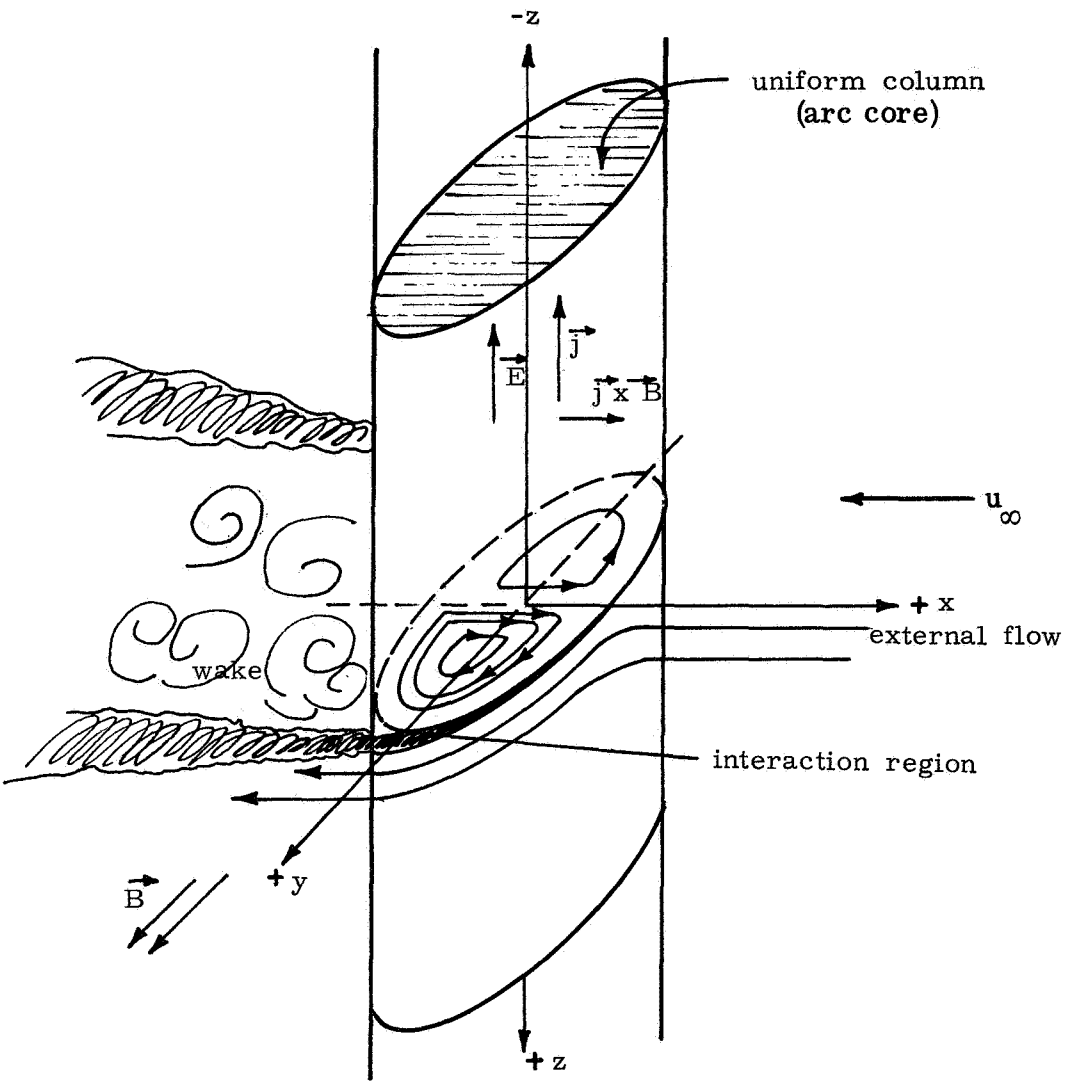

Fig. 14 Physical model of the balanced convected arc

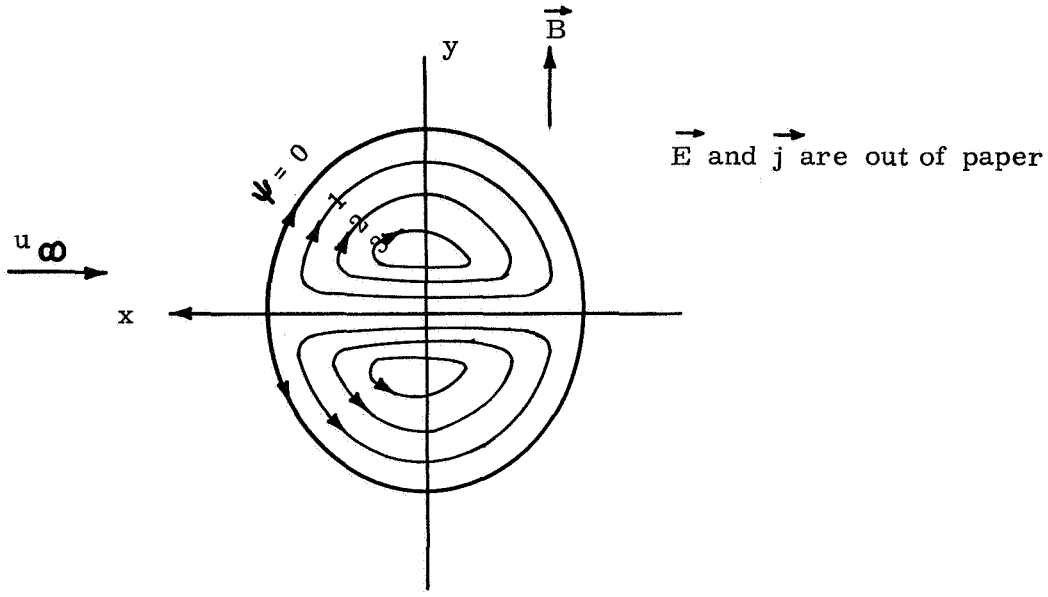

Fig. 15 Streamline pattern for simplified model

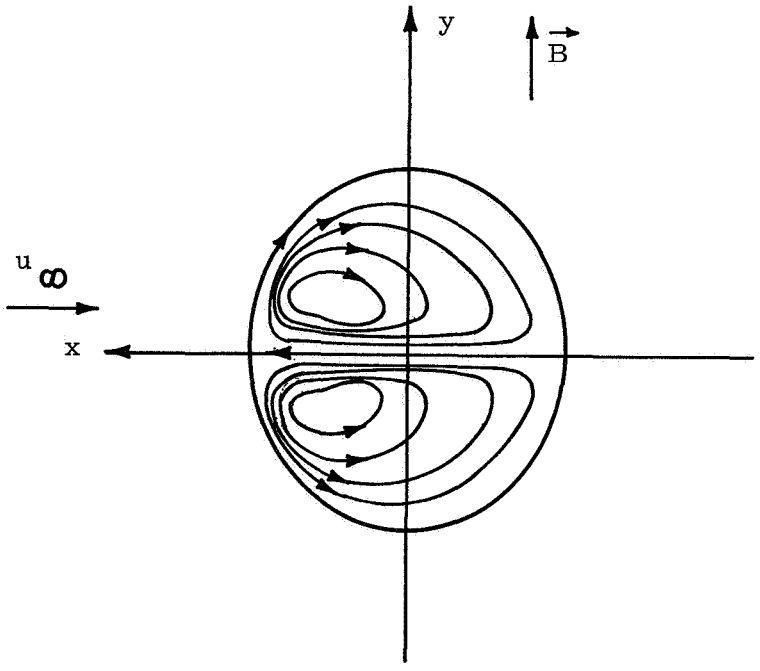

Fig. 16 Possible streamline pattern for no source and no heat conduction in arc interior

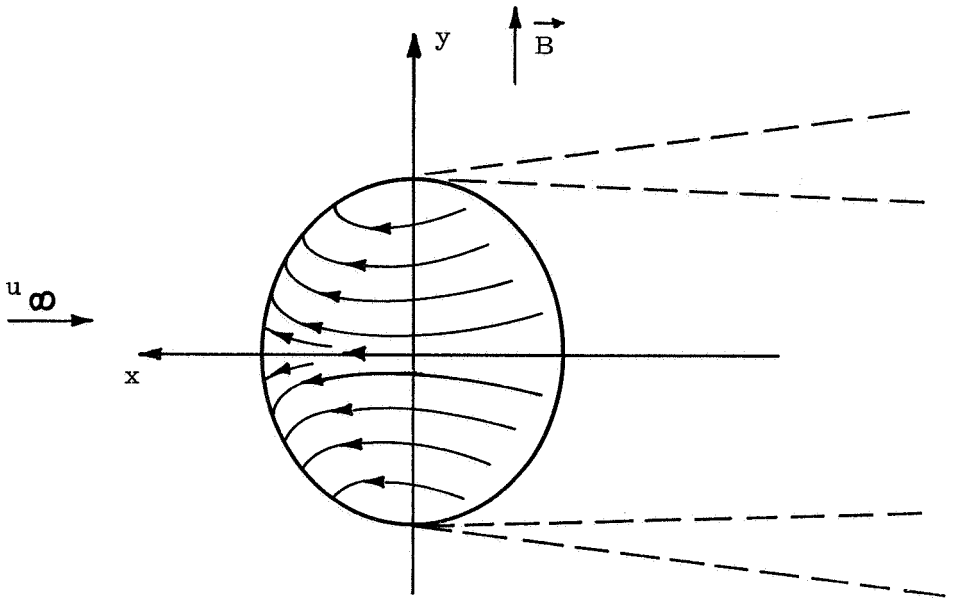

Fig. 17 Possible streamline pattern for source flow

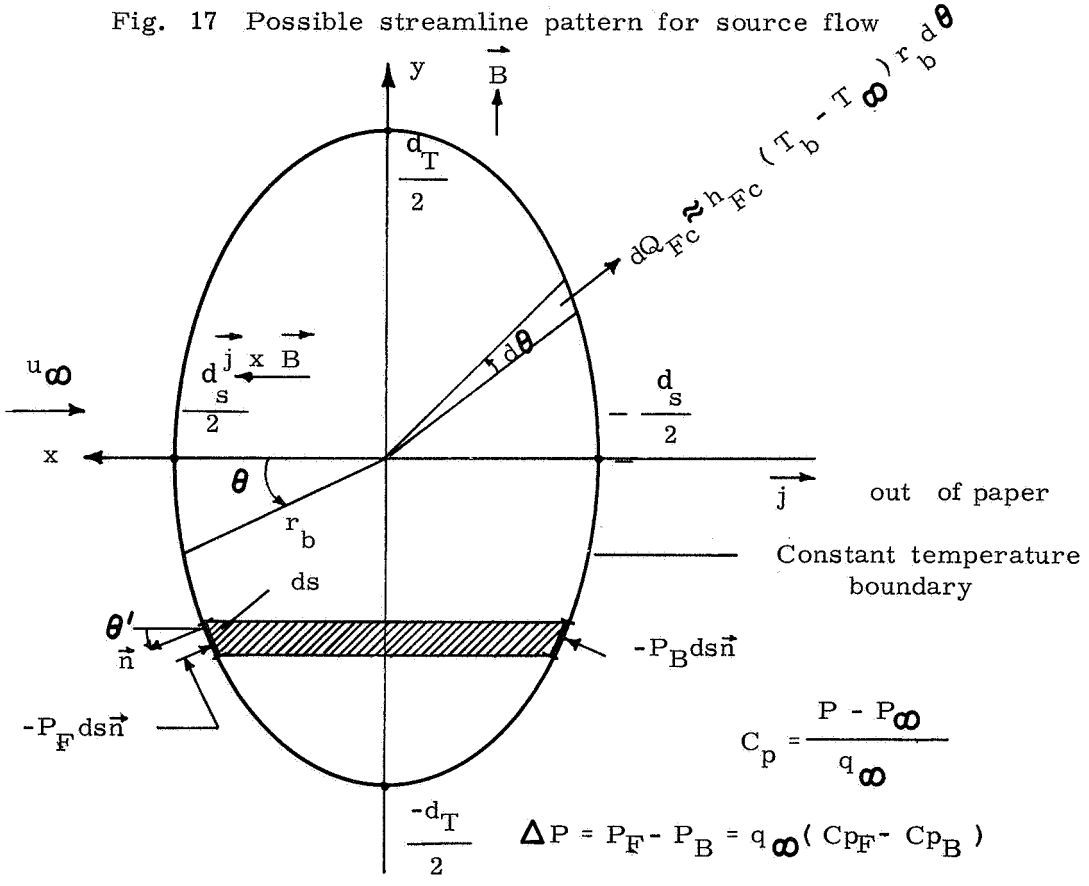

Fig. 18 Diagram for force and energy balance

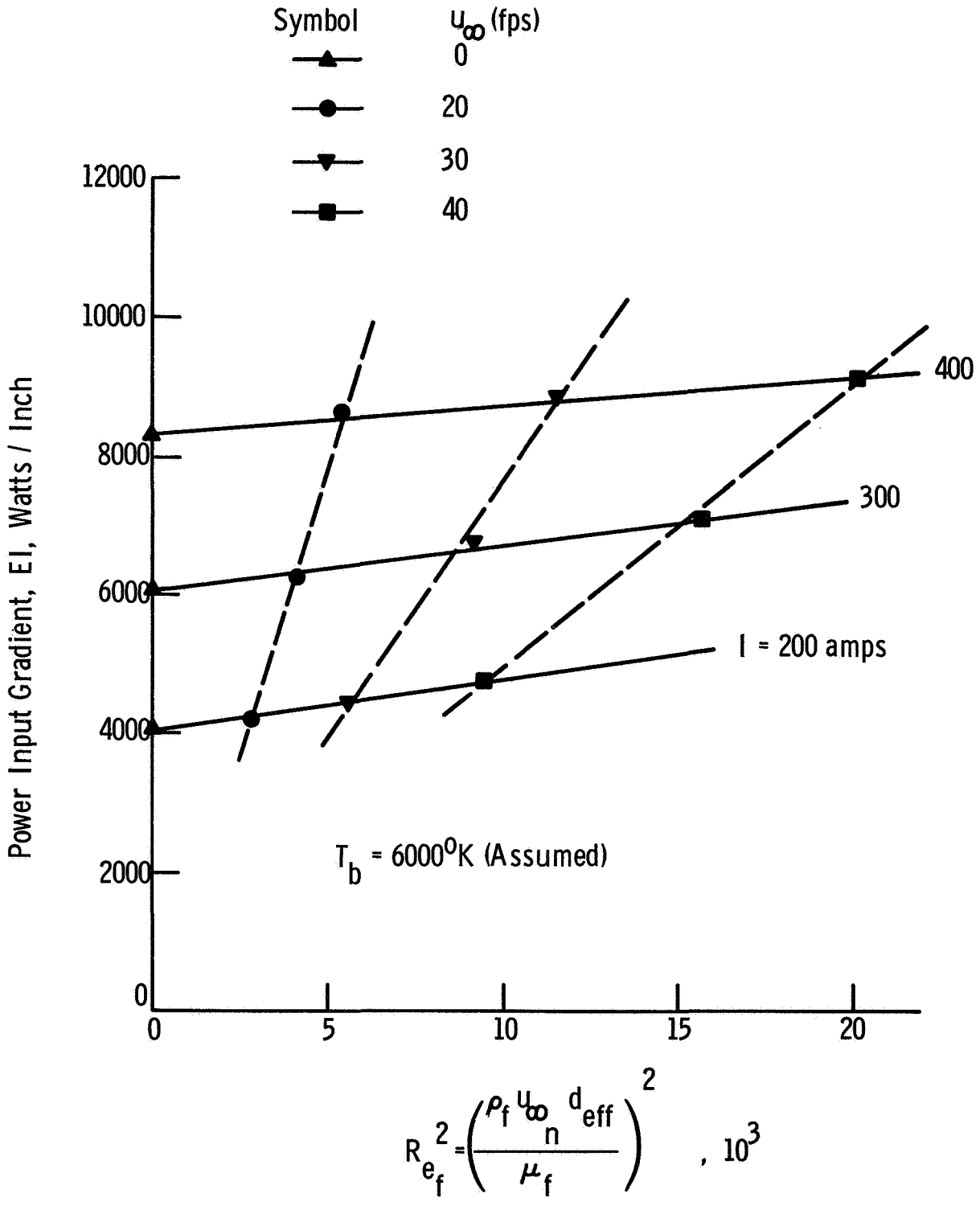

Fig. 19. Power input gradient versus Re_f^2 for Roman's data.

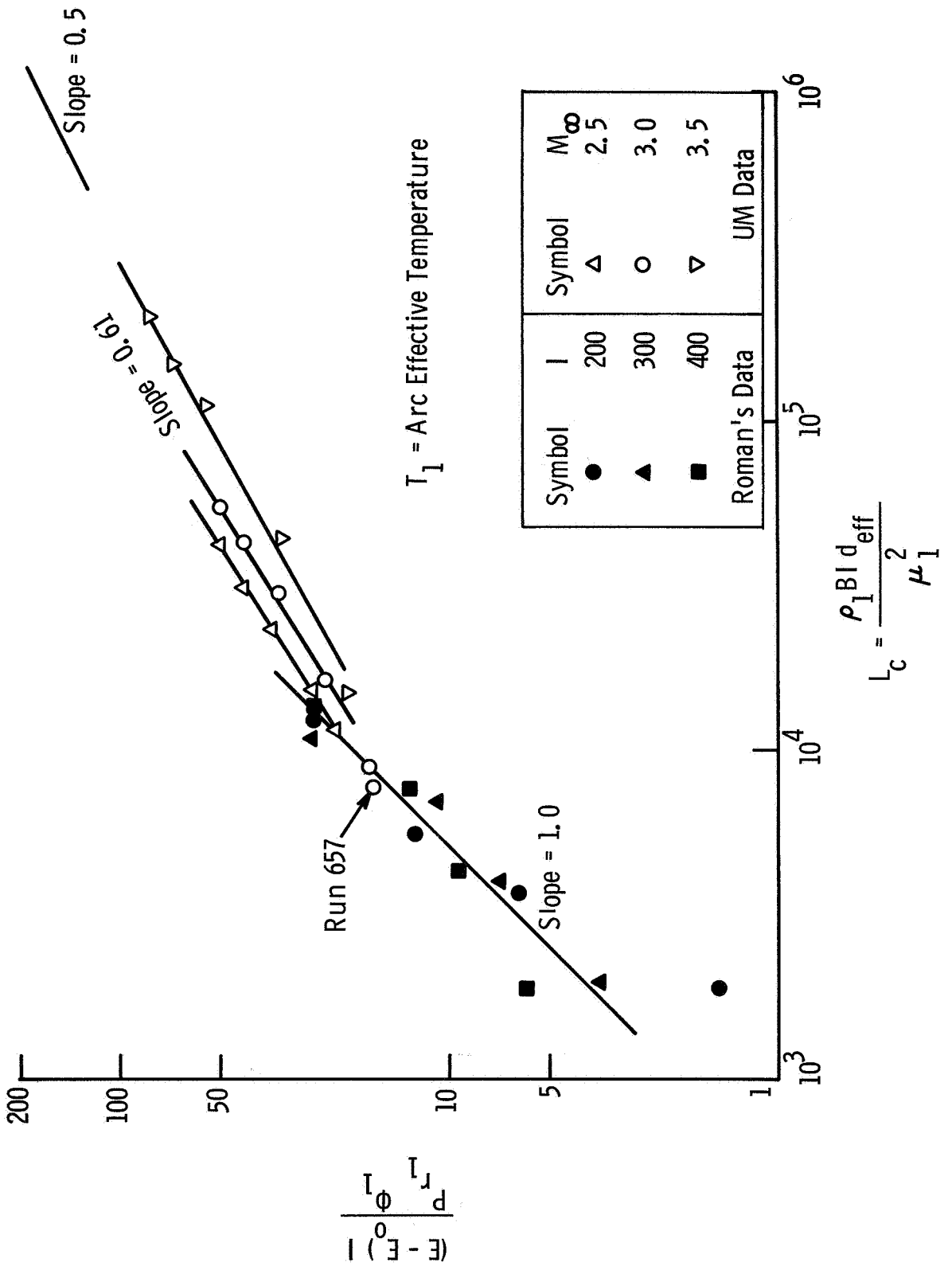

Fig. 20. Variation of $(E - E_o)I/Pr_1\phi_1$ with L_c.

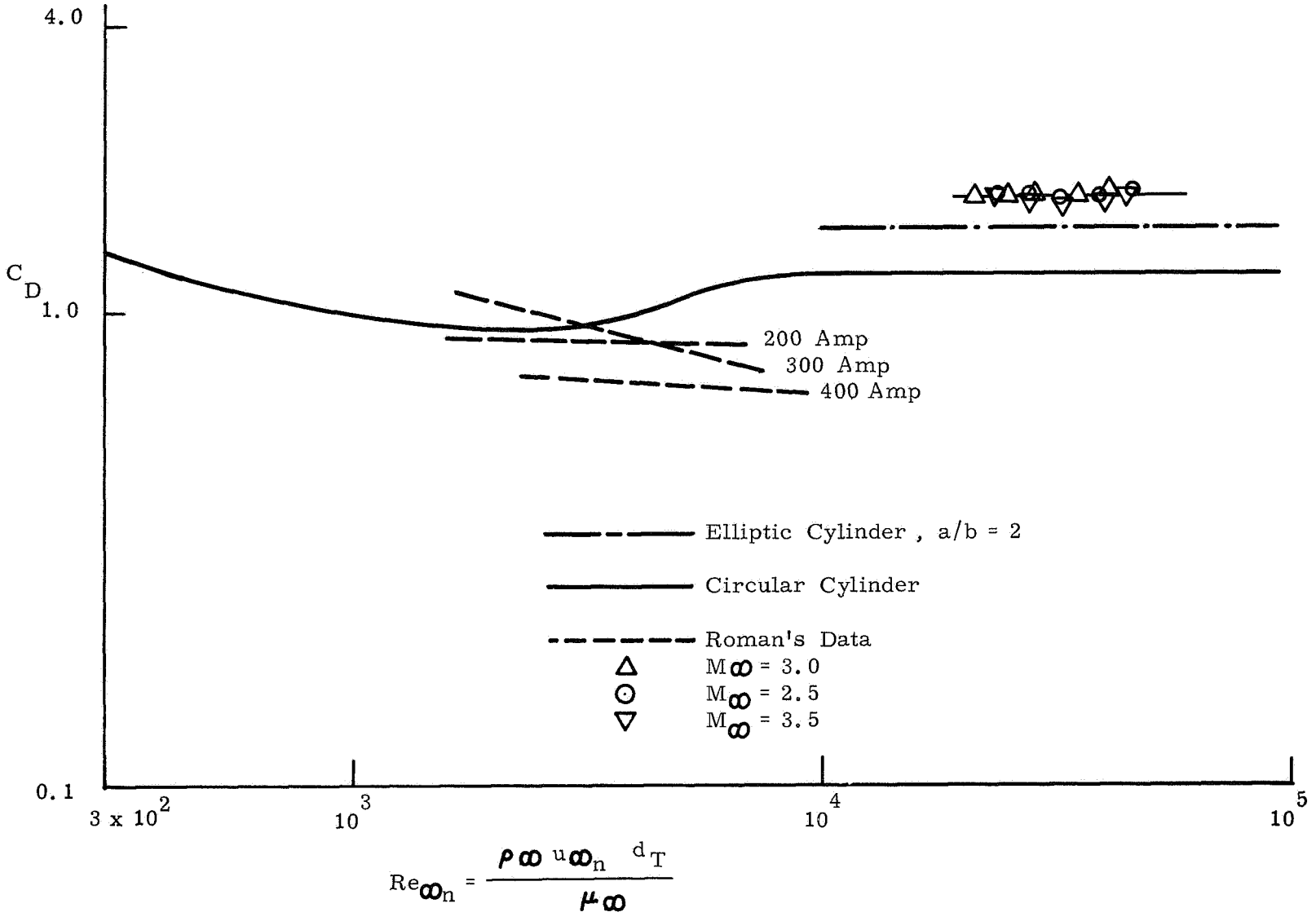

Fig. 21 Experimental normal force coefficients for balanced convected arcs

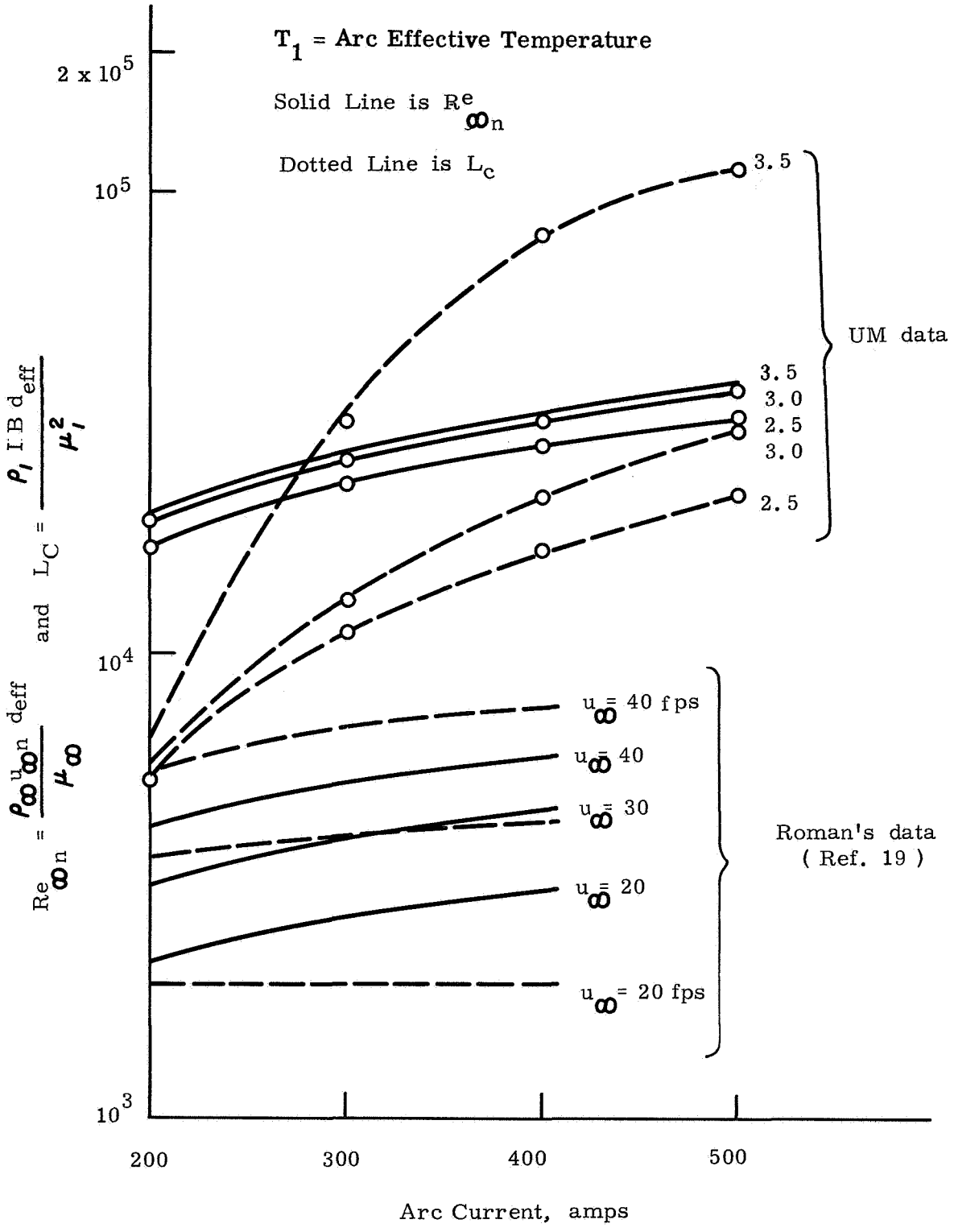

Fig. 22 Range of $Re_{\infty n}$ and L_C In ARL and UM Experiments

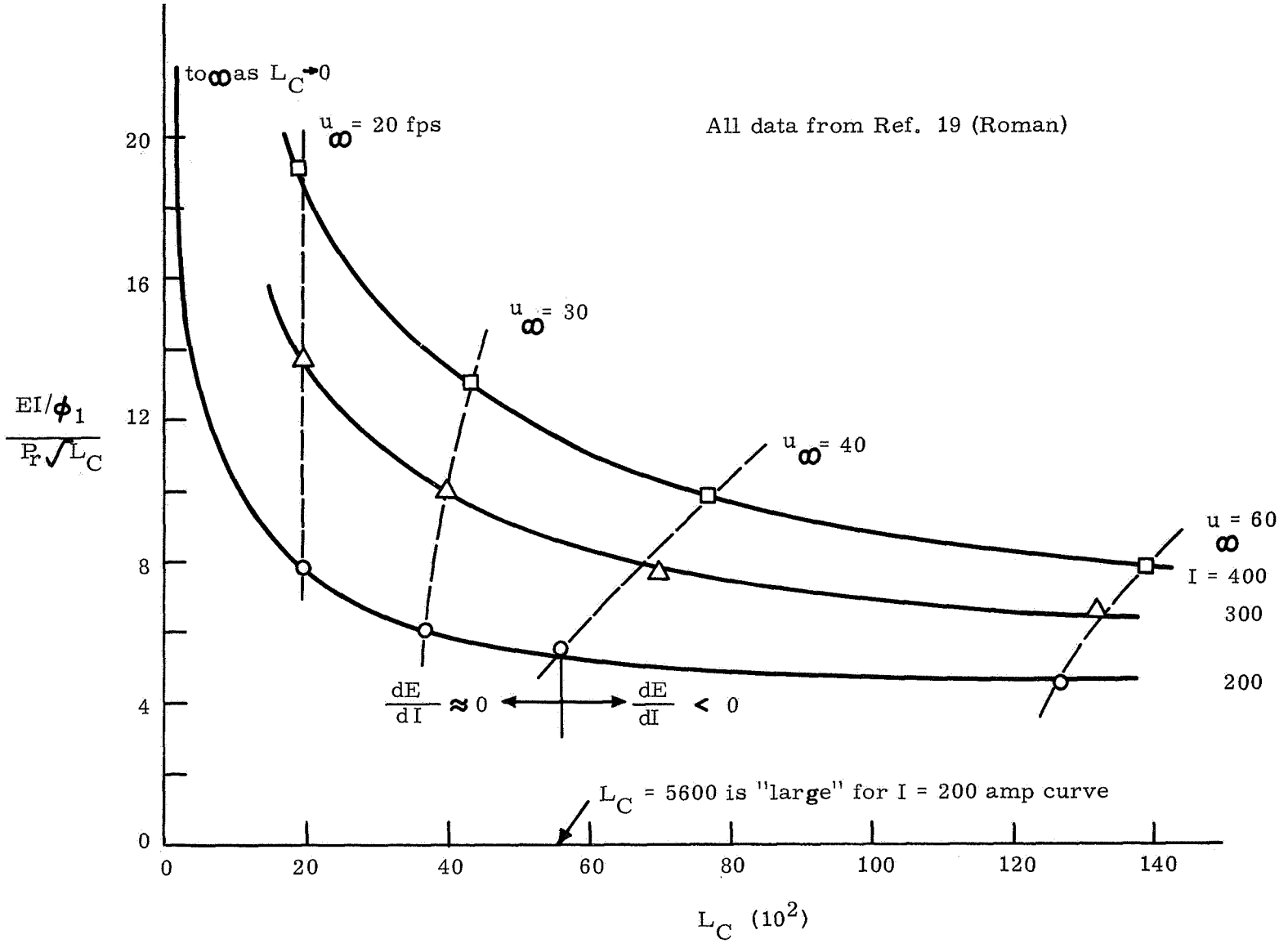

Fig. 23. Behavior of the Joule heating parameter as L_C increases for Roman's data

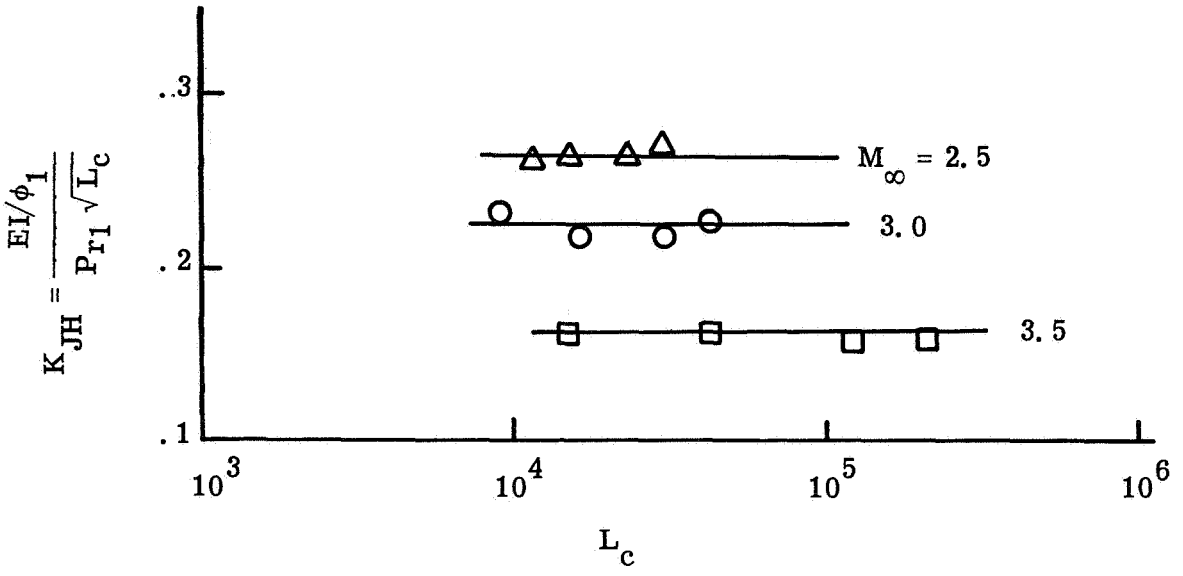

Fig. 24. Behavior of the Joule heating parameter for UM data.

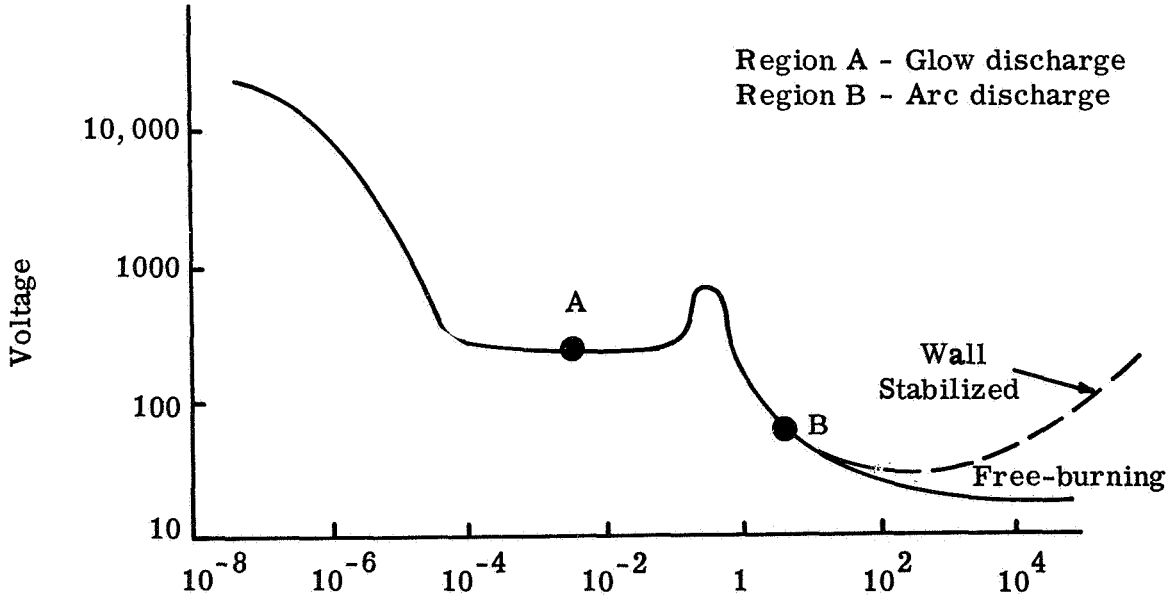

Fig. 25. Static characteristics of self-sustaining gaseous discharges.

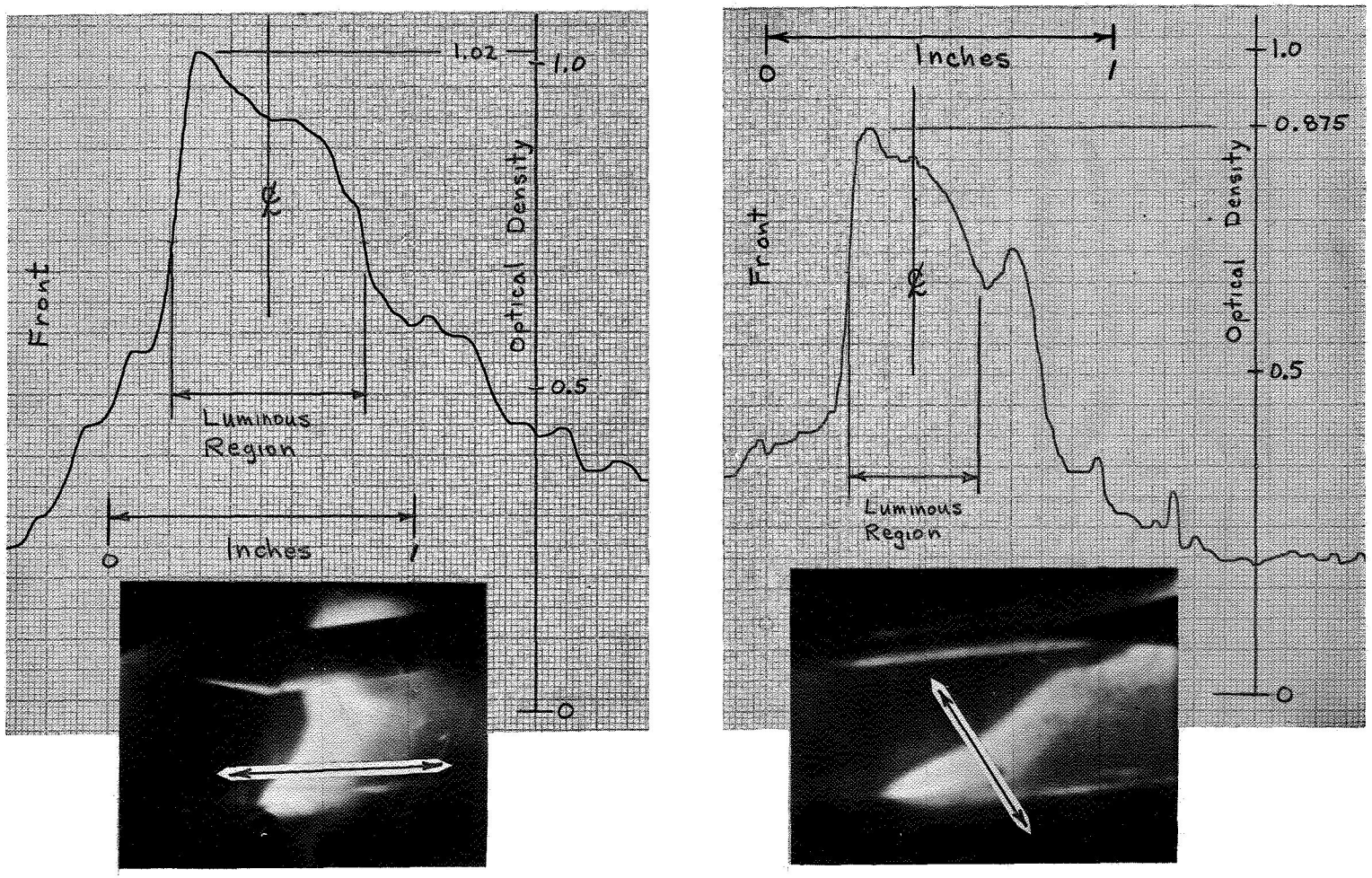

(a) Near head-on view

(b) Near side-on view

Figure 26 Microdensitometer scans of Run 657

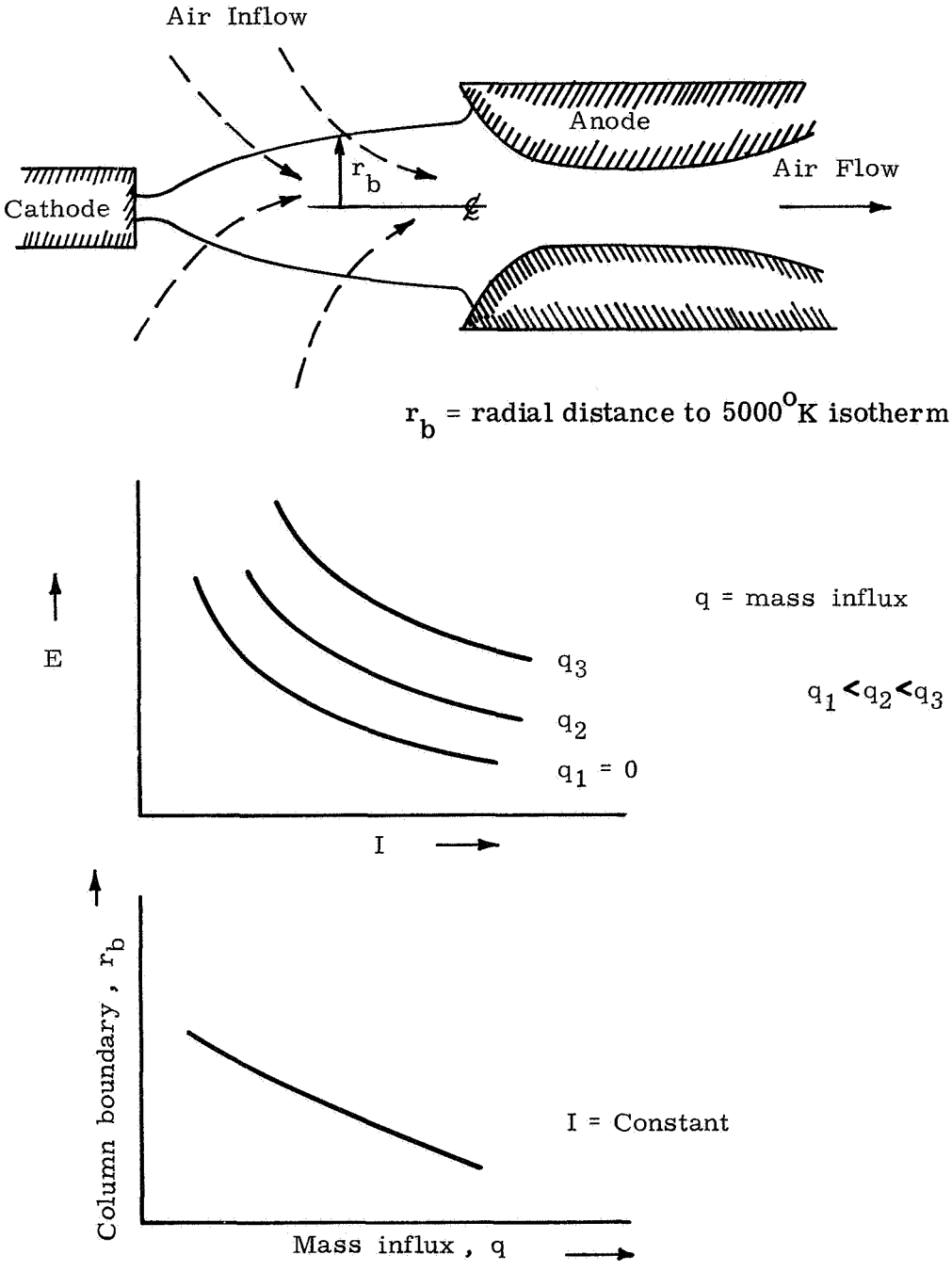

Fig. 27 Results and arc heater design considered in Reference 64

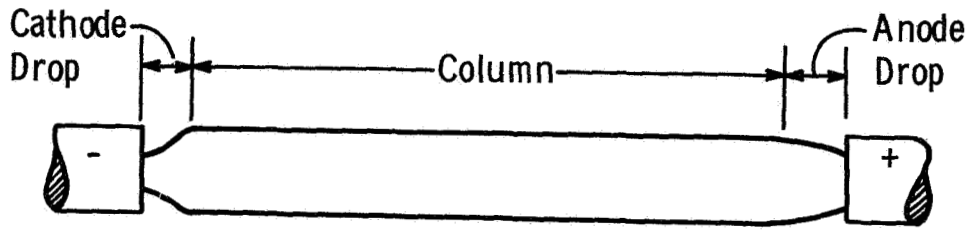

(a) Electric arc showing regions of cathode and anode drop (distances exaggerated) and positive column. Note severe contraction at cathode and less severe contraction at anode.

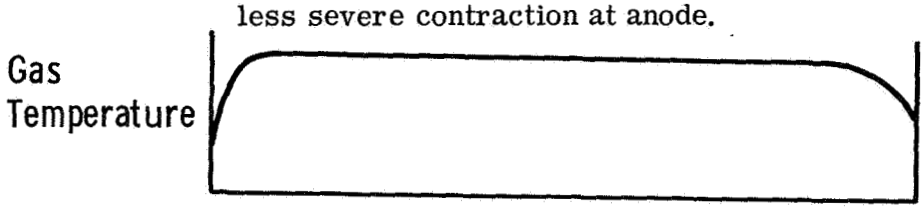

(b) Gas temperature along arc (electron temperature equal to gas temperature at elevated pressures).

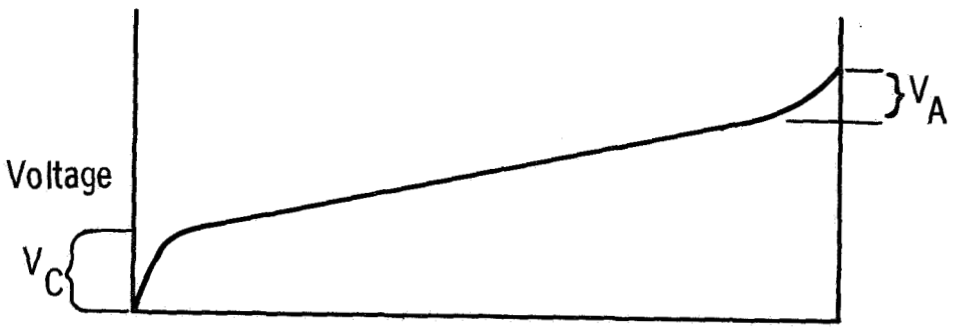

(c) Voltage, V, along arc showing potential falls in cathode and anode drop regions. Note constant voltage gradient (electric field strength) in column.

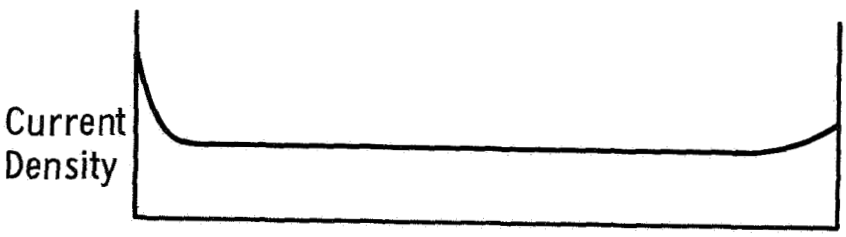

(d) Current density (amperes/cm^2) along arc.

Fig. 28. Schematic of an electric arc.

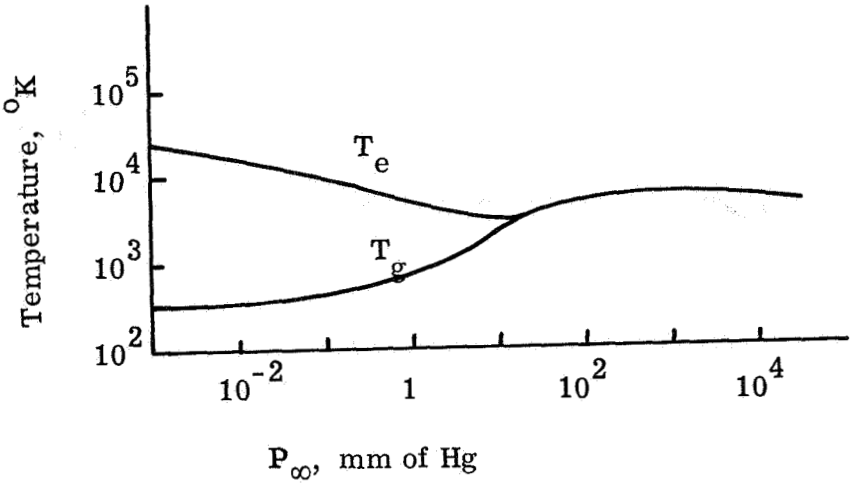

Fig. 29. Dependence on gas pressure of electron and gas temperature of an electric arc (from Ref. 4).

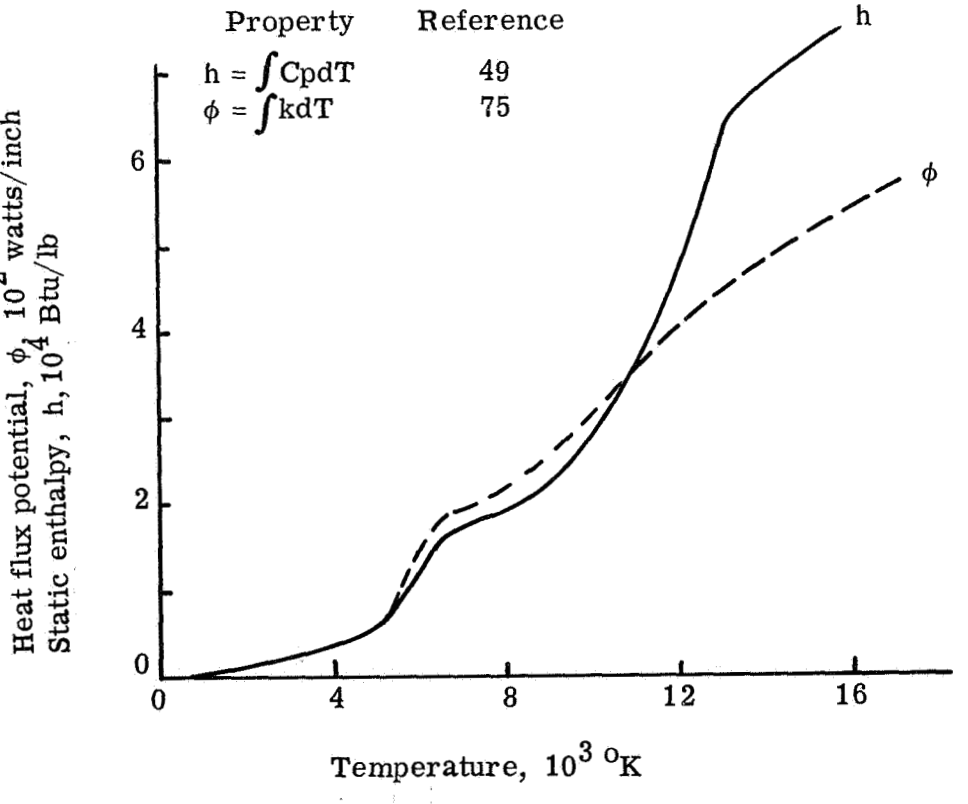

Fig. 30. Equilibrium air data at P_∞ = .0191 atm.

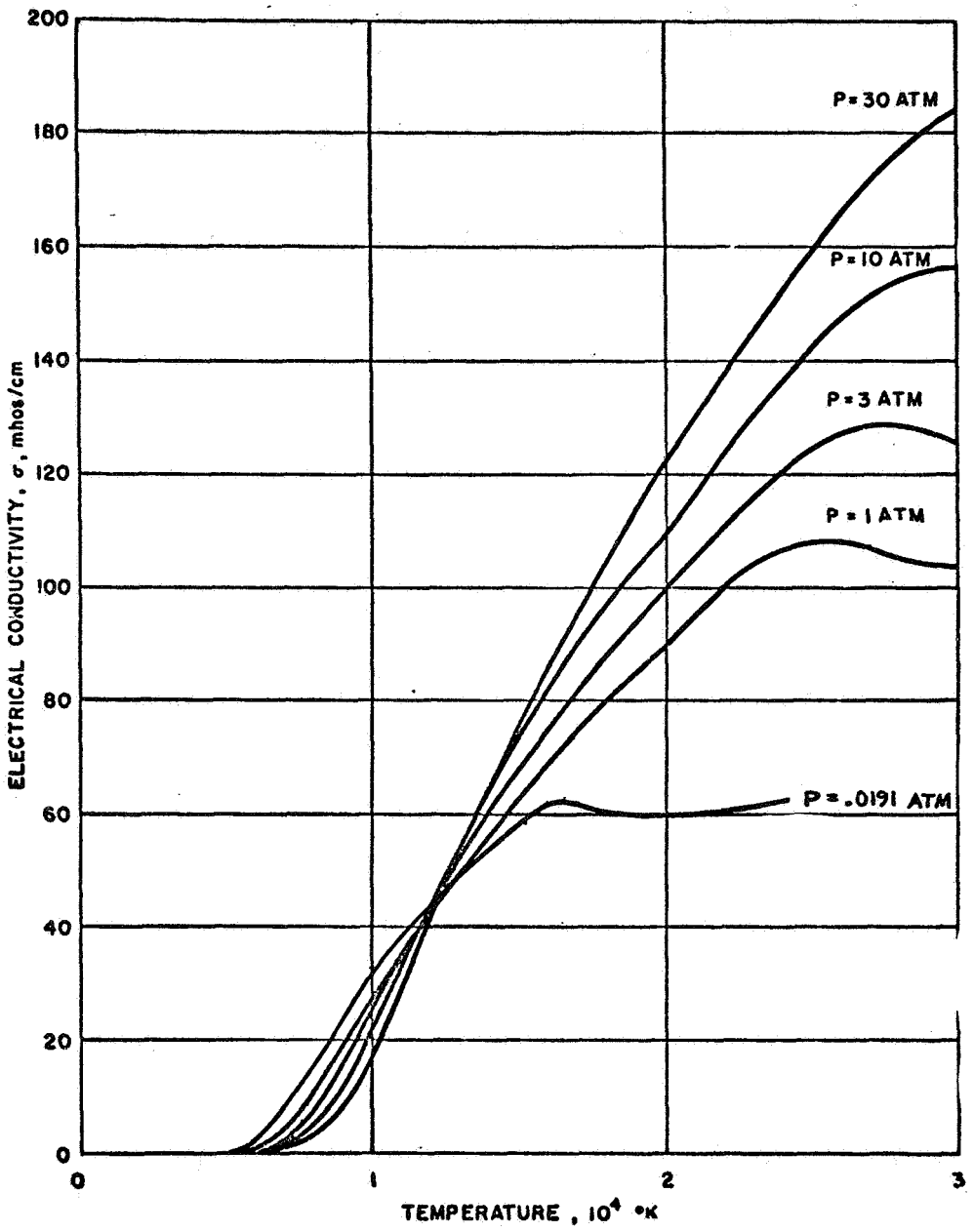

Fig. 31. Electrical conductivity for equilibrium air from Reference 34 ($P \geq 1$ atm) and References 25 and 47 ($P < 1$ atm).

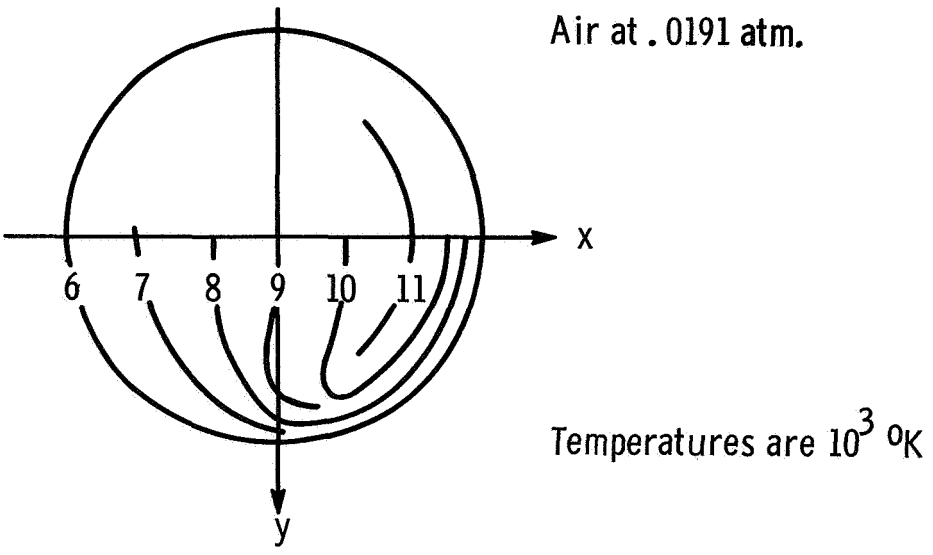

Fig. 32. Temperature distribution for two-dimensional model with T_b = 6000°K, B = 1430 gauss, E = 21 v/inch, d_S = 0. 335 inches, $T_1 = T_b$, L_c = 469 and K_{JH} = 0. 136.

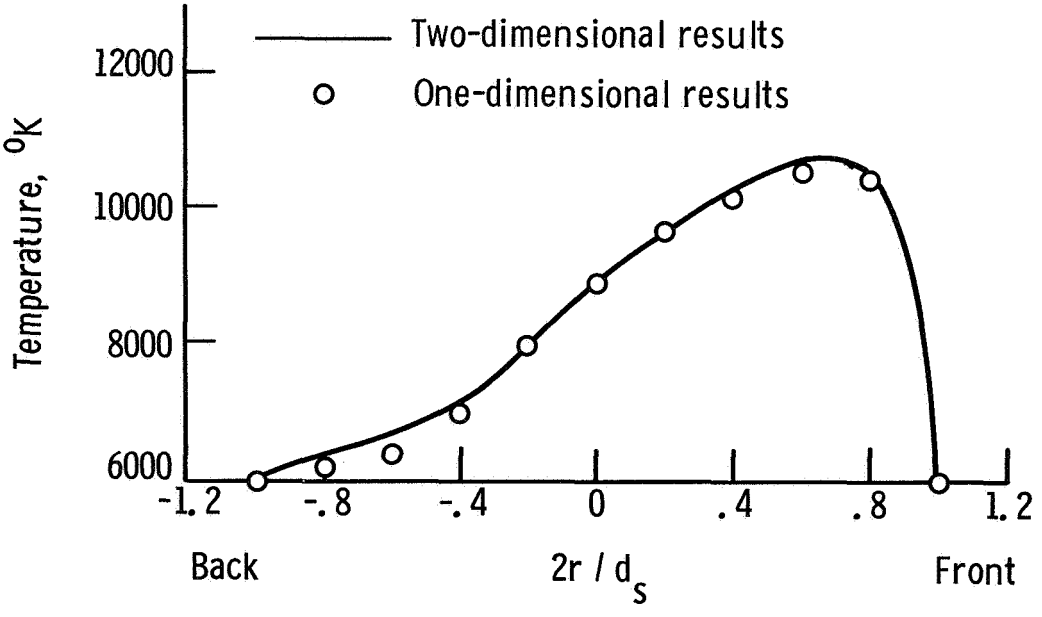

Fig. 33. Comparison of temperature distributions for one- and two-dimensional models (conditions same as for Fig. 32).

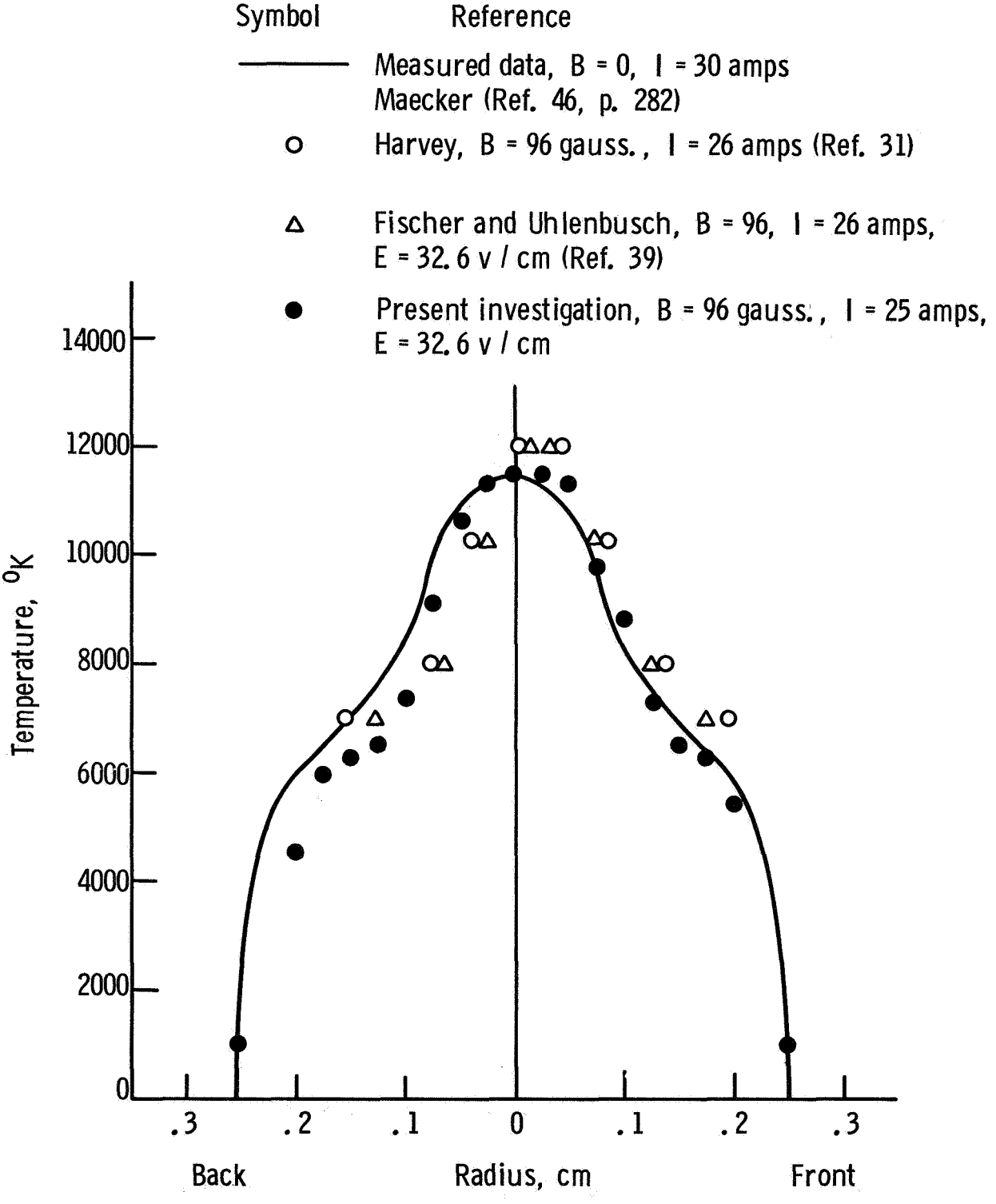

Fig. 34. Comparison of measured and calculated temperature distributions for 1 atm Nitrogen arc.

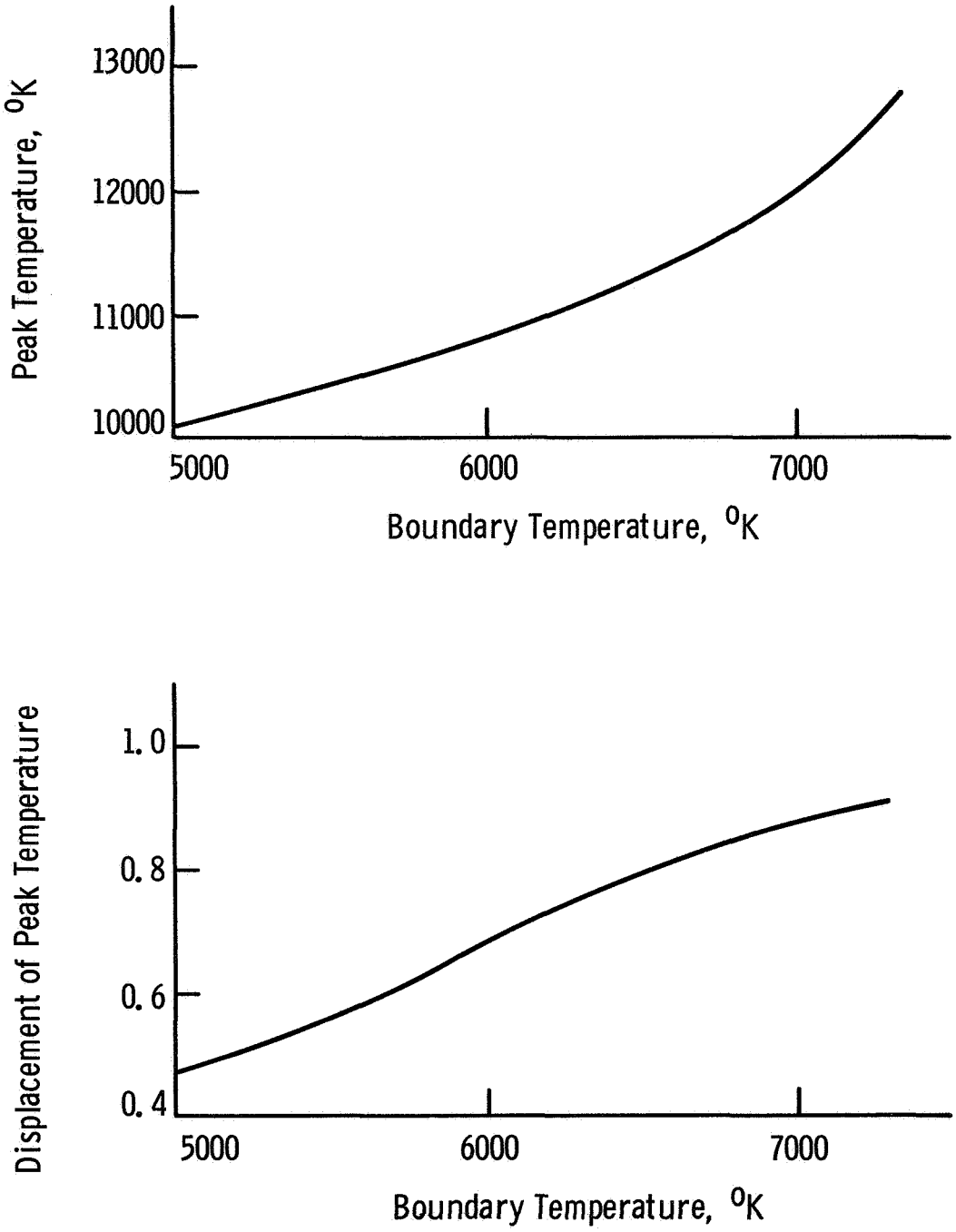

Fig. 35. Effect of boundary temperature on peak temperature and displacement of peak temperature for air at .019 atm, B = 1430 gauss, E = 21 v/inch and d_s = 0.335 inches.

Case No.	75	86	88
Inputs	RUN 657	Estimated	Estimated
T_b (^oK)	7200	7200	7200
T_1 (^oK)	7200	7200	7200
E (v/in)	21	13.5	7.7
B (gauss)	1430	390	63
d_S (in)	.335	.433	.627
u_{∞_n} (fps)	655	300	100
K_{JH}	.22	.248	.33
L_c	1338	505	143

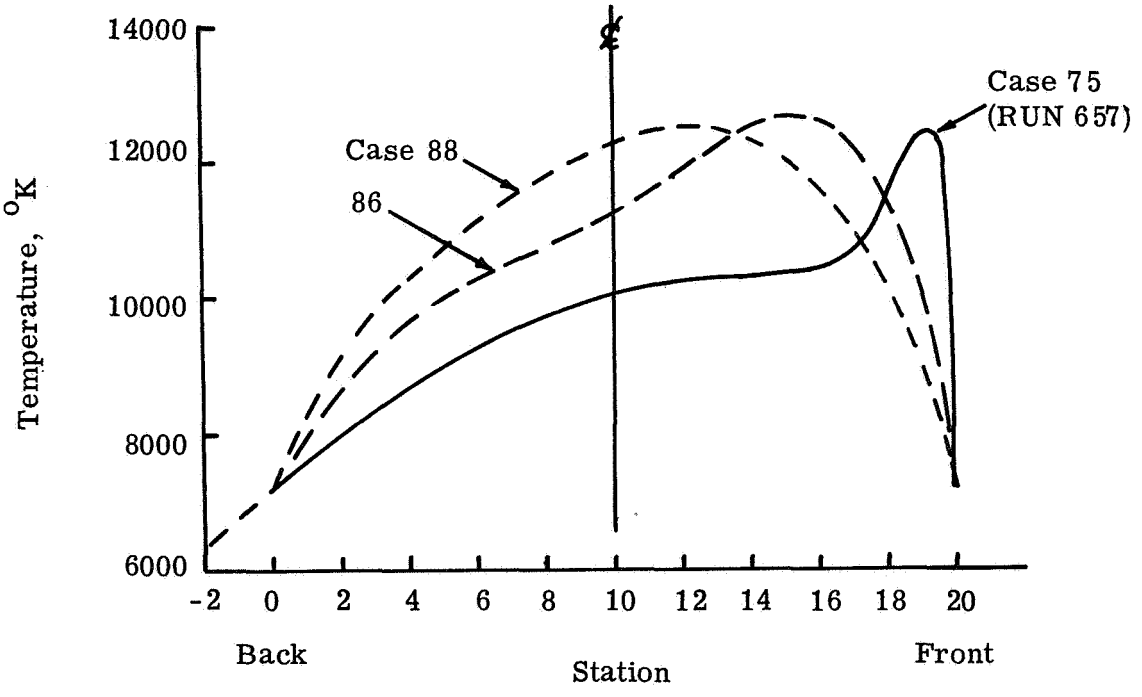

Fig. 36. Calculated temperature distributions for air at P_∞ = .0191 atm and I = 216 amps.

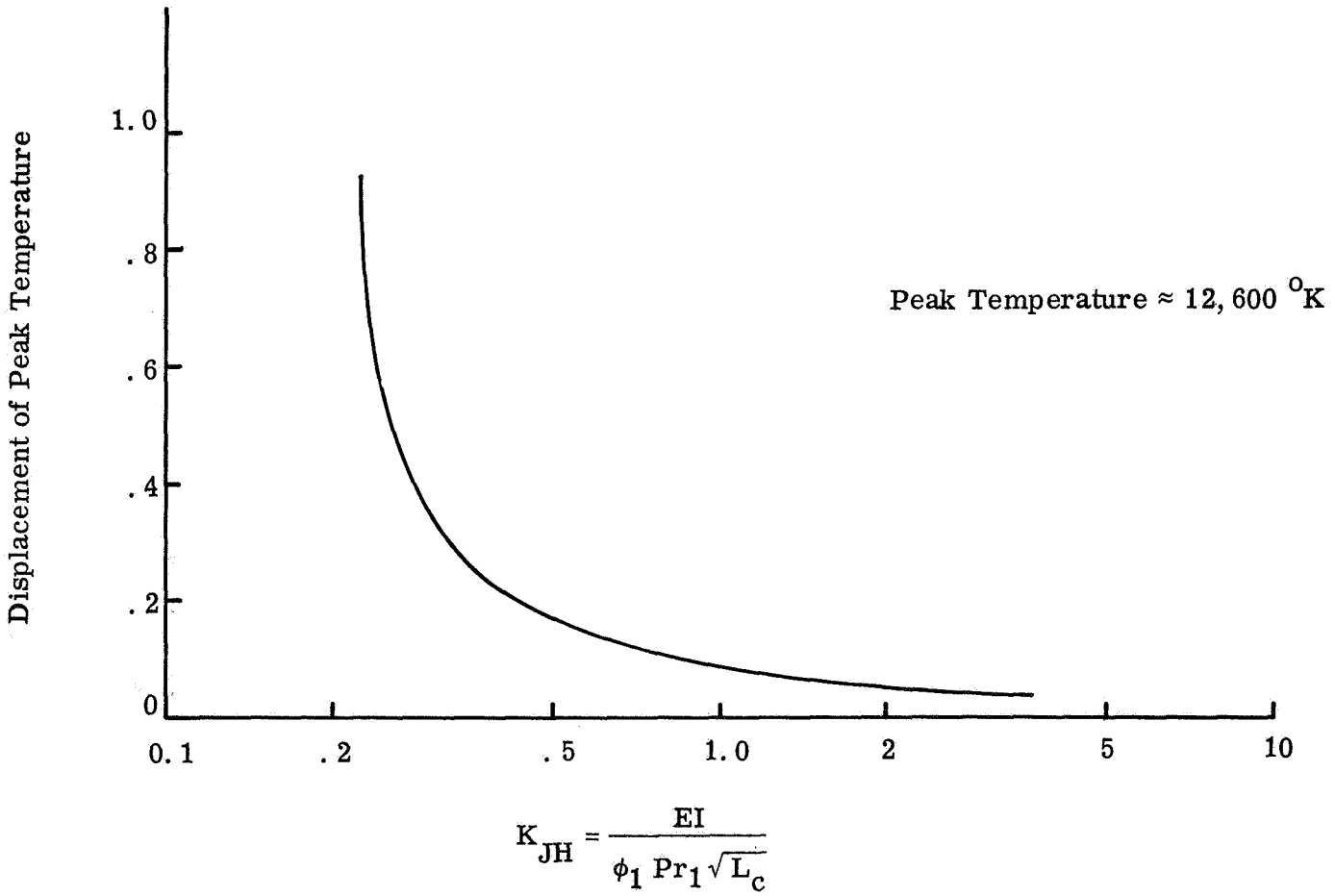

Fig. 37. Displacement of peak temperature versus K_{JH} for air at P_∞ = .0191 atm, I = 216 amps and T_b = 7200 °K.

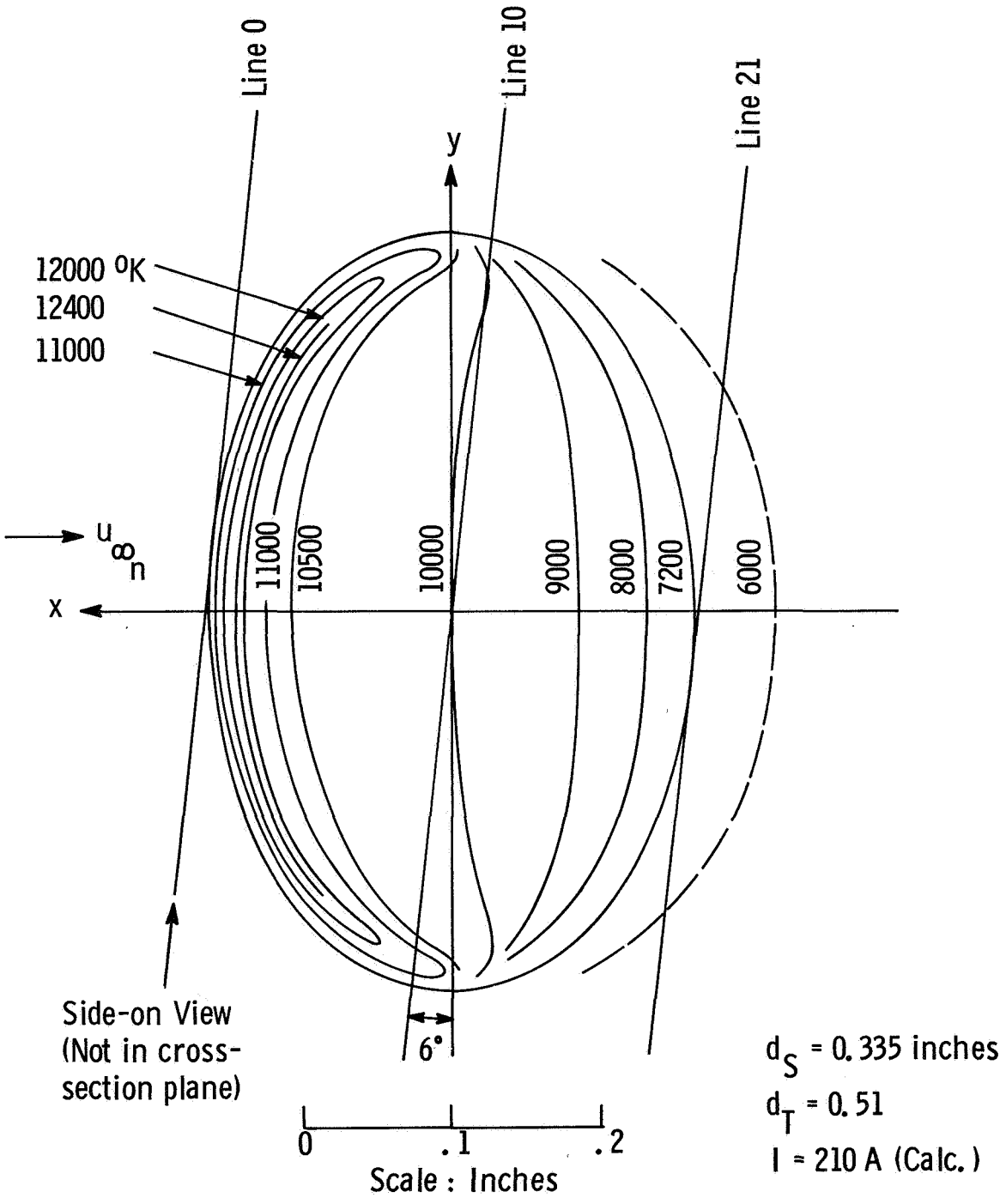

Fig. 38. Calculated temperature distribution for RUN 657.

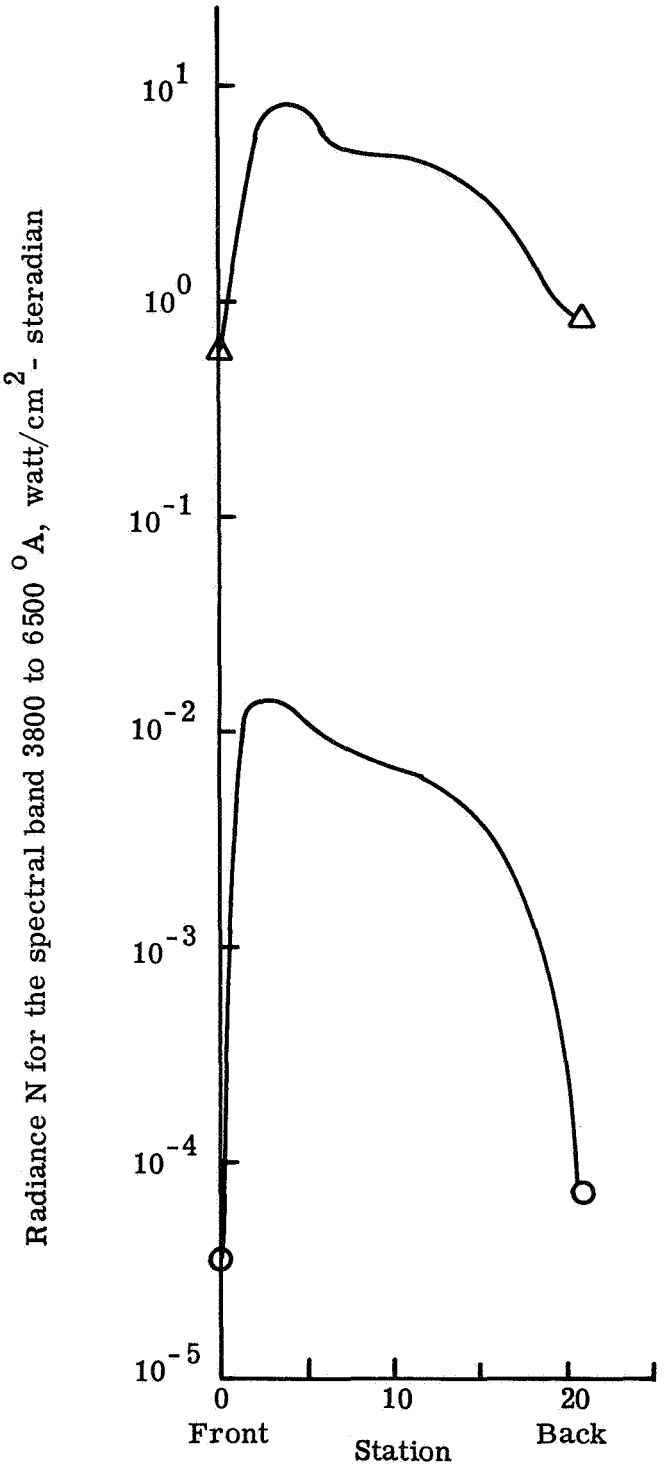

Fig. 39. Measured and calculated radiance distributions for RUN 657 (side-on view).

Appendix A

ANALOGY WITH NATURAL CONVECTION OF HEAT IN A HORIZONTAL TUBE

Information about the balanced convected arc can be obtained by considering a related problem; that of natural convection of heat in a horizontal tube. The analogy between the two problems is that conduction and convection are the primary heat transfer mechanisms in the interior (for arcs where radiation is small) and they both have an external volume force; the Lorentz force in one case and the buoyancy force in the other.

Weinbaum (Ref. 32)* considered theoretically a horizontal tube of circular cross section whose wall was maintained at the temperature distribution $T_{wall} = T_o + \Delta T \cos(\theta + \theta_o)$ (shown in Fig. A1). In natural convection problems the important parameters are (subscript zero denotes conditions at the origin):

$$\text{Gr} = \text{Grashoff number} = \frac{\beta' g \Delta T \rho_o^2 r_o^3}{\mu^2} \qquad \text{(A-1)}$$

= ratio of body force (due to buoyancy) to viscous force

where $\beta' = 1/\rho \, (\partial\rho/\partial T)_P$, thermal expansion

$\text{Pr} = \text{Prandtl number} = \mu C_p/k$

$u_o = \text{Characteristic velocity} = \sqrt{\beta' \Delta T g r_o}$ (A-2)

*Ostrach and Menold in Ref. 33, discuss Weinbaum's work and extend it for other temperature distributions.

u_o comes from the effective increase in kinetic energy of the fluid due to the work done on the fluid by buoyancy forces.

For small pressure changes we can express $\rho/\rho_o = 1 - \beta' (T - T_o)$. The governing equations are

$$\frac{\partial}{\partial x}(\rho u) + \frac{\partial}{\partial y}(\rho v) = 0 \tag{A-3}$$

$$u \frac{\partial u}{\partial x} + v \frac{\partial u}{\partial y} = - \frac{1}{\rho} \frac{\partial P}{\partial x} + \frac{\mu}{\rho} \left[\nabla^2 u + \frac{1}{3} \frac{\partial}{\partial x} \left(\frac{\partial u}{\partial x} + \frac{\partial v}{\partial y} \right) \right] \tag{A-4}$$

$$u \frac{\partial v}{\partial x} + v \frac{\partial v}{\partial y} = - \frac{1}{\rho} \frac{\partial P}{\partial y} - g + \frac{\mu}{\rho} \left[\nabla^2 v + \frac{1}{3} \frac{\partial}{\partial y} \left(\frac{\partial u}{\partial x} + \frac{\partial v}{\partial y} \right) \right] \tag{A-5}$$

$$u \frac{\partial T}{\partial x} + v \frac{\partial T}{\partial y} = \frac{k}{\rho C_p} \nabla^2 T \tag{A-6}$$

where we have assumed constant specific heat, thermal conductivity, viscosity and negligible viscous dissipation. The constant properties imply that $\Delta T/T_o \ll 1$. Weinbaum expresses $\Theta = (T - T_o)/\Delta T$ and rewrites Eq. (A-3) through (A-6) as

$$\frac{1}{\sqrt{Gr}} \nabla^4 \psi + \frac{1}{r} \frac{\partial \psi}{\partial \theta} \nabla^2 \psi - \frac{\partial \psi}{\partial \theta} \frac{\partial}{\partial r} \nabla^2 \psi = \cos \theta \frac{\partial}{\partial r} - \frac{\sin \theta}{r} \frac{\partial}{\partial \theta} \Theta \tag{A-7}$$

$$\frac{1}{Pr \sqrt{Gr}} \nabla^2 \Theta + \frac{1}{r} \frac{\partial \psi}{\partial r} \frac{\partial}{\partial \theta} - \frac{\partial \psi}{\partial \theta} \frac{\partial}{\partial r} \Theta = 0 \tag{A-8}$$

where $V_r = \frac{1}{r} \frac{\partial \psi}{\partial \theta}$ and $V_\theta = - \frac{\partial \psi}{\partial r}$ are the nondimensional radial and tangential velocities. Equations (A-7) and (A-8) together with the b.c.

$\partial\psi/\partial r = \partial\psi/\partial\theta = 0$ and $\Theta = \cos(\theta + \theta_o)$ at $r = 1$ complete the statement of the problem.

Equations (A-7) and (A-8) are of the boundary layer type as the coefficients of the highest order terms get very small as Gr gets very large. For large Gr the viscous and heat conducting terms become negligible everywhere except in the immediate vicinity of the boundary where their presence is essential if the b.c. at $r = 1$ are to be satisfied. Thus, for large Gr the flow in the interior is governed by the inviscid equations:

$$\frac{\partial\psi}{\partial r}\frac{\partial\Theta}{\partial\theta} - \frac{\partial\psi}{\partial\theta}\frac{\partial\Theta}{\partial r} = 0 \qquad \text{(A-9)}$$

$$-\frac{1}{r}\left(\frac{\partial\psi}{\partial r}\frac{\partial}{\partial\theta} - \frac{\partial\psi}{\partial\theta}\frac{\partial}{\partial r}\right)\nabla^2\psi = \left(\cos\theta\,\frac{\partial}{\partial r} - \frac{\sin\theta}{r}\frac{\partial}{\partial\theta}\right)\Theta \qquad \text{(A-10)}$$

For large Gr the region where velocity and temperature gradients are large (i.e. the boundary layer) must be very small because these gradients must be very large in order to make the viscous and heat conduction terms significant.

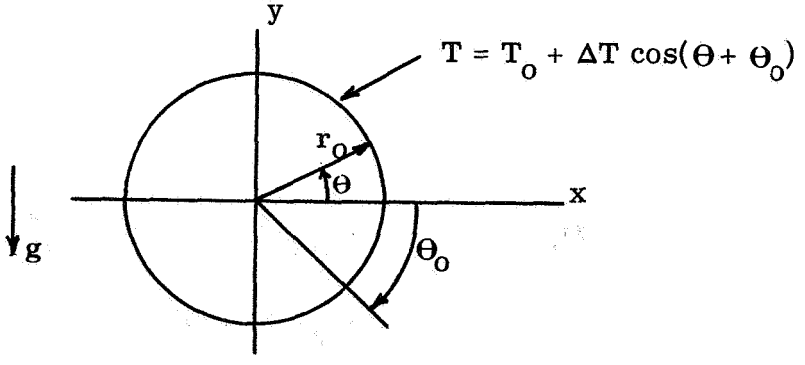

Figure A-1. Configuration for the problem of natural convection of heat in a horizontal tube (Ref. 32).

Appendix B

FORCED AND NATURAL CONVECTION HEAT TRANSFER FROM HEATED SOLID CYLINDERS

The convection heat transfer from heated solid cylinders with surface temperature T_s is expressed as:

$$Q = \pi \, Nu \, k_f \, (T_s - T_\infty) \tag{B-1}$$

where

$Nu = h2r_s/k_f$, Nusselt number

h = heat transfer coefficient

r_s = radius of solid cylinder

k_f = thermal conductivity evaluated at the film temperature $T_f = T_s + T_\infty/2$

The Nu is a function of the product of the Grashoff number (Gr) and Prandtl number (Pr) for free or natural convection, and of a characteristic Reynolds number (Re) for forced convection. For solid circular cylinders with ΔT's of at most $1000^{o}K$ the experimental data correlates very nicely when (Gr Pr) and Re are evaluated at the film temperature T_f. For this we get:

Natural Convection $$Nu_{NC} = \text{const} \, (Gr \, Pr)_f^m \tag{B-2}$$

Forced Convection $$Nu_{FC} = \text{const}' \, (Re_f)^n \tag{B-3}$$

The values of the constants, m and n for the equations (B-2) and (B-3) are obtained from correlation curves of the experimental data (Ref. 37, pp 529 and 38). The Hilpert correlation curve is used for forced convection and is shown in Fig. B-1. McAdams' correlation curve is used for natural convection heat transfer from horizontal cylinders (Fig. B-2) and King's correlation curve for natural convection heat transfer from vertical cylinders (Fig. B-2). The correlation curves for natural convection from horizontal and vertical cylinders overlap each other and a single curve is usually drawn through both data as shown in Fig. B-2.

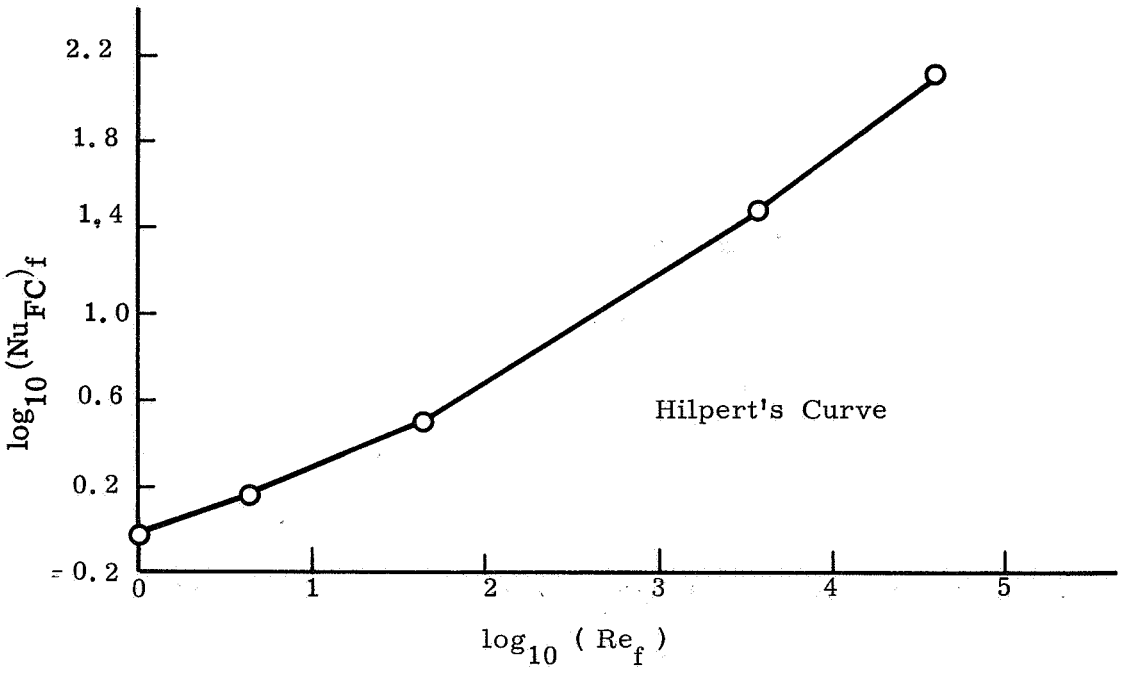

Fig. B-1 Correlation curve for forced convection normal to circular cylinders

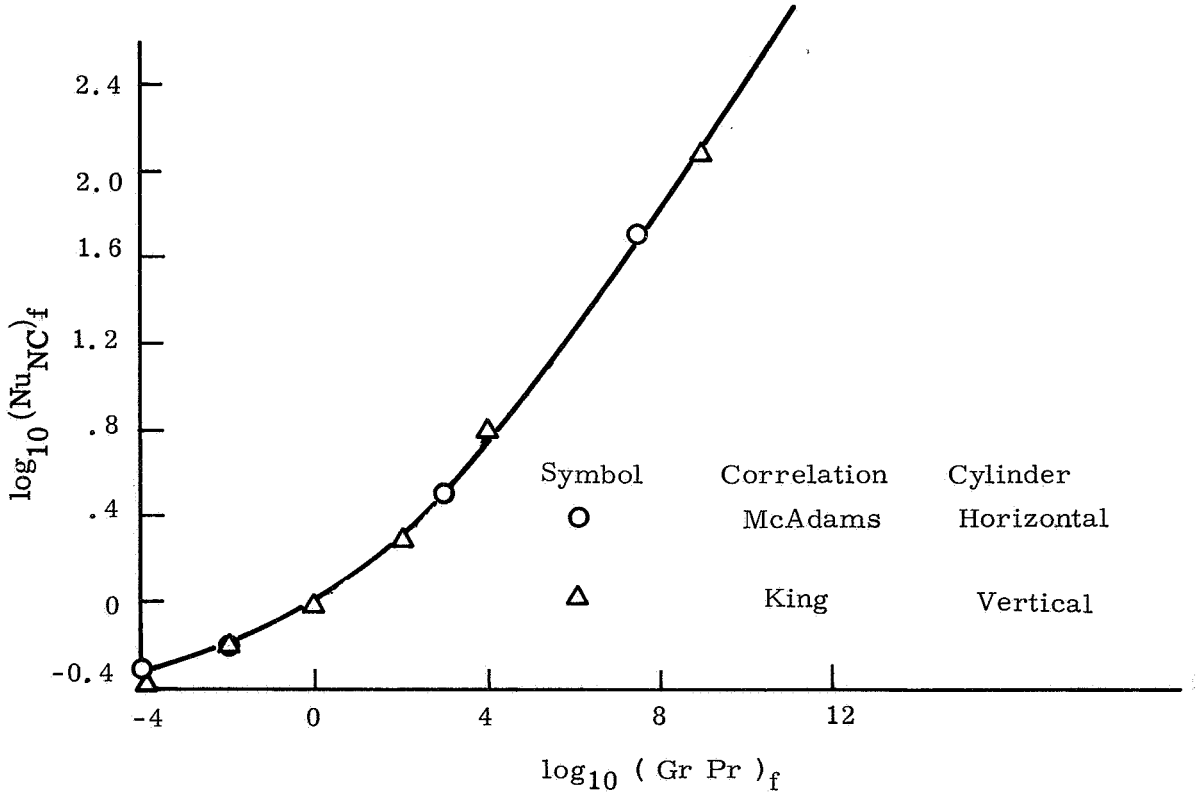

Fig. B-2 Correlation curve for natural convection from horizontal and vertical cylinders

Appendix C

ARC SLANT AND CONFIGURATION

A striking observation of a balanced convected arc in a supersonic airstream is the slant of the arc column. The arc slant is usually in a direction and at an angle such that considering the Hall effect could qualitatively explain the behavior. This appendix indicates that the slanting is not an electro-magnetic effect (i. e., Hall effect) but rather a fluid-mechanical effect and is related to the shock wave pattern between the electrodes.

The general Ohms law can be expressed as (Ref. 25, pg. 190)

$$\vec{j} = \sigma(\vec{E} + \vec{V} \times \vec{B}) - \omega_e \tau_e \vec{j} \times (\vec{B}/B) + (\text{ion slip}) \qquad \text{(C-1)}$$

Hall Current

where ion slip accounts for a current due to the ions having a large velocity relative to the neutral particles. Ion slip can be neglected for weakly ionized gases and $(\omega_e \tau_e)^2 < \sqrt{m_i/m_e}$. The other terms in Eq. (C-1) are defined in Section 3. 2. Equation (C-1) also neglects a conduction current due to diffusion of species and currents due to a non-uniform magnetic field.

We take the vector product of Eq. (C-1) with $\vec{B}$ to obtain $\vec{j} \times \vec{B}$ and substitute this back into Eq. (C-1). The explicit expression for $\vec{j}$ (neglecting ion slip) is

$$\vec{j} = \frac{\sigma}{1 + \omega_e^2 \tau_e^2} \left[\vec{E} + \vec{V} \times \vec{B} - \omega_e \tau_e^2 (\vec{E} + \vec{V} \times \vec{B}) \times (\vec{B}/B) \right] \qquad (3\text{-}10a)$$

The components of $\vec{j}$ are (using Figure 14)

$$j_x = \frac{\sigma}{1 + \omega_e^2 \tau_e^2} \left[E_x - \omega_e \tau_e^2 (E_z + uB) \right] \qquad (C\text{-}2)$$

$$j_z = \frac{\sigma}{1 + \omega_e^2 \tau_e^2} \left[E_z + uB + \omega_e \tau_e^2 E_x \right] \qquad (C\text{-}3)$$

If the electrodes are continuous electrical conductors (equipotential surfaces), any electric fields in the stream or x direction that might be generated will in essence be short circuited, such that $E_x = 0$. For a plasma sheet between these continuous or rail electrodes a streamwise current j_x will flow due to the Hall effect and the total current vector will be slanted in the channel. This slant is given by

$$\tan \alpha = \frac{j_z}{j_x} = \frac{1}{\omega_e \tau_e^2} \qquad (C\text{-}4)$$

where α is measured from the x axis.

For pin electrodes or segmented electrodes (individual electrodes separated by insulators and each having its own power supply) a current in the stream direction cannot flow, so that the Hall current $j_x = 0$ and $\alpha = 90^o$. There is now an x component of the electric field given by $E_x = \omega_e \tau_e^2 (E_z + uB)$ and called the Hall field (References 25 and 27).

Zauderer (Ref. 22) used a segmented electrode arrangement in a channel accelerator and observed a travelling arc that was straight up and down regardless of the value of $\omega_e \tau_e$. As the arc moved down the channel it would extinguish and re-ignite for each electrode segment.

It was not clear whether the cone cylinder rail electrodes used in this investigation were behaving like rail electrodes or skewed (i. e., off set) pin electrodes. The values of $\omega_e \tau_e$ at Mach 2. 5, 3. 0 and 3. 5 were such that the angle α from Eq. (C-4) was near the observed slant angles. The convected balanced arc with cone cylinder electrodes always slanted in the Hall direction (i. e., cathode downstream of the anode). Thus it appeared as though the Hall effect might be the reason for the arc slant.

Podalsky and Sherman (Ref. 70) investigated theoretically the influence of the Hall current on a plasma sheet flowing between rail electrodes. They considered a "tilted" electric field (using skewed electrodes) and showed that the direction of the total current is very much affected by the angle of "tilt".

If we assume that the electrodes used in this investigation behave like rail electrodes and the arc slant is due to a Hall effect, then altering the electric field should alter the arc slant angle. Following

this assumption, the electrode Models A through F, shown on Figure C-1, were used in different combinations to examine the effect of tilting $\vec{E}$ *.

The results were that the arc slant was identical for all combinations of electrode Models A through F. Three of the more extreme electrode combinations are shown on Figure C-2. The arc configurations were all similar and the arcs were steady in most cases. Runs 596 and 599, shown on Figure C-2, exhibited a slight unsteadiness (voltage fluctuations of $\pm$ 5 volts). This behavior is attributed to the circumstance that the cathode spot of Run 596 and anode spot of Run 599 were located at a nylon-copper junction on the electrodes.

The different electrode combinations did not produce a tilting of the electric field vector, thus the electrodes were not behaving as rail electrodes, but rather as skewed pin electrodes. Hence the Hall current was zero and the use of the simple Ohm's law was valid, i. e. ,

$$\vec{j} = \sigma(\vec{E} + \vec{V} \times \vec{B}) \qquad (3\text{-}10b)$$

It appeared from these observations that the slant was fluid-mechanical in nature. It was therefore of interest to examine how the arc configuration varied with changes in the flow pattern between the electrodes. These changes were accomplished by generating different combinations of strong and weak shock waves off the front of the

---

*This experiment was first suggested by Charles Bond in 1965.

electrodes using electrode Models A and G. The operating conditions for the first set of runs described in this appendix were: $M_\infty = 3.0$, $P_\infty = 14.5$ mm Hg, gap = 1.0 inch, I = 218-224 amperes. The location of the field coils was fixed.

The shock wave patterns are shown on Figure C-4 and the arc shapes on Figure C-3. The weak conical shocks were darkened slightly with a soft lead pencil on the schlieren photographs. It was not possible to obtain schlieren photographs of the balanced connected arc because of the location of the magnets. It was assumed that the presence of the arc would not affect the shock wave pattern very much and the schlieren photographs of Figure C-4 would be representative of the shock wave patterns for the arcs shown on Figure C-3.

Figure C-3 (a) shows a convected balanced arc with a blunt cathode (top electrode) and a cone-cylinder anode. This arrangement produced an arc configuration which slanted opposite to the normal slant (i. e., Hall direction). This was the first observation of a balanced convected arc having a slant opposite to the Hall direction and is further proof that the arc slant is not due to the Hall effect. The apparent arc slant shown on Figure C-3 (a) is 42.5°; after correcting for the viewing angle the actual angle of slant is 35°. The cathode spot was about 1.5 inches from the electrode base and the anode spot was at the junction of the electrode hose and the teflon washers (Figure 1).

With a blunt anode and a cone cylinder cathode the arc configuration is as shown on Figure C-3 (b). The interesting observation here is the absence of the kink in the arc leading edge and a constant slant angle of 27. 5^{o} From Figure C-4 (b) we observe that the bow shock slants at about 28^{o}. The center of the anode spot is about 1/4 inch from the blunt nose and the arc appears to position itself just behind the bow shock. The conical shock and expansion wave from the cathode are not strong enough to influence the flow field very much. The current through the magnetic field coils was 1820 amperes and this provided a B of 1500 gauss at the reference station. The arc was very steady.

With blunt electrodes for both the anode and cathode the arc configuration is as shown on Figure C-3 (c). Here again the anode spot is 1/4 inch back from the blunt nose and the arc has a lower leading edge slant of 30. 5^{o} and an upper leading edge slant of 34^{o}. The pronounced kink half way up the column is at the location of the intersection of the two bow shocks. From Figure C-4 (c) the bow shocks have a lower angle of about 31^{o} and an upper angle (after the shock intersection) of 35^{o}. Here again it appears as though the arc positions itself just behind the shock.

A second set of runs was made using the same electrode combinations shown on Figure C-3 but the current range was increased to 370-390 amperes and the field coils were moved downstream one

quarter inch. The other run conditions were identical to the previous runs. The arc configurations and root locations were the same as the previous runs at the lower currents. The arc slant angles were equal to or at most one degree greater for the higher current runs and corresponding electrode arrangements. The current through the field coils was 1740 amperes. This lower coil current and the more rearward location of the field coils produced a 25 per cent decrease in the magnetic field strength at the reference station. For example, Run 733 had a blunt cylinder anode and cone cylinder cathode electrode arrangement (some as Run 668, Figure C-3), an arc current of 390 amperes and a B of 1200 gauss. The dynamic pressure q_{∞_n} is the same for Runs 733 and 668 so that the

$$B \sim 1/I^{1/3}$$

behavior of Eq. (4-28) is demonstrated.

The arc for the normal electrode arrangement (i. e., two Model A electrodes) is located well behind the attached conical shocks as the anode spot is always behind the shoulder of the cone-cylinder (about 2. 0 inches from the tip for the $M_\infty = 3.0$ runs). Since the arc is not positioned directly behind the shock it can adjust its slant somewhat depending on the current as shown on Figure 7. This behavior is indeed puzzling and a possible explanation might be as follows. The convected balanced arc cannot withstand (maintain a steady condition) the steep pressure gradient of a leading edge shock. Thus it slants

slightly behind the local Mach angle. As the arc current increases, the local temperature might increase such that the local Mach angle and hence the arc slant angle would increase accordingly.

The details of the slanting mechanism are still in question. However, it does appear as though the slanting behavior of the convected balanced arc is directly related to the flow field and shock wave pattern between the electrodes.

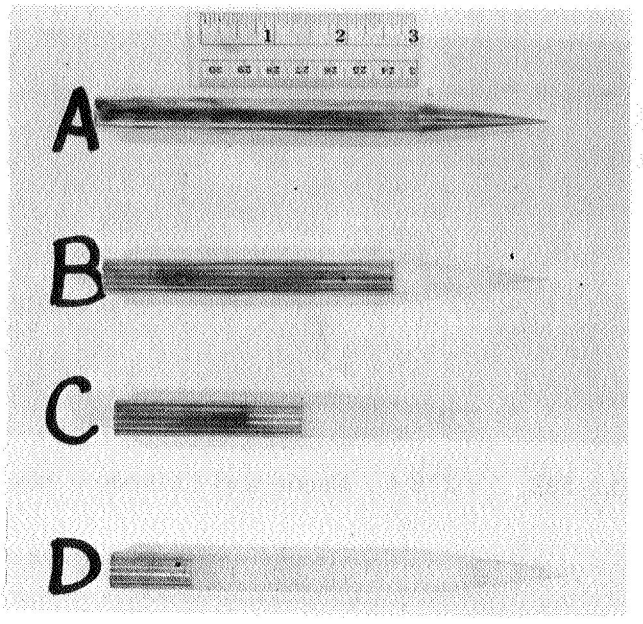

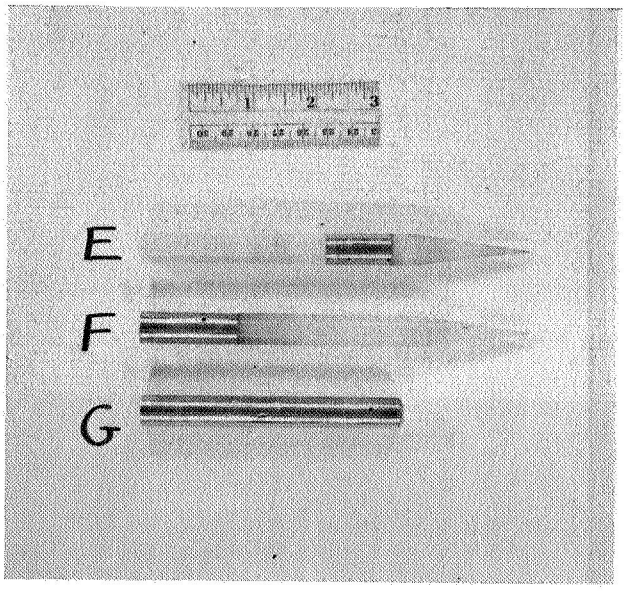

Note: All electrodes are 0.5 inches in diameter
The conducting parts are OFHC copper and
the non-conducting parts are nylon.

FIGURE C-1 Electrode configuration models

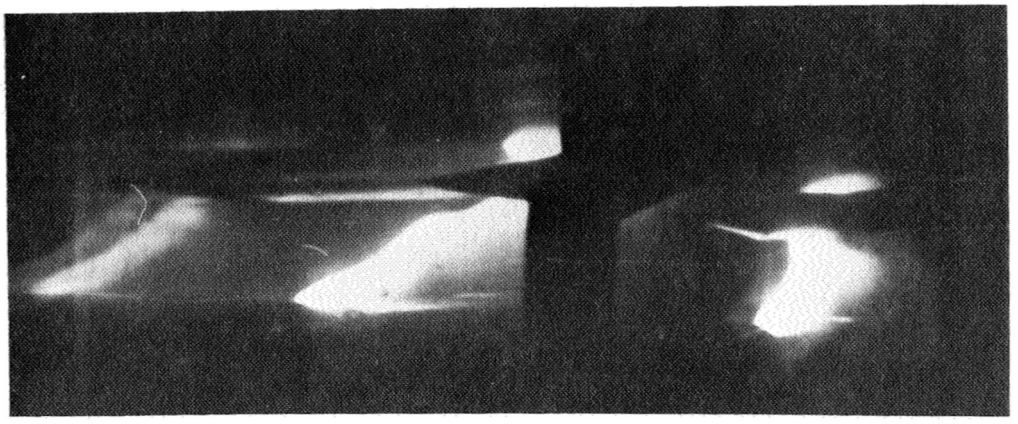

(a) Run 592, I = 216 A, Anode and Cathode - Model A (normal)

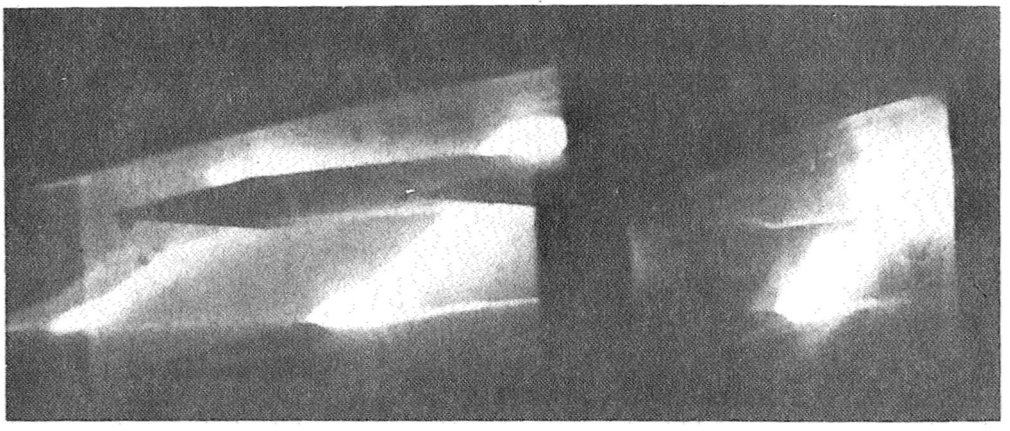

(b) Run 596, I = 216 A, Anode-Model A and Cathode-Model D

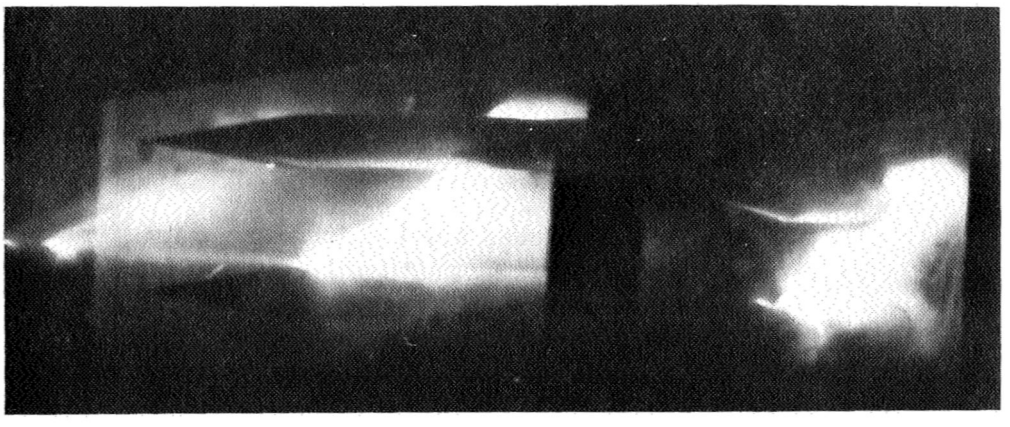

(c) Run 599, I = 224 A, Anode-Model E and Cathode-Model F

FIGURE C-2 Photographs of Mach 3.0 runs showing effects of electrode configurations

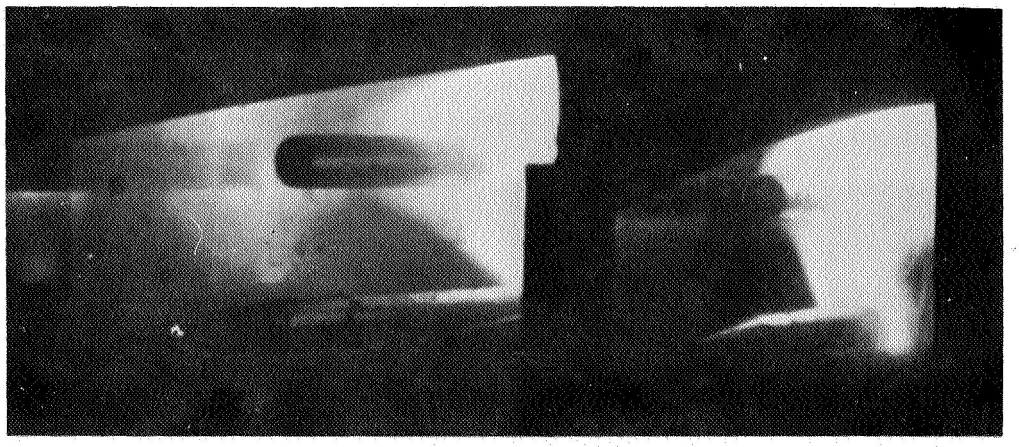

(a) Run 600, I = 218 A, Cathode - Model G and Anode - Model A

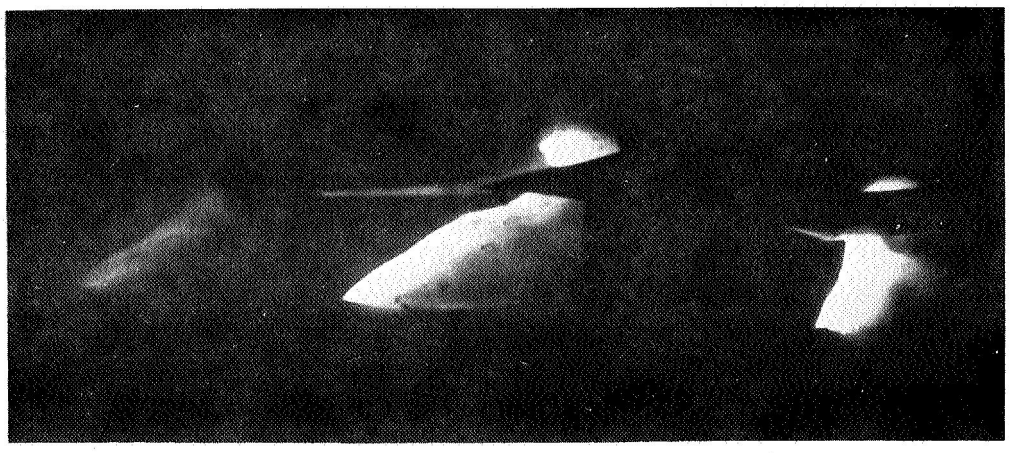

(b) Run 668, I = 221 A, Cathode - Model A and Anode - Model G

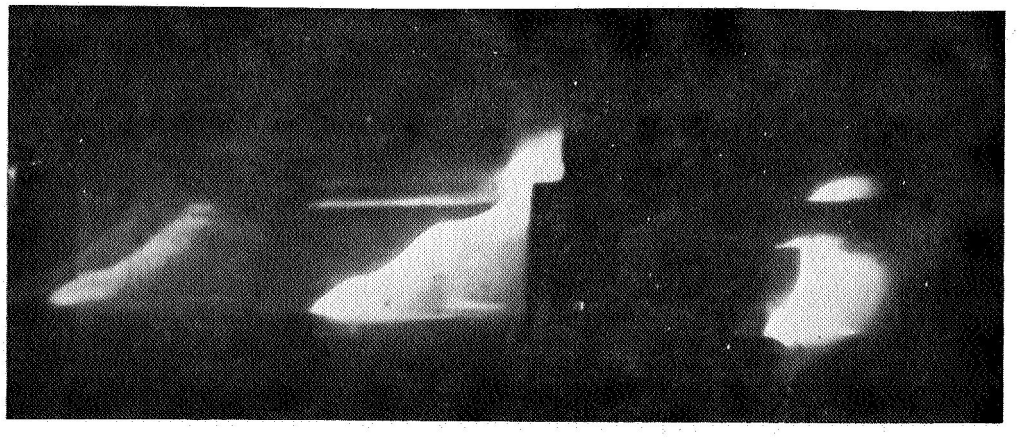

(c) Run 601, I = 224 A, Both Cathode and Anode are Model G

FIGURE C-3 Photographs of Mach 3.0 runs showing effect of electrode shape

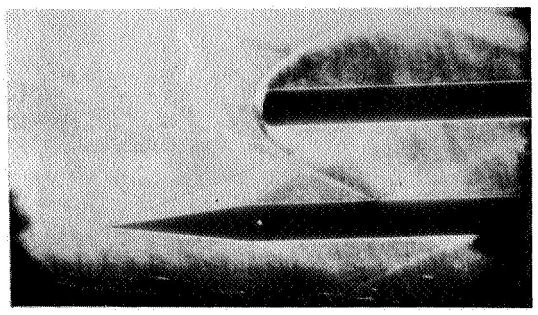

(a) Cathode - Model G
Anode - Model A

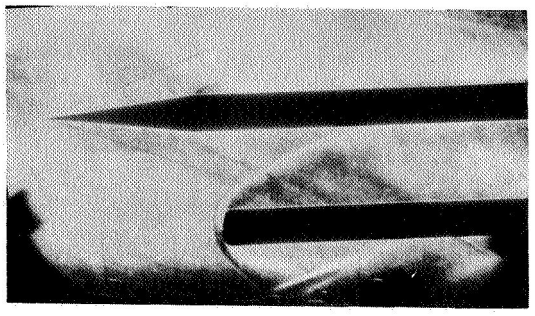

(b) Cathode - Model A
Anode - Model G

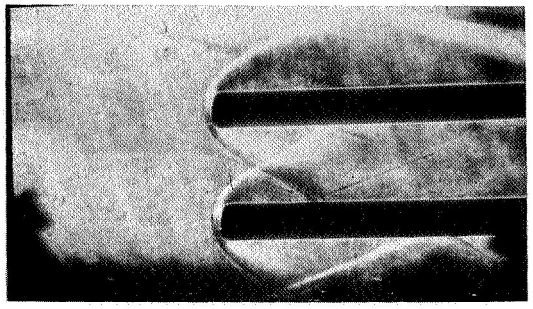

(c) Cathode - Model G
Anode - Model G

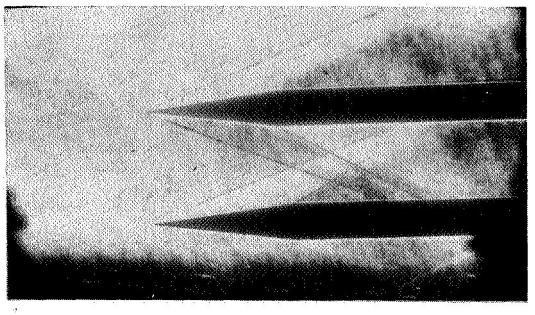

(d) Cathode - Model A
Anode - Model A

Figure C-4 Schlieren photographs of electrode combinations at Mach 3.0 (cathode on top)

Appendix D

FREE-BURNING ARC MEASUREMENTS

It was of interest to know what the characteristic curve looked like for a free-burning arc in air at low pressures and high currents. Specifically the curve at P_∞ = 14. 5 mm Hg and a current range of 190 to 400 amps would represent the limiting characteristic for the M_∞ = 3. 0 runs as $L_c \rightarrow 0$.

The apparatus for a free-burning arc was installed in the 4 x 4 supersonic tunnel. By closing the upstream valve and opening the downstream valve, P_∞'s from one atmosphere down to 9 mm Hg were obtained. The apparatus is shown in Fig. D-2. OFHC copper electrodes, 1/2 in. in diameter were used with the cathode always on the bottom. Electrode gaps of 1. 0 to 2. 4 in. were studied. Figure D-2 shows a 190 amp free-burning arc in air at one atmosphere and an electrode gap of 1. 2 in. Pressures of 1. 0, 0. 627, 0. 1 and 0. 019 (14. 5 mm Hg) atmospheres were examined over the current range of 190 to 400 amps.

The measured electric fields are shown in Fig. D-1 along with results from other investigations. The data at one atmosphere is consistent with King's data for a nitrogen arc (Ref. 57), Roman's data for an argon arc burning in air (Ref. 18) and Reider's data for low current air arcs (Ref. 44).

The electric fields at one atmosphere and 0.627 atmosphere showed a slight positive characteristic over the current range of 190 to 400 amps. This observation is in agreement with King (Ref. 57) and appears to be due to the strong electrode jets. The characteristic curves at 0.1 and 0.0191 atmosphere were fairly flat over the current range.

The electric field was difficult to determine at 0.0191 atmosphere for two reasons. First, the arc was electrode stabilized* for gaps less than 2.0 in. Thus the data from gaps at 2.0 and 2.4 in. were for arcs at the onset of convection stabilization and the electric fields were not completely independent of electrode gap. The second reason was that the voltage differences were very small and their measurement was difficult. For these reasons E at $P_\infty = 0.0191$ atmospheres is represented as a range from 2.0 to 4.0 volts/in. in Fig. D-1 and D-3. The extrapolation of the data at higher pressures in Fig. D-3 indicates that an E = 2.5 volts/in. is a reasonable value for $P_\infty = .0191$ atmosphere. The data does indicate that E is fairly constant over the current range examined.

The presence of anode jets are very noticeable in the arcs at 1.0 and 0.627 atmosphere as shown in Fig. D-4. King remarks that the cathode and anode jets are responsible for the positive characteristic. The jets will augment the natural convection of heat from the column,

*The total voltage was not linear with arc length. See also Section 1.4.

thereby causing the input power to increase (Section 4.6). If the arc is made long enough the characteristic curve is again flat as the effect of the electrode jets on the arc column is made negligible (King, Ref. 57). These jets are not observed in photographs of the arc at the two low pressures.

We can again apply heat transfer ideas to measured arc data as was done in Section IV and by Suits and Poritsky in Ref. 41. The measured data will be for the free-burning arcs and we will try to determine the functional form of $Nu_{NC} = f(Gr\ Pr)$ (Appendix B).

We will assume that the energy transfer out of the arc by mass transfer and radiation is small compared to the energy transfer by natural convection at the boundary $r = r_b$ (Ref. 56). We also assume that for a constant P_∞ and T_∞ the effective temperature T_σ is fairly constant over the current ranges $I < 50$ amps and $I > 100$ amps (Ref. 41).

Thus, Ohm's law is given by Eq. (4-1).

$$I = \text{const}\ D^2\ E \tag{4-1}$$

where $D = 2r_b$ and r_b is a characteristic dimension of the arc cross-section, i.e. the radius of the luminous region or some appropriate isotherm. Krinberg (Ref. 56) used $5000^\circ K$ and $6000^\circ K$ for his boundary temperature.

The energy balance at the boundary is given by Eq. (3-30) and (B-2):

$$EI = \text{const}' \, \pi \, (Gr \, Pr)^m \, \phi_b \qquad \text{(D-1)}$$

where Gr and Pr are based upon film temperature properties and r_b.

For P_∞, T_∞ and T_σ constant Eq. (D-1) becomes

$$EI = \text{const}'' \, D^{3m} \qquad \text{(D-2)}$$

Eliminating D between Eq. (4-1) and (D-2) gives

$$E = \frac{\text{const}'''}{I^n}$$

where $n = (2 - 3m)/(2 + 3m)$. (D-3)

Rieder's data (Fig. D-1) for currents less than 50 amps has a slope of approximately - 1/3 (i.e. $n = 1/3$). For currents greater than 100 amps, this investigation indicates a flat characteristic ($n = 0$). Putting this information into Eq. (D-3) gives:

$$\begin{aligned} Nu_{NC} &\sim (Gr \, Pr)^{1/3} \quad \text{for} \quad I < 50 \text{ amps} \\ Nu_{NC} &\sim (Gr \, Pr)^{2/3} \quad \text{for} \quad I > 100 \text{ amps} \end{aligned} \qquad \text{(D-4)}$$

The current interval $50 \leq I \leq 100$ appears to be a transition.

The Nusselt number relation for vertical heated solid cylinders is (from Fig. B-2):

Turbulent range , $10^9 < Pr \, Gr < 10^{12}$ $\quad Nu_{NC} = 0.13 \, (Pr \, Gr)^{1/3}$

Laminar range , $10^4 < Pr \, Gr < 10^9$ $\quad Nu_{NC} = 0.55 \, (Pr \, Gr)^{1/4}$

We observe that the natural convection heat transfer coefficients for the free-burning arc appear to be higher than those for the vertical solid cylinders of equivalent dimensions and boundary temperatures. This is reasonable since the free-burning arc has the additional heat transfer process of mass flow along the column axis and through the boundary. This internal convection is generated by buoyancy forces and the electrode jets.

Rowe (Ref. 58) considered the theoretical problem of the free-burning arc and concluded that the relation

$$Nu_{NC} = 2 (Pr\ Gr)^{1/3} \qquad (D\text{-}5)$$

was valid for all currents. He assumed that Pr and Gr were based upon film temperature properties ($T_B = T_S = 5000^{\circ}K$) and an axial length Z for the characteristic dimension. The exponent equal to 1/3 in Eq. (D-5) is a consequence of the fact that the effect of Z must vanish from the problem, since the column is uniform and independent of distance from the electrodes. There is partial agreement between Eq. (D-4) and Rowe's equation (D-5). The reasons for the difference at the high current range are not clear.

The assumption that T_σ is fairly constant for changing current and the experimental fact that E is constant give us

$$D = \text{const}\sqrt{I} \qquad (D\text{-}6)$$

which is the same relation for the convected balanced arc.

Now let us hold current constant and determine the relation between E and P_∞. We consider I and T_∞ constant. Ohm's law is

$$I = \text{const } D^2 E P_\infty^{\Gamma-1} \tag{D-7}$$

where $P_\infty^{\Gamma-1}$ accounts for the change in electrical conductivity as the pressure P_∞ is varied. Suits and Poritsky (Ref. 41) discuss this term in detail and conclude that $\Gamma = 1.44$ for air. Equation (D-1) becomes

$$EI = \text{const } P_\infty^{2m} D^{3m} \tag{D-8}$$

Now eliminating D between Eq. (D-7) and (D-8) and considering I as a constant we get

$$E = \frac{\text{const}'}{P_\infty^{n}}$$

where

$$n = \frac{m\,[3(\Gamma - 1) - 4]}{3m + 2} \tag{D-9}$$

Substituting $\Gamma = 1.44$ and $m = 2/3$ into (D-9) gives $n = -0.448$. Thus

$$E = \text{const}' P_\infty^{.448} \tag{D-10}$$

Figure D-3 shows Eq. (D-10) compared with the experimental results. The failure of Eq. (D-10) to agree better with the experimental data is perhaps due to the value for Γ. $\Gamma = 1.44$ was determined for low current arcs (up to 30 amps) and pressures of 1 to 30 atmospheres.

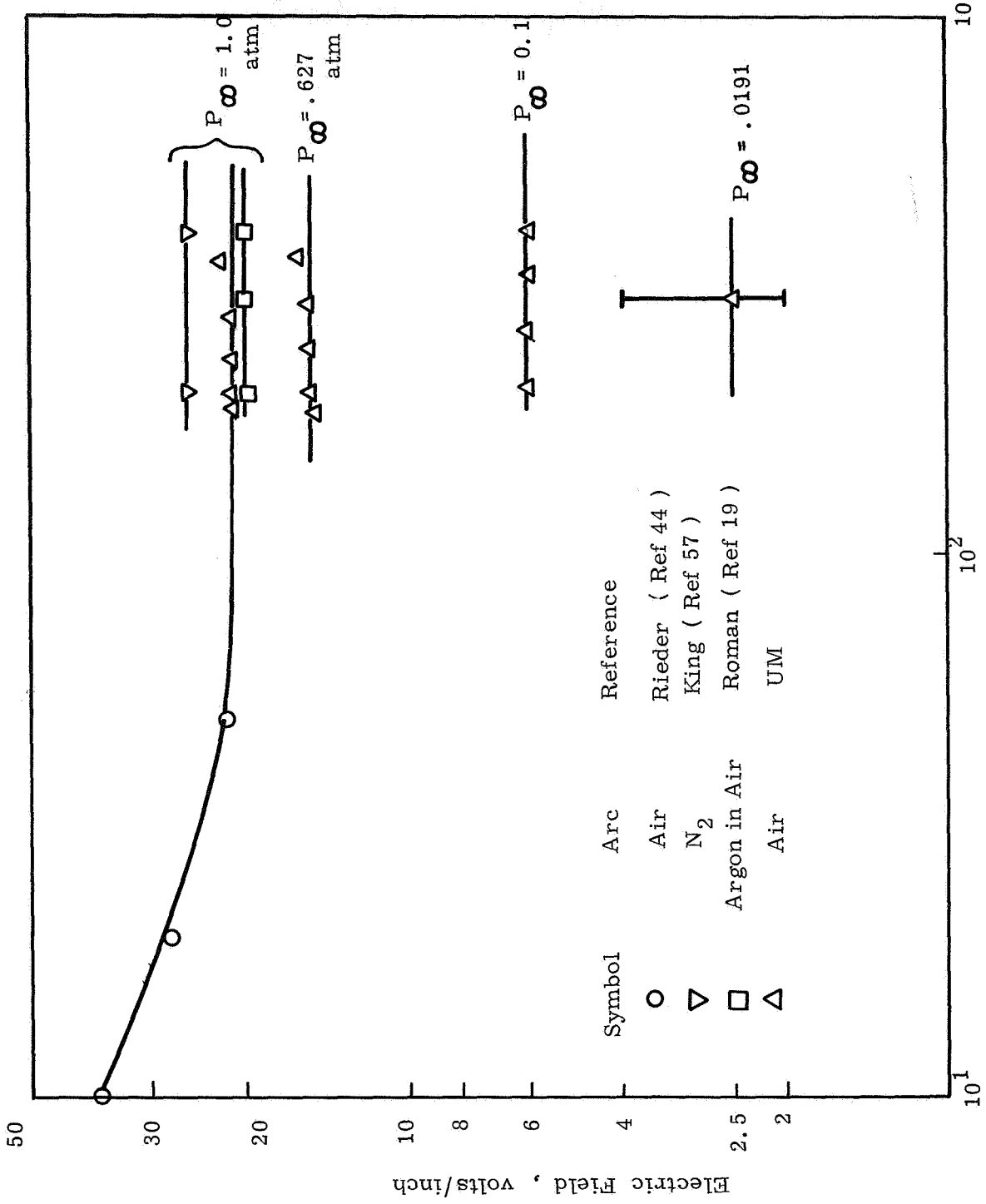

Figure D-1 Free - burning arc characteristic curves

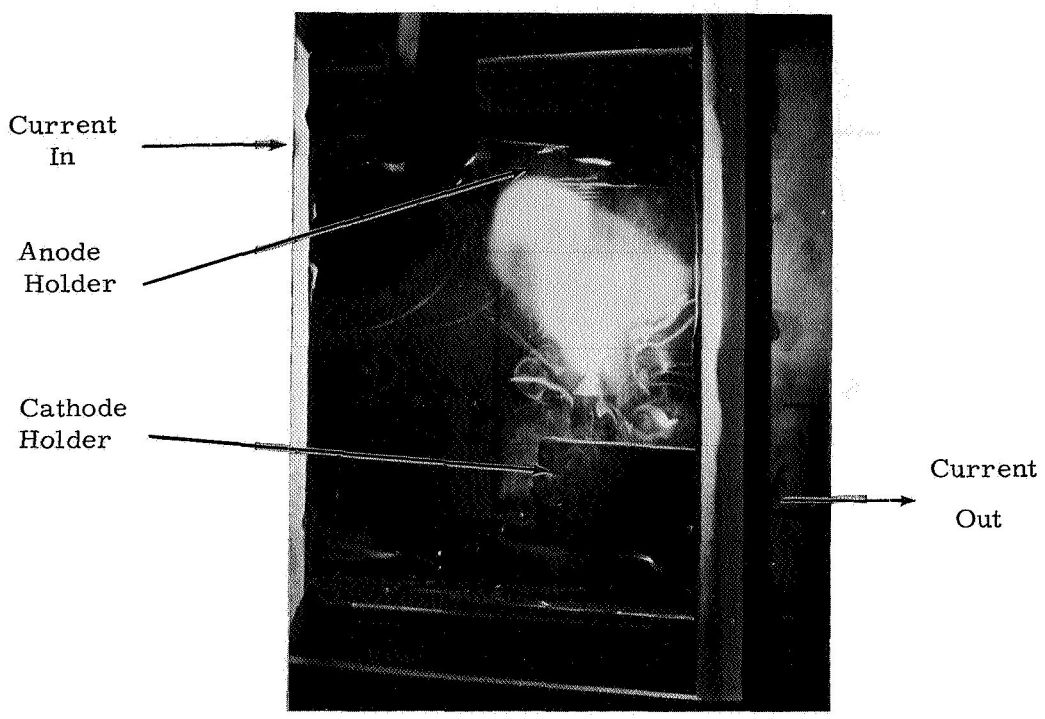

Fig. D-2 Set-up for free - burning experiments showing a 190 amp arc in air at one atmosphere and a 1.2 inch gap

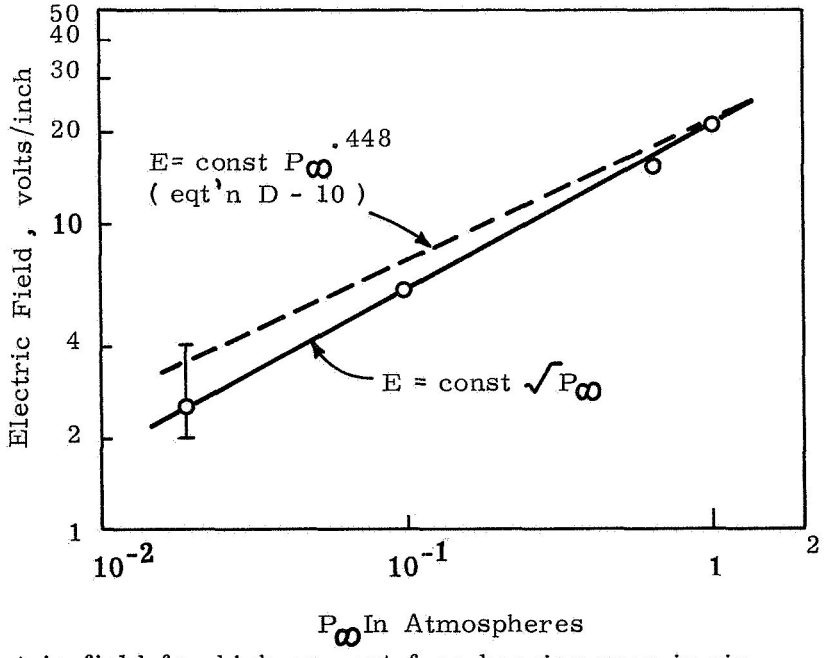

Fig. D-3 Electric field for high current free-burning arcs in air

P_∞ = 1.0 atm, I = 300 A, gap = 1.2"

P_∞ = .627 atm, I = 298 A, gap = 1.2"

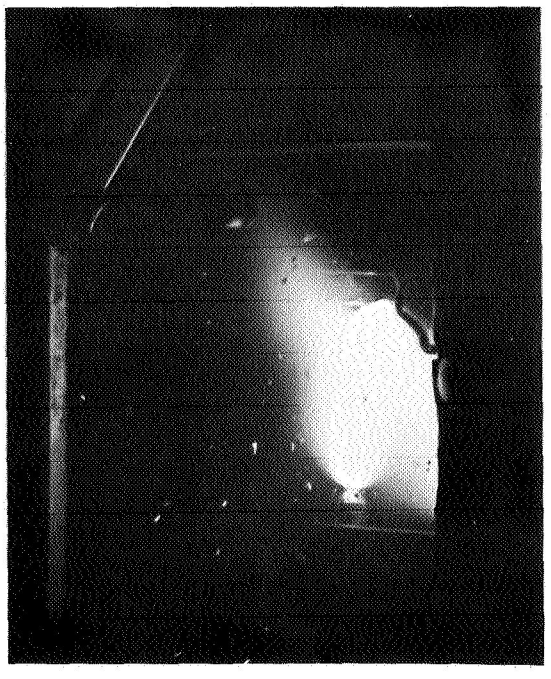

P_∞ = 0.1 atm, I = 196 A, gap = 2.0"

P_∞ = .0191 atm, I = 318 A, gap = 2.0"

FIGURE D-4 Typical photographs of high current free-burning arcs on copper electrodes

"The aeronautical and space activities of the United States shall be conducted so as to contribute . . . to the expansion of human knowledge of phenomena in the atmosphere and space. The Administration shall provide for the widest practicable and appropriate dissemination of information concerning its activities and the results thereof."

—NATIONAL AERONAUTICS AND SPACE ACT OF 1958

NASA SCIENTIFIC AND TECHNICAL PUBLICATIONS

TECHNICAL REPORTS: Scientific and technical information considered important, complete, and a lasting contribution to existing knowledge.

TECHNICAL NOTES: Information less broad in scope but nevertheless of importance as a contribution to existing knowledge.

TECHNICAL MEMORANDUMS: Information receiving limited distribution because of preliminary data, security classification, or other reasons.

CONTRACTOR REPORTS: Scientific and technical information generated under a NASA contract or grant and considered an important contribution to existing knowledge.

TECHNICAL TRANSLATIONS: Information published in a foreign language considered to merit NASA distribution in English.

SPECIAL PUBLICATIONS: Information derived from or of value to NASA activities. Publications include conference proceedings, monographs, data compilations, handbooks, sourcebooks, and special bibliographies.

TECHNOLOGY UTILIZATION PUBLICATIONS: Information on technology used by NASA that may be of particular interest in commercial and other non-aerospace applications. Publications include Tech Briefs, Technology Utilization Reports and Notes, and Technology Surveys.

Details on the availability of these publications may be obtained from:

SCIENTIFIC AND TECHNICAL INFORMATION DIVISION

NATIONAL AERONAUTICS AND SPACE ADMINISTRATION

Washington, D.C. 20546